INFLATION MODELS IN LIGHT OF COSMIC MICROWAVE BACKGROUND OBSERVATIONS

By

SUKANNYA BHATTACHARYA

PHYS05201304003

A thesis submitted to the

Board of Studies in Physical Sciences

In partial fulfillment of requirements

For the Degree of

DOCTOR OF PHILOSOPHY

of

HOMI BHABHA NATIONAL INSTITUTE

February, 2019

Homi Bhabha National Institute

Recommendations of the Viva Voce Committee

As members of the Viva Voce Committee, we certify that we have read the dissertation prepared by **Sukannya Bhattacharya** entitled **"Inflation Models in light of Cosmic Microwave Background Observations"** and recommend that it maybe accepted as fulfilling the thesis requirement for the award of Degree of Doctor of Philosophy.

Asitkrde ______________________ Date: 6/5/2019

Chairman - Prof. Asit Kumar De

Koushik Dutta ______________________ Date: 06.05.2019

Guide / Convener - Prof. Koushik Dutta

______________________ Date:

Co-guide - (if any)

L. Sriramkumar ______________________ Date: 6/5/19

Examiner - Prof. L. Sriramkumar

______________________ Date: 6/5/19

Member 1 - Prof. Amit Ghosh

Debasish Majumdar ______________________ Date: 06/05/2019

Member 2 - Prof. Debasish Majumdar

Final approval and acceptance of this thesis is contingent upon the candidate's submission of the final copies of the thesis to HBNI.

I/We hereby certify that I/we have read this thesis prepared under my/our direction and recommend that it may be accepted as fulfilling the thesis requirement.

Date: 06.05.2019

Place: Saltlake, Kolkata **Guide:** Koushik Dutta

STATEMENT BY AUTHOR

This dissertation has been submitted in partial fulfillment of requirements for an advanced degree at Homi Bhabha National Institute (HBNI) and is deposited in the Library to be made available to borrowers under rules of the HBNI.

Brief quotations from this dissertation are allowable without special permission, provided that accurate acknowledgement of source is made. Requests for permission for extended quotation from or reproduction of this manuscript in whole or in part may be granted by the Competent Authority of HBNI when in his or her judgement the proposed use of the material is in the interests of scholarship. In all other instances, however, permission must be obtained from the author.

Sukannya Bhattacharya

Sukannya Bhattacharya

DECLARATION

I, hereby declare that the investigation presented in the thesis has been carried out by me. The work is original and has not been submitted earlier as a whole or in part for a degree / diploma at this or any other Institution / University.

Sukannya Bhattacharya

Sukannya Bhattacharya

List of Publications Arising from the Thesis

Journal:

1. *Attractor Models in Scalar-Tensor Theories of Inflation*

   Sukannya Bhattacharya, Kumar Das, Koushik Dutta, Int. J. Mod. Phys. D 27, 1850079 (2018), arXiv: 1706.07934 [gr-qc]

   DOI: http://doi.org/10.1142/S0218271818500797

2. *Constrains on Kähler Moduli Inflation from Reheating*

   Sukannya Bhattacharya, Koushik Dutta, Anshuman Maharana, Phys. Rev. D 96, 083522 (2017), arXiv: 1707.07924 [hep-ph]

   DOI: http://doi.org/10.1103/PhysRevD.96.083522

3. *Constraining Warm Inflation with CMB data*

   Mar Bastero-Gil, **Sukannya Bhattacharya**, Koushik Dutta, Mayukh Raj Gangopadhyay, JCAP02 (2018) 054, arXiv: 1710.10008 [astro-ph.CO]

   DOI: http://iopscience.iop.org/article/10.1088/1475-7516/2018/02/054

4. *Confronting Kähler moduli inflation with CMB data*

   Sukannya Bhattacharya, Koushik Dutta, Mayukh R. Gangopadhyay, Anshuman Maharana, Phys. Rev. D 97, 123533 (2018), arXiv: 1711.04807 [astro-ph.CO]

   DOI: http://doi.org/10.1103/PhysRevD.97.123533

5. *A study in non-canonical domain of Goldstone inflation*

   Sukannya Bhattacharya, Mayukh R. Gangopadhyay, (Communicated to journal), arXiv: 1812.08141 [astro-ph.CO]

Chapters in Books and Lecture Notes: None

Conferences:

1. Talk presented "Constraining Warm Inflation with CMB observations" at *Advances in Astroparticle Physics and Cosmology - AAPCOS* , Saha Institute of Nuclear Physics, Kolkata, India, 6-9 March, 2018

2. Talk presented "Constraining Warm Inflation with CMB observations" at *DESY Theory Workshop: Fundamental Physics in the Cosmos*, DESY, Hamburg, Germany, 26-29 September, 2017

3. Talk presented "Constraining Warm Inflation with CMB observations" at *Meeting on fundamental Cosmology*, Centro de Estudios de Fisica del Cosmos de Aragon, Teruel, Spain, 11-13 September, 2017

4. Talk presented "Attractor Models in Scalar-Tensor Theories of Inflation" at *29 th meeting of Indian Association for General Relativity and Gravitation - IAGRG-29* , IIT Guwahati, Guwahati, India, 18-20 May, 2017

5. Poster presented “Constraining Kähler moduli inflation using CMB data" at*Conference on Shedding Light on the Dark Universe with Extremely Large Telescopes*, International Centre for Theoretical Physics (ICTP), Trieste, Italy, 2-6 July, 2018

6. Poster presented “Constraining Warm Inflation with CMB observations" at*Summer School on Cosmology, 2018*, International Centre for Theoretical Physics (ICTP), Trieste, Italy, 18-29 June, 2018

7. Poster presented “Constraining Warm Inflation with CMB observations" at*Post-Planck Cosmology: Enigma, Challenges and Vision*, Inter-University Centre for Astronomy and Astrophysics (IUCAA), Pune, India, 9-12 October, 2017

Others: None

Sukannya Bhattacharya

Sukannya Bhattacharya

To *my loving Parents*.

ACKNOWLEDGEMENTS

"It's not the destination, but the journey that matters."

This journey has been possible due to the continuous support of my parents. My father is a tremendous inspiration to me with his urge for knowledge and truth. My mother is a constant motivation with her strength and perseverance. I owe this journey to their brave defense for me against the odds of the unreasonable demands of a typical Indian suburban society.

My Ph.D. supervisor, Prof. Koushik Dutta, has thoroughly guided me with his expertise and a mere thank you is not enough to express my gratitude towards him. His advises, comments and our numerous academic discussions have ushered me into the path of research and encouraged me to attain a broader perspective of science. He has been a great source of enthusiasm and strength in both academic and non-academic situations and I am forever thankful to him for that.

I sincerely thank my collaborators Dr. Kumar Das, Dr. Mayukh Raj Gangopadhyay, Prof. Mar Bastero-Gil and Prof. Anshuman Maharana, with whom I had very useful academic discussions. I have learned a lot while working with them and hope to collaborate again in future. I also thank Prof. Supratik Pal, Prof. Pravabati Chingangbam, Dr. Dhiraj Hazra, Prof. Akhilesh Nautiyal and Dr. Jayanti Prasad who have helped me academically during visits or over online communications. I sincerely thank Prof. Asit De, Prof. Palash Baran Pal, Prof. Amit Ghosh and Prof. Debasish Majumdar for their help in many scenarios. I also thank the theory division for giving me access to the divisional cluster computing facility, which I have used extensively in my research. I thank the system administrators Kaushik da (CMP), Sangita di (Theory) and Richard for helping me with the cluster systems on many occassions.

I thank Saha Institute of Nuclear Physics for providing me with adequate infrastructure to pursue my research work and I thank Council of Scientific and Industrial Research (CSIR) for financial support through five years of my doctoral research.

I thank my uncle and aunt (*Jethu* and *Jethi*) in Dinhata for reminding me of the simple unconditional love of ‘family’ and of the peace and quiet of ‘home’. I thank my aunt and uncle (*Pisi* and *Piso*) in Baranagar for being a home away from home for more than 10 years in Kolkata. I also thank my brother for our long conversations about struggle and responsibilities, which have reminded me of the same regularly. My higher secondary physics tutor Dulal da, who had introduced me to the pure joy of science, has always been a friend, philosopher and guide, and I remain grateful to him for that.

In my time in SINP, I have met a huge number of marvellous people. I have made wonderful memories with Rome, Shamik, Roopam, Shramana, Sudeshna, Sourav, Mugdha, Maireyee, Aranya, Gourab, Sayan, Pritam and many more. The endless *adda*s about science, philosophy, music, drama, art, poetry and what not and the unforgettable on-stage ventures with you guys have made it possible to get through rough times. I learned some of neutrino physics from Rome and Roopam and eventually co-authored with them in a project. I have been fortunate to come across some superb seniors like Aminul da, Arindam da, Goutam da, Amit da, Aritra da, Chiru da, Naoshad da, Anshu da, Susnata di, Debasree di, Chaitrali di and Nilu da. In Theory division, I have encountered some highly motivating colleagues and juniors like Mugdha, Rohit, Kuntal, Avik (Jr. and Sr.), Bithika, Supriyo, Aranya, Augniva, Ritesh, Pritam, Arunima, Ayan and Madhurima.

I thank my M.Sc. friends Arpita, Deya and Pritha for the nice friendship that we share. I also thank my cousin Tua, my school friends Jayita and Purbasha for their love and support. Last, but not the least, I thank Suman for simply being there through thick and thin and for being a continuous source of strength to me. His passion for life is contagious, which has

been an elemental driving force for many years.

All your love and support have helped me through these five years and

“Miles to go before I sleep.”

Sukannya Bhattacharya

Sukannya Bhattacharya

CONTENTS

SYNOPSIS

The theory of inflation, predicting a quasi-exponential expansion of the universe at very early times (energy scale $\sim 10^{16}\mathrm{GeV}$), was proposed as a solution to the horizon and flatness problems of hot big bang cosmology [1]. Moreover, quantum perturbations during inflation can act as seeds for generation of the large-scale structures in the universe. The observations of the cosmic microwave background (CMB) through the decades (COBE, 1989 [2]; WMAP 2003 [3]; PLANCK 2018 [4]) have mapped the free streaming photons from the last scattering surface (LSS) (at redshift ~ 1100) to measure the temperature and polarization power spectra in the sky. The latest observed power spectra are in excellent agreement with the predictions of the $\Lambda\mathrm{CDM}$ cosmology considering the primordial spectra to be generated from inflation [4].

The simplest dynamics of inflation is given by constructing a model where a single scalar field ϕ (inflaton), minimally coupled to gravity, is slowly rolling down a potential $V(\phi)$ [5]. The action S for such a simple scenario can be written (in natural units and with reduced Planck mass set to unity) as:

$$S = \int d^4x\sqrt{-g}\left[\frac{1}{2}R + \frac{1}{2}g_{\mu\nu}\partial^\mu\phi\partial^\nu\phi - V(\phi)\right], \tag{1}$$

where $g_{\mu\nu}$ is the Friedman-Robertson-Walker (FRW) metric, $\sqrt{-g}$ is the determinant of $g_{\mu\nu}$ and R is the Ricci scalar.

The scalar field can be decomposed into a background homogenerous part and fluctuations as: $\phi(t, \mathbf{x}) = \phi(t) + \delta\phi(t, \mathbf{x})$. The spacetime can also be written as a summation of a background part $\tilde{g}_{\mu\nu}$ and perturbations $\delta g_{\mu\nu}$ (contains scalar, vector and tensor components) in a similar way. The background equations of motion can be derived from the action in Eq. (1) with only the background field and metric. The fluctuations in the field and spacetime, which can be combined in a gauge-invariant form $\mathcal{R}$ known as the *comoving curvature perturbation*, grow during inflation and eventually exit the horizon [5, 6]. The perturbations can be decomposed into various modes of different wavenumbers $k = 2\pi/\lambda$, and horizon exit for a particular mode occurs when the wavelength of that mode becomes larger than the horizon size. These perturbations are frozen in the superhorizon regime and they re-enter the horizon only after the end of inflation to evolve further. Later at the time of recombination, photons decouple from the thermal bath and free-stream through the universe to reach us as the cosmic microwave background radiation. Therefore, the perturbations at the surface of last scattering of the photons are embedded as fluctuations in the CMB sky.

The 2-point correlation functions of the primordial fluctuations can be written as scalar and tensor power spectra, which can be paramterised in almost scale-invariant forms as:

$$\Delta^2_{\mathcal{R}}(k) = A_s \left(\frac{k}{k_*}\right)^{n_s - 1} \qquad \text{and} \qquad \Delta^2_t(k) = A_t \left(\frac{k}{k_*}\right)^{n_t} \tag{2}$$

where k_* is a pivot scale that exits the horizon N_{pivot} e-folds before the end of inflation. A_s and A_t are the amplitude of the scalar and tensor power spectra at the pivot scale, and n_s and n_t are the respective spectral indices at the pivot scale. The ratio r of the tensor and scalar fluctuations: $r = \Delta_t^2(k)/\Delta_{\mathcal{R}}^2(k)$ is a measure of the energy scale of inflation. Therefore, precise measurement of r, which is a challenge even in modern CMB experiments, is very useful to understand the inflationary energy scale, which is theoretically predicted to be different for different models of inflation.

Model building in the inflationary scenario is attributed to different forms of $V(\phi)$, non-minimal gravitational coupling of the inflaton and non-canonical kinetic function. Different models of inflation in the literature are constrained by mainly using their predictions of n_s and r and comparing them with their observed values from CMB experiments. Single-field models can be either large-field models where the field excursion $\Delta\phi$ is larger than the Planck mass $M_{\rm Pl}$, or small-field models where $\Delta\phi < M_{\rm Pl}$ or hybrid of these two cases. Several canonical single-field models have been studied and compared statistically [7, 8] using CMB observations. Specifically, power law models of single-field inflation of the form $V(\phi) = \lambda\phi^p$ are tightly constrained by observations, where $p \geq 2$ cases are strongly disfavoured by the PLANCK2018+BK14 data [4]. Latest observations have ruled out the particle physics motivated quartic inflation model $V(\phi) = \lambda\phi^4$ [9] by more than $3-\sigma$ confidence level. On the other hand, observations strongly favour single-field plateau inflation models where the inflaton rolls very slowly in a flat part of the potential for a large number of e-folds. Plateau inflation models include Starobinsky inflation [10], where the dynamics is driven by a R^2 term in the Lagrangian, and the Einstein frame potential has a large flat plateau. The value of r for Starobinsky inflation ($r \simeq 0.003$) acts as a point of convergence for α-attractor models (E models and T models) [11] and for models where the inflaton is non-minimally coupled to gravity (e.g. ξ-attractors) [12].

In [13], we have studied cosmological attractor models of inflation (α and ξ-attractors) to explore their connection with scalar-tensor theories of gravity, e.g $f(R)$ gravity and Brans-Dicke theory. We have demonstrated the conditions on the Lagrangian under which

$f(R)$ and Brans-Dicke theories exhibit the attractor mechanism and converge to the Starobinsky prediction. We have also explored the stability of the attractor mechanism by varying the functional degrees of freedom of (i) the non-minimal coupling and (ii) the non-canonical kinetic term. We have shown that the attractor has a robust dependence on the functional forms and coefficients present in those forms.

Since the pivot number of e-folds of inflation N_{pivot} can be related to n_s using $n_s = 1 - 2/N_{\text{pivot}}$, the existence of non-trivial post-inflationary epochs in a model can lead to interesting predictions in the $n_s - r$ plane. Different non-standard scenarios like non-minimal gravitational coupling, energy dissipation of inflaton during the time of inflation and non-canonical kinetic functions can modify the n_s and r values and change the significance of different inflationary models by allowed by data.

Evidently, it is interesting to statistically explore different theoretically inspired scenarios of inflation with rigorous numerical analysis, e.g. Markov Chain Monte Carlo (MCMC) analysis, in light of present CMB data. COSMOMC [14] is a publicly available package that uses the Boltzman solver CAMB and MCMC simulations to constrain the cosmological parameters. The default algorithm uses spatially flat 6-parameter ΛCDM model where the varying cosmological parameters are baryon density Ω_b, cold dark matter density Ω_c, acoustic peak angular scale θ, reionization optical depth τ and inflationary parameters A_s and n_s. Extensions of this model in the inflationary sector can include other parameters like r, running of the spectral index α_s etc. The primordial power spectra (scalar and tensor) depend on the underlying inflationary model. Given an almost scale-invariant primordial spectrum of the form Eq. (2), different modes (k) of inflation can be evolved from the time each of them re-enter the horizon in a matter dominated epoch upto the LSS through a transfer function. The cumulative amplitude of different modes at LSS can be written in terms of spherical harmonics with amplitude $\mathcal{C}_\ell$. The $\mathcal{C}_\ell$ generated by simulations in COS-

MOMC are compared with observed $\mathcal{C}_\ell$ values at different CMB experiments and the best fit to data is obtained by χ^2 minimization. The parmeters of the model can be constrained using Bayesian analysis, where marginalized posterior probabilities for the parameters are calculated using their prior probabilities and likelihood functions.

One of the non-trivial inflationary scenarios is warm inflation [15], where the inflaton is energetically coupled to relativistic degrees of freedom (d.o.f.) present during inflation and therefore the inflaton energy density is continuously transformed into radiation energy density. Different warm inflation theories can be constructed based on which fields are present in the radiation bath and the nature of energy dissipation of inflaton into the thermal bath For the case of "warm little inflation" [16], the inflaton is a pseudo Nambu-Goldstone Boson (pNGB), coupled to the light relativistic d.o.f., and the inflation potential is protected from quantum corrections using symmetries. In [17], we have constrained the warm little inflation scenario using PLANCK2015+BICEP2 [18] data where the inflation potential is quartic chaotic $V(\phi) = \lambda\phi^4$ and the maximum contribution to dissipation is linear in temperature T (dissipative coefficient: $\Upsilon = C_T T$). The posterior probabilities and best-fit values of the model parameters C_T, λ and g_* (effective number of relativistic d.o.f. in the thermal bath) are calculated using COSMOMC for non-thermal (inflaton excluded from thermal bath) and thermal (inflaton included in thermal bath) scenarios. The predictions for the cosmological observables are within $1-\sigma$ limit of the current observations by PLANCK for the thermal ($n_s = 0.9631$ and $r = 0.03$) case and just at the $2-\sigma$ limit for the non-thermal case ($n_s = 0.9736$ and $r = 0.06$). These predictions re-establish the quartic potential as a possible candidate for inflation in a warm dissipative picture. Moreover, since by the end of warm inflation most of the inflaton energy is already converted into radiation, the (p)reheating epoch can be avoided without loss of generality. Therefore, for instant reheating we have also kept $N_{\rm pivot}$ as a variable which is computed to be $N_{\rm pivot} = 58$ and

$N_{\rm pivot} = 58.5$ for the mean values of the model parameters in non-thermal and thermal cases respectively.

String theory can also provide potential candidates for inflation through different mechanisms. Models evolving from the Large Volume Scenario (LVS) in string theory [19] are widely explored as inflationary models due to their predictions of low values for tensor-to-scalar ratio (r) and post-inflationary modular cosmology. Such a model, the Kähler moduli inflation [20], is set in LVS for moduli stabilisation of IIB flux compactifications and the complex structured moduli can be stabilised and integrated out. The heavy moduli particles are stable during inflation, but at the end of inflation with sufficient decrease in the value of the Hubble parameter, these moduli particles dominate and then decay. Therefore, the moduli dominated epoch and reheating by moduli decay alter the predictions for inflationary and reheating number of e-folds. In [21], we have studied the Kähler moduli inflation, to explore the possible predictions about reheating in such a scenario. With the number of e-folds $N_{\rm mod}$ of muduli domination given in terms of the model parameters, in [21] we have computed the inflationary number of e-folds $N_{\rm pivot}$ while keeping the model parameters at theoretically inspired values. Then using the relation between $N_{\rm pivot}$ and n_s, we have inspected the dependence of the reheating number of e-folds $N_{\rm re}$ and reheating temperature $T_{\rm re}$ on n_s for different reheating equations of state $w_{\rm re}$. We have shown that $w_{\rm re} = 2/3$ exotic reheating case reaches closest to the observed central value of n_s.

In [22], we have done MCMC analysis for the Kähler moduli inflation where we have constrained the model parameters for general reheating scenario ($w_{\rm re}$ not specified) and for particular values of $w_{\rm re}$ in the range $-1/3 < w_{\rm re} < 1$. This analysis was done using CosmoMC with modified version of ModeCode [23], where the later is a public package to calculate the primordial power spectra for a given inflationary model which allows to vary the model parameters and $N_{\rm pivot}$ directly. We found that the central value $n_s = 0.953$

from simulations for the general reheating case is shifted to the left from the observed central value of n_s(from PLANCK 2015 [18]). Analysis with fixed $w_{\rm re}$ showed that the exotic reheating scenarios are preferred with the maximum value $n_s = 0.9575$ reached for $w_{\rm re} = 1$. r has a very low value $\sim 10^{-8}$ for all these cases, complying to the current upper limit for r [18].

In my doctoral work, I have studied the phenomenology of the above inflationary cases in light of CMB data.

List of Figures

List of Tables

CHAPTER 1

INTRODUCTION

Curious minds of ancient times were baffled by the exquisite design in the night sky. Looking at the spectacular celestial objects, they wondered about the enormity of ‘space’ and inquired about the beginning of ‘everything’. Technological development allowed humankind to be amazed by “the grand design” of stars and galaxies using telescopes. The relentless effort in scientifically understanding the laws of nature with respect to observations resulted in several fundamental theories. The study of the origin and evolution of our universe is known as *Cosmology*.

Tremendous technological advances have enabled the modern-day telescopes to reach immense precision and sensitivity in observations. Current experiments in cosmology use much more sophisticated telescopes to explore the universe at different length scales and at different frequency windows of the electromagnetic spectrum, and now, even with the gravitational wave. The huge influx of data from such observations helps test the viability of the theories in cosmology. Thus, validating and constraining the cosmological theories with data from different experimental surveys (known as “phenomenological analysis”) is crucial to converge towards a complete theory describing the correct dynamics of our universe.

Although the universe looks clustered and clumpy at a glance, several galaxy surveys have observed it as homogeneous and isotropic at large scales (> 100 Mpc) [36, 37]. The dynamics of the universe is derived using the theory of general relativity (GR), where the spacetime is described by a fundamental quantity known as a metric and is related to the constituents in the universe through Einstein's equations. Our homogeneous and isotropic universe is described by the Friedmann-Lemaitre-Robertson-Walker (FLRW) metric [38], which is characterized by two quantities: the curvature of the spatial geometry and the scale factor. The scale factor $a(t)$ describes the expansion of the universe over cosmic time t such that any length scale d becomes $a(t) \times d$ after time t when the scale factor grew from 1 to $a(t)$ over that time. The rate of expansion is described in terms of the Hubble parameter $H(t)$, which, by definition, is the ratio of the velocity with which two galaxies are receding from each other to their distance. Therefore, $H(t)$ can also be written as:

$$H(t) = \frac{\dot{a}}{a}, \tag{1.1}$$

where the dot signifies derivative with respect to t. The curvature κ of the 3-space is observed to be extremely close to zero at present, which means that we live in a spatially flat universe. We will discuss about the FLRW metric extensively in the next chapter.

The standard model that predicts the cosmological evolution starting from a radiation dominated universe filled with relativistic fields is known as the hot big bang model. These relativistic particles eventually cooled down with the expansion of the universe and a matter dominated epoch began. With further expansion, matter density fell below the constant energy density of dark energy, which is the dominating component now. The average equation of state parameter $w = p/\rho$ for radiation, matter and dark energy are different, where p is the pressure and ρ is the energy density. The evolution of the $a(t)$ with t depends on w and therefore, the universe expands differently according to the energy-dominant component at each epoch. However, both radiation and matter domination predict decelerating expansion of the universe, whereas dark energy domination results in accelerated expansion due to its negative pressure.

In the time that takes the light from distant objects to reach us, the expansion of the universe stretches the wavelength of the incoming light. The redshift z is thus defined as:

$$z = \frac{\lambda_{\rm obs} - \lambda_{\rm em}}{\lambda_{\rm em}} = \frac{\lambda_{\rm obs}}{\lambda_{\rm em}} - 1 = \frac{a_{\rm obs}}{a_{\rm em}} - 1, \tag{1.2}$$

where $\lambda_{\rm em}$ and $\lambda_{\rm obs}$ are the emitted and observed wavelengths respectively; $a_{\rm em}$ and $a_{\rm obs}$ are the scale factors at the time of emission and observation respectively. Evidently $(1+z)$ is a measure of the evolution of the scale factor where $z = 0$ signifies the present time. In Fig. 1.1, the energy density of the universe is shown as a function $(1+z)$.

The thermal history of the universe predicts that different constituent particles fell out of the thermal equilibrium when their rate of interaction became smaller than the rate of expansion of the universe. At a certain point during matter domination, when the universe cooled down below 0.1 eV, the photons decoupled from the electrons which went on to recombine with the protons to form the first neutral hydrogen atoms. These photons have traveled almost unscattered from decoupling to reach us now with redshifted energy in the microwave range. The snapshot of the last scattering surface (LSS) of the photons is thus known as the cosmic microwave background (CMB) radiation. The CMB, first discovered by Penzias and Wilson, is an excellent probe to the cosmology of the early universe. Almost three decades ago the Cosmic Background Explorer (COBE) [2] satellite

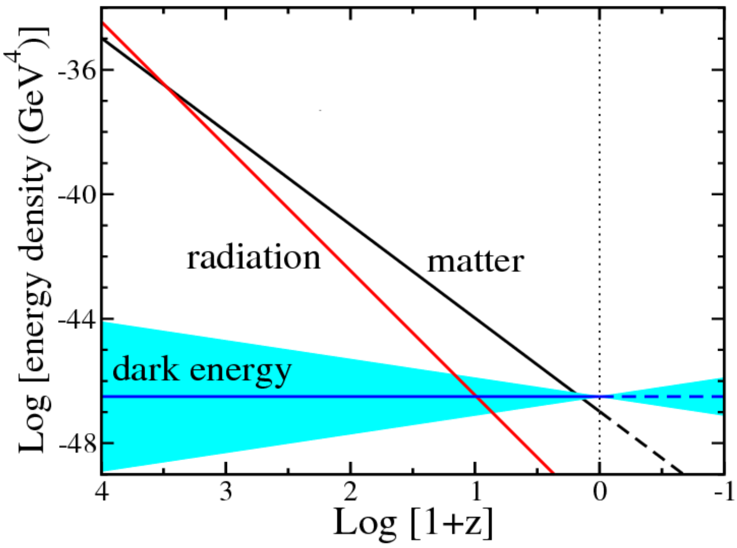

Figure 1.1: Variation of the energy density with the evolution of the universe. Figure borrowed from ref. [24].

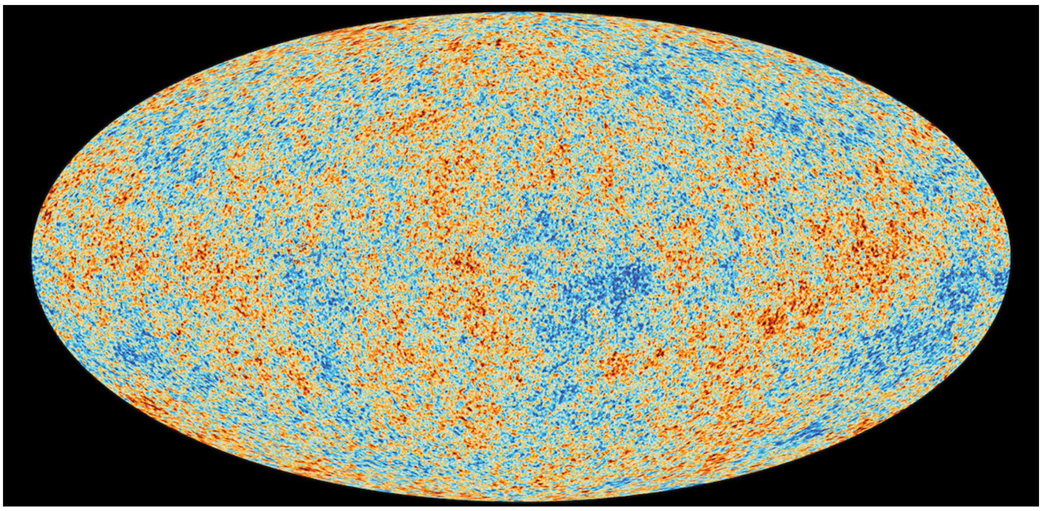

Figure 1.2: The Cosmic Microwave background as observed by PLANCK 2018 mission. The hot spots are coloured red whereas the colored spots are shown in blue. The anisotropy of the hottest and coldest spots are measured to be $|\Delta T| \sim 300\ \mu$K. Picture credit: ESA/PLANCK Collaboration (www.esa.int).

observed that CMB temperature follows an almost exact black-body spectrum with very small anisotropies. The latest results from modern-day telescopes like WMAP [3] and PLANCK [39] (Fig. 1.2) have observed the temperature of CMB to be is almost constant all over the sky at $T_{\rm CMB} = 2.725$ K with very small average fluctuations $\langle \delta T/T \rangle \sim 10^{-5}$. It is essential to have early causal connections between different patches of the CMB sky to achieve such a homogeneous temperature distribution at the last scattering. However, the hot big bang model predicts decelerating radiation and matter dominated expansions before LSS and therefore, cannot explain early causal history among different length scales that entered the horizon at different times. This fault of the standard model to explain the high degree of homogeneity in the CMB sky is known as the *homogeneity problem* or *horizon problem*. On the other hand, the hot big bang cosmology predicts that the initial curvature of the universe has to be tuned to an unnaturally small value to reach the observed flatness of the current universe. This issue is known as the *flatness problem*. The *horizon* and *flatness* problems, both explained in details in the next chapter, are the main two pitfalls of the standard picture which compelled cosmologists to think beyond.

The theory of inflation proposed by Alan Guth in 1981 [40] suggested that an additional early (pre-radiation) epoch of accelerated expansion of the universe can take care of the problems mentioned above through its default mechanism. This accelerated phase of the universe is known as inflation, during which the physical horizon maintained an almost constant size, whereas the physical length scales grew due to expansion and eventually exited the horizon. These scales re-enter the horizon at later epochs of decelerating expansion during radiation and matter domination. Therefore, the addition of the inflationary paradigm to the standard picture ensures that two points, which are separated even by the largest distance in the CMB sky, were causally connected when the corresponding length scale was inside the inflationary horizon before growing out of it.

The virtue of inflation is that it not only solves the horizon and flatness problems of the hot big bang model but also the quantum perturbations during this epoch can serve as initial seeds for structure formation in the universe. Eventually, the temperature fluctuations in the CMB sky can be related to the primordial density fluctuations during inflation. Latest CMB surveys such as PLANCK [39] observes two-point correlations in temperature (T) as well as polarization (E and B type) at CMB. These observed power spectra for temperature and polarization are in excellent agreement with the predictions of the ΛCDM model of the universe.

The ΛCDM model, also known as the concordance model, predicts that the present universe is mainly constituted of dark energy ($\sim 70\%$) and dark matter ($\sim 25\%$), both of whose exact physical nature are still under speculation. The baryons (i.e. visible matter) and photons (i.e. radiation) constitute only about 5% of the energy density of the current universe. In this model, the primordial fluctuations are theorized to be produced during inflation which, after horizon re-entry, evolve up to the last scattering surface through radiation and/or matter dominated epochs. Therefore, the ΛCDM model includes six basic cosmological parameters: two (or more) parameters to describe the inflationary power spectra, 3 parameters accounting for the evolution of the primordial spectra up until CMB and one parameter accounting for the reionization epoch of the universe, which affects the propagation of the CMB photons at very late times.

The phenomenology of the early universe involves comparing the theoretically produced ΛCDM power spectra with the observed spectra in CMB to constrain these parameters of the model. Particularly, constraints on the inflationary model parameters in this method helps uncover the details about the dynamics of inflation. But the most prominent motive of inflationary phenomenology is to resolve between the predictions of different inflationary models with CMB data so that we can converge towards the correct theory of inflation.

Models of inflation are plenty in number and design in current literature, the number of only single field models being ~ 50 as per reference [7]. The simplest yet elegant model of inflation is where a single scalar field slowly rolls down an almost constant potential, which will be discussed in detail in the following chapter. Other than single field models, there are models where two or more fields participate in the inflationary dynamics [41–43]. The CMB observations predict that the universe expanded 50-60 e-folds during inflation which indicates that the energy scale of inflation can be as large as 10^{16} GeV. Therefore, it is always a challenge to embed models of inflation in ultraviolet complete theories at such high energies. Moreover, the predictions of big bang nucleosynthesis (BBN) confirm that the universe was in thermal equilibrium below the energy scale 10 MeV. There is no independent constraint on the post-inflationary reheating (or preheating) epoch when the scalar field driving inflation decays into (beyond) standard model fields (in particle physics) through oscillation. Therefore, observationally there is no way to distinguish between a purely inflationary epoch and any post-inflationary (p)reheating epoch that may contribute to the observed number of e-folds together up until the onset of BBN. This confusion about the beginning and end of inflation and therefore the indetermination about the exact number of inflationary e-folds gives room for exquisite models of inflation.

Especially, models of inflation which are motivated by high energy theories are particularly interesting from the phenomenological perspective, even by allowing such models in non-trivial dynamical settings such as non-minimal gravitational coupling, energetic coupling to radiation etc. The phenomenology of such theoretically inspired models of inflation in light of the CMB data is the main focus of this thesis.

The rest of this thesis is arranged as follows:

♣ Chapter 2 discusses the basics of the standard big bang model, the 'homogeneity' and ‘flatness’ problem encountered in this model and how the theory of inflation solves these problems. This chapter also derives a basic inflationary dynamics, both at the background and perturbation level, through the single field slow roll model of inflation, focusing on the prediction of cosmological observables for such models.

♣ Chapter 3 discusses the cosmological implications of the cosmic microwave background (CMB) radiation in terms of the angular power spectra. The basic construction of the numerical simulations and statistical analysis required to perform precision phenomenology of inflation with this power spectra is also described in detail at the end of this chapter.

♣ Chapter 4 involves the phenomenology of attractor models of inflation emerging from scalar-tensor theories such as $f(R)$ theory and Brans-Dicke gravity. Here, we derive the attractor dynamics for two cases: the α-attractor and the ξ-attractor and discuss the robustness of this mechanism upon the parameters and functional forms in the Lagrangian with their implications on the inflationary observables.

♣ Chapter 5 describes how a warm inflation model can be constrained with observations. In a generic setting where inflaton is energetically coupled to radiation during inflation, the dynamics gets modified and depends on the thermal parameters as well as couplings in the theory. We discuss the constraints from CMB data on a particular model, the ‘warm little inflation’ and show that the $V(\phi) = \lambda\phi^4$ model of inflation that is theoretically motivated, but ruled out in its default cold inflation scenario, can be consistent with the observations in a warm setting.

♣ In Chapter 6, we discuss the effects of post-inflationary moduli domination and reheating for Kähler moduli inflation. We first analyze the model for typical order-of-magnitude values of the model parameters to understand the possible reheating scenarios allowed in such a case. In the next part, we provide a full numerical analysis of the Kähler moduli inflation using various statistical tools and constrain the reheating parameters in this case. Through precision analysis, we find that the Kähler moduli inflation predicts a lower scalar spectral index than observed unless an exotic reheating epoch with matter decaying faster than radiation is considered.

♣ Chapter 7 presents a phenomenological analysis of the theoretically motivated Goldstone inflation scenario in the non-canonical regime. Here, we embed the Goldstone potential in two types of generic non-canonical scenarios: one where the kinetic term in the Lagrangian depends only on the inflaton field and another where the term depends on the derivatives of inflaton. We find that the first case lowers the predicted primordial tensor amplitude only in the super-Planckian symmetry breaking scales, whereas the second case has moderate predictions for the primordial tensor amplitude in the sub-Planckian breaking scales.

♣ In Chapter 8, we present a full summary of the analysis done for several inflationary models throughout this doctoral thesis. We also provide a brief outlook for the contemporary research in inflationary phenomenology.

CHAPTER 2

MOTIVATION FOR INFLATION

This chapter encloses the background dynamics of standard big bang cosmology leading up to the inflationary paradigm. The evolution of the radiation and matter dominated universe are discussed in Sec. 2.1.2, whereas the inadequacy of the standard picture in terms of the horizon and flatness problem are discussed in Sec. 2.1.3 and Sec. 2.1.4. Sec. 2.2 introduces the basic notion of inflation and Sec.2.2.2 discusses the solution of the horizon and flatness problem through inflation. Sec. 2.2.3 and Sec. 2.2.5 are dedicated to the background and perturbation dynamics of inflation respectively. The reader may consult references [5, 10, 44–47] for further detailed analysis of the inflation picture.

2.1 The standard big bang theory

2.1.1 Metric

The $(3+1)$ dimensional FLRW metric $g^{\mu\nu}$ representing our homogeneous and isotropic universe has the following line element:

$$ds^2 = -dt^2 + a^2(t)\left(\frac{dr^2}{1-\kappa r^2} + r^2(d\theta^2 + \sin^2\theta d\phi^2)\right), \tag{2.1}$$

where $a(t)$ is the scale factor and κ is the spatial curvature. κ can take values -1,0 and $+1$ when the spatial geometry is open, flat and closed respectively. It is to be noted here that the equations throughout this text are written in natural units unless otherwise specified[1]. Now, various observations suggest that the present universe is spatially flat. Therefore, in terms of the conformal time $\tau = \int dt/a(t)$, the flat FLRW metric is:

$$ds^2 = a^2(t)(-d\tau^2 + d\mathbf{x}^2), \tag{2.2}$$

where $\mathbf{x} = (r, \theta, \phi)$ is the vector in 3-dimensional space. The components of the universe are described in the simplest case as an ideal fluid such that the corresponding stress-energy tensor is:

$$T^{\mu\nu} = (\rho + p)u^\mu u^\nu - pg^{\mu\nu}, \tag{2.3}$$

where ρ and p are the energy density and pressure of the fluid respectively. u^μ is the 4-velocity of the fluid, which in the rest frame takes the form: $u^\mu = (1, 0, 0, 0)$. Therefore, in

[1]The natural unit here refers to $\hbar = c = 1$. The reduced Planck mass $M_{\text{Pl}} = \frac{1}{\sqrt{8\pi G}}$ is equated to unity unless written explicitly.

the rest frame of the fluid, the stress-energy tensor takes the following simpler form:

$$T^{\mu\nu} = \mathrm{diag}(\rho, -p, -p, -p). \tag{2.4}$$

2.1.2 Background dynamics

The Einstein equations relating spacetime with constituents of the universe are:

$$G_{\mu\nu} = R_{\mu\nu} - g_{\mu\nu}R = 8\pi G T^{\mu\nu}, \tag{2.5}$$

where $R_{\mu\nu}$ is the Ricci tensor, R is the Ricci scalar, $G_{\mu\nu}$ is the Einstein tensor, G is the universal gravitational constant. In a FLRW universe of line element as given in Eq. (2.1) with the stress-energy tensor given in the form of Eq. (2.4), the Einstein equations are:

$$H^2 = \left(\frac{\dot{a}}{a}\right)^2 = \frac{8\pi G}{3}\rho - \frac{\kappa}{a^2}, \tag{2.6}$$

$$\dot{H} + H^2 = \frac{\ddot{a}}{a} = -\frac{4\pi G}{3}(\rho + 3p). \tag{2.7}$$

Eq. (2.6) and Eq. (2.7) are also known as Friedman equations. In addition to the Friedman equations, the conservation of the stress-energy tensor gives the equation of continuity as:

$$\dot{\rho} + 3H(\rho + p) = 0. \tag{2.8}$$

Now, the equation of state for a constituent matter species is defined as $w = p/\rho$. Therefore, Eq. (2.8) yields the dependence of energy density on the scale factor as:

$$\rho \propto a^{-3(1+w)}. \tag{2.9}$$

In case of a flat universe, Eq. (2.6) combined with Eq. (2.9) gives

$$a(t) \propto t^{2/3(1+w)}, \qquad \text{if } w \neq -1, \tag{2.10}$$

$$\propto e^{Ht}, \qquad \text{if } w = 1. \tag{2.11}$$

The evolution of the energy density and scale factor for different epochs are given in Table 2.1 below.

Table 2.1: The energy density $\rho(a)$, scale factor $a(t)$ and Hubble parameter $H(t)$ for different cosmological epochs from FLRW solutions in a flat universe

Epoch	w	$\rho(a)$	$a(t)$	$H(t)$
Radiation dominated (RD)	$1/3$	a^{-4}	$t^{1/2}$	$1/2t$
Matter dominated (MD)	0	a^{-3}	$t^{2/3}$	$2/3t$
Cosmological constant (Λ) dominated (ΛD)	-1	$Const.$	e^{Ht}	$Const.$

In case of an universe with multiple constituents, the total energy density is $\rho = \sum_i \rho_i$ and pressure is $p = \sum_i p_i$, where ρ_i and p_i are respectively the energy density and pressure i-th component. The energy density of the i-th component can also be written in a dimensionless form as

$$\Omega_i = \frac{8\pi G \rho_i}{3H^2}, \tag{2.12}$$

such that the first Friedman equation can be rewritten as

$$\sum_i \Omega_i + \Omega_\kappa = 1, \tag{2.13}$$

where $\Omega_\kappa = -\kappa/a^2H^2$ is the curvature density, which vanishes for an exactly flat spacetime. The quantity $\rho_c = 3H^2/8\pi G$ is known as the critical density. Cosmological observations claim that the total energy density of the universe today is extremely close to the critical density with the Hubble parameter given in its present value $H_0 = 67.66$ km/s/Mpc, which means that we live in a spatially flat universe so that the curvature density now is $\Omega_\kappa^0 \approx 0$.

This standard picture of cosmology starting from a radiation dominated universe after the big bang is also termed as the hot big bang theory. As discussed previously, radiation domination was followed by matter domination when the constituents became non-relativistic with the expansion of the universe. Therefore, the Friedman equation can be written as:

$$\frac{H^2}{H_0^2} = \Omega_{\mathrm{r}}^0 \left(\frac{a_0}{a}\right)^4 + \Omega_{\mathrm{m}}^0 \left(\frac{a_0}{a}\right)^3 + \Omega_\Lambda^0, \tag{2.14}$$

where Ω_{r}^0, Ω_{m}^0 and Ω_Λ^0 represent the dimensionless density parameters today for radiation, matter and cosmological constant Λ and a_0 is the scale factor in the present universe. The superscript 0 stands for the present time and, by convention, $a_0 = 1$. It is to be noted that the cosmological constant Λ can be considered as a particular form of dark energy, for which the energy density is constant over time and the pressure is exactly negative of the energy density.

The standard hot big bang model is excellent in describing the thermal history of the universe. Given seed fluctuations at very early times, the hot big bang model can predict the generation and evolution of the large scale structures in the late-time universe. However, there are certain puzzles related to the initial state from which the hot universe started to expand in a standard model. The two most important and interesting of these puzzles are the *horizon problem* and the *flatness problem*.

2.1.3 Horizon problem

The particle horizon is defined as the maximum distance that a particle can travel throughout the age of the universe. Therefore, the comoving particle horizon is:

$$\tau_H = \int_0^t \frac{dt'}{a(t')} = \int_{a_i}^{a_f} \frac{d \ln a}{aH}, \tag{2.15}$$

where the lower limit signifies initial big bang (scale factor a_i) in the standard cosmological model and t is the age of the universe when the scale factor is a_f. It can be seen from Table 2.1 that for both the cases of radiation and non-relativistic matter dominated epochs, the comoving particle horizon increases with the expansion of the universe ($\tau_H \sim a$ for RD and $\tau_H \sim \sqrt{a}$ for MD). In general, the universe dominated by any perfect fluid satisfying the strong energy condition (SEC) of GR $1 + 3w > 0$ will always have a monotonically increasing comoving horizon $\tau_H \sim a^{(1+3w)/2}$. Therefore, according to the standard model, the comoving length scales that enter the comoving particle horizon at any time could never have causal contact among them at an earlier epoch.

The COBE satellite first measured the CMB sky to be extremely homogeneous in temperature, which was later verified and precisely quantified by WMAP [3] and PLANCK [39]. But the hot big bang model predicts that the scales at last scattering were never causally connected which definitely contradicts the observed high degree of homogeneity. In Fig. 2.1, it is shown that the past light cones of two points separated in the CMB sky do not overlap in the standard big bang scenario starting from $\tau_i = 0$, implying that the causal histories of those two points are disconnected. This caveat of the standard theory is known as the *horizon problem* or the *homogeneity problem*.

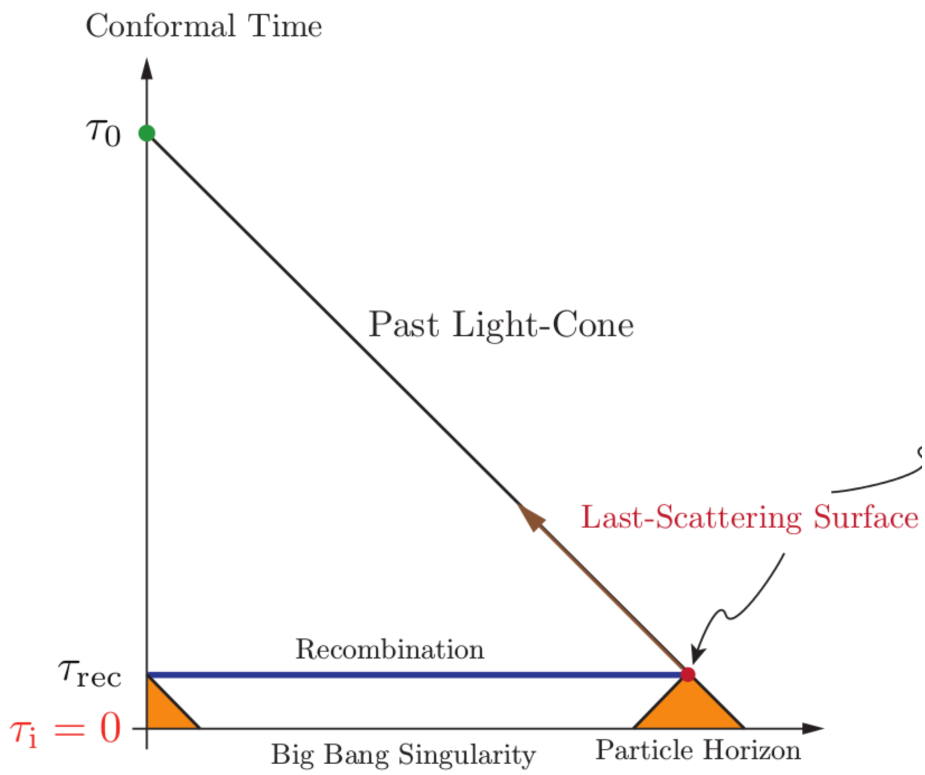

Figure 2.1: Representation of the horizon problem in terms of light cones. The past light cones of two points separated at the last scattering surface do not overlap back in time in the standard big bang picture. Figure borrowed from [5].

2.1.4 Flatness problem

Eq. (2.13) can be rewritten as:

$$1 - \Omega(a) = -\frac{\kappa}{(aH)^2}, \tag{2.16}$$

where $\Omega(a) = \sum_i \Omega_i(a)$ is the total energy density of the universe (dimensionless). In the standard model, the comoving Hubble radius $(aH)^{-1}$ increases with time $\big((aH)^{-1} \sim a^{(1+3w)/2}\big)$. Therefore, $\Omega(a)$ deviates from the unstable fixed point $\Omega = 1$ with the expansion of the universe. The curvature density $|\Omega_\kappa|$ also increases with time.

Several cosmological surveys at different scales and by different probes observe the present universe to be spatially flat. The exact value of present curvature density is measured to be very small $\Omega_\kappa^0 = -0.0106 \pm 0.0065$ by PLANCK 2018[2] [4]. It can be shown that to achieve such a negligible spatial curvature now, the initial conditions have to be tremendously fine-tuned (e.g. $|1 - \Omega(a)| \sim \mathcal{O}(10^{-64})$ at the Planck scale). Such a constricted value of the initial parameters required in the standard case definitely contradicts the generic nature of the theory. This is known as the *flatness problem* (Fig. 2.2).

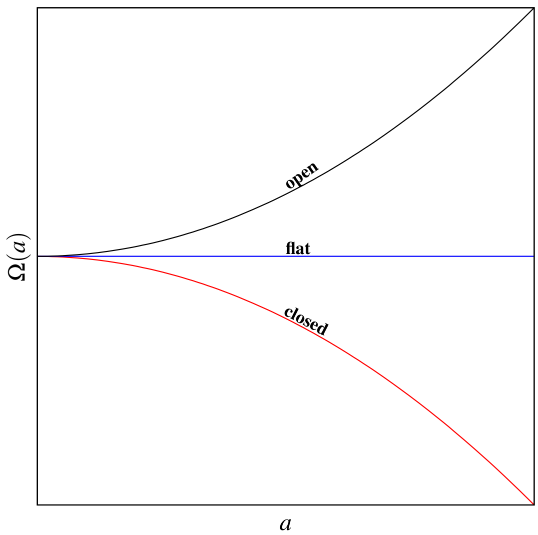

Figure 2.2: Representation of the flatness problem which shows that the tiniest deviation in the initial conditions in the standard hot big bang model would be very different from the flat universe (black curve).

2.2 Inflation

The theory of inflation was proposed [40] as a solution to the above mentioned initial condition problems of standard big bang cosmology. The paradigm of inflation is introduced as an early epoch of expansion, even before radiation domination, where a tiny

[2]The quoted value of Ω_κ^0 is at 68% confidence level for the data combination: PLANCK TT+TE+EE + lowE + lensing.

homogeneous and isotropic patch of the universe expanded quasi-exponentially and the comoving Hubble radius decreased in size (Fig. 2.3). Such an accelerating expansion of

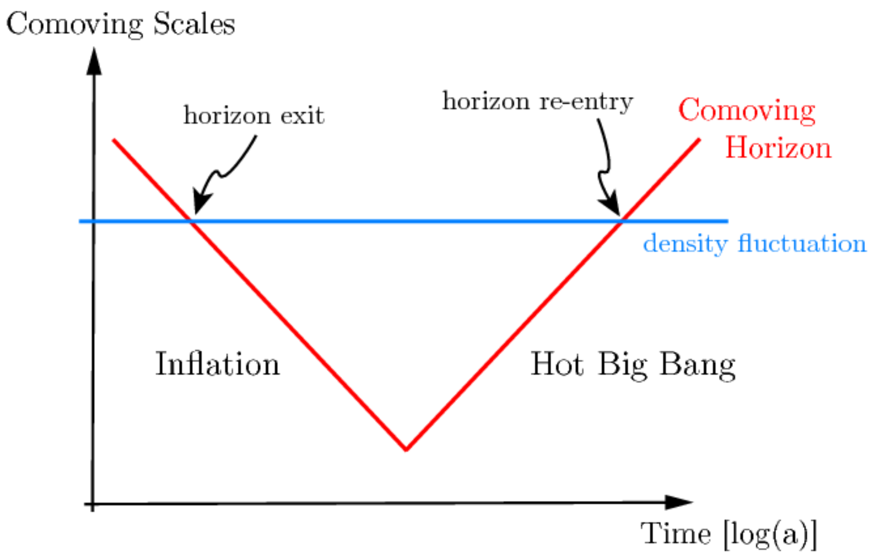

Figure 2.3: The evolution of the comoving horizon during and after inflation with time. Figure courtesy [5]

the universe is characterized by a quasi-de Sitter manifold, where the Hubble parameter remains almost constant. The addition of the inflationary epoch to the standard picture of cosmological evolution not only aids to the shortcomings of the standard theory (see Sec. 2.2.2) but also the quantum fluctuations during inflation (see Sec. 2.2.5) act as initial seed perturbations for the evolution of large scale structures.

2.2.1 Basic dynamics of inflation

The shrinking comoving Hubble radius implies an accelerated expansion phase:

$$\frac{d}{dt}(aH)^{-1} < 0 \Rightarrow \ddot{a} > 0. \tag{2.17}$$

This accelerating epoch can be expressed in terms of a quasi-de Sitter metric where the scale factor grows nearly exponentially $a \sim e^{Ht}$ and the Hubble parameter H is almost constant. In such a scenario, Eq. (2.7) satisfies:

$$\rho + 3p < 0 \Rightarrow p < -\frac{\rho}{3} \Rightarrow 1 + 3w < 0. \tag{2.18}$$

Therefore, the inflationary universe was filled with some matter that does not comply with the SEC. In the simplest scenario, the inflationary universe is described in terms of a single scalar field whose potential energy is much larger than its kinetic energy (see Sec. 2.2.3), which is consistent with the violation of the strong energy condition.

2.2.2 Solution to the puzzles in standard theory

The key to solving the shortcomings of the hot big bang theory is the modified causal history of the universe with an additional early universe inflationary epoch when the comoving Hubble radius $(aH)^{-1}$ decreased with time.

• Due to the shrinking of the comoving Hubble radius, the scales inside the same Hubble patch exit the comoving horizon during inflation. These scales re-entered the comoving horizon at later epochs of decelerating expansion and evolved through the standard dynamics. Therefore, the scales that are observed at the CMB sky are all expected to have early causal connections at the time of inflation before their horizon exit. Even the largest scale that went out of the inflationary horizon at the earliest and enters the comoving horizon now is also expected to have a causal connection to the other length scales at the beginning of inflation (Fig. 2.4). This early causal contact between different length scales efficiently describes the homogeneity in the CMB sky and therefore inflation evidently solves the *horizon/ homogeneity* problem in the standard theory.

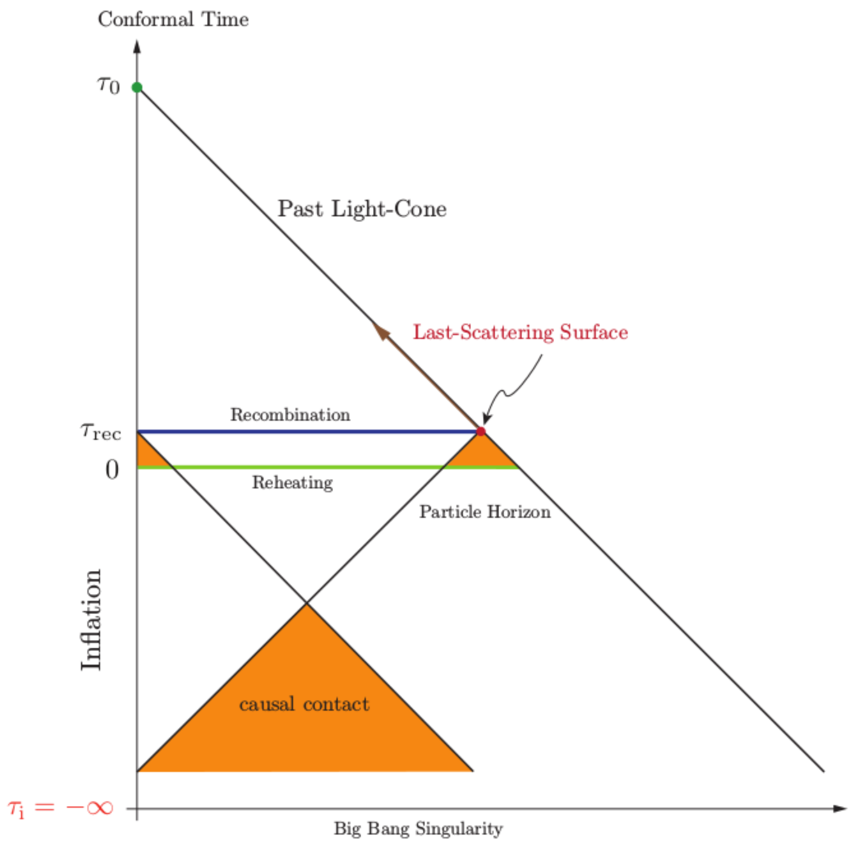

Figure 2.4: Solution of the horizon problem in terms of light cones is shown here. The past light cones of two points separated at the last scattering surface are now causally connected in the past as addition of the inflationary paradigm pushes the conformal time for big bang singularity back to $\tau_i \approx -\infty$. Figure borrowed from [5].

• The curvature density of the universe $|\Omega_\kappa| = \kappa/(aH)^2$ decreases in an inflationary universe. So, even if the universe starts with an arbitrary spatial curvature at the beginning of inflation, spatial flatness is rapidly restored due to the exponential expansion during inflation. So, the introduction of the inflationary epoch helps to include the initial curvature of the universe as a generic initial condition rather than a fine-tuned value, thereby taking care of the *flatness* problem of the standard big bang theory.

2.2.3 Single field slow roll dynamics of inflation

As mentioned earlier, in the simplest scenario, the dynamics of inflation can be expressed in terms of a single scalar field (known as 'inflaton') rolling down an almost constant potential 2.6. The action $\mathcal{S}$ for the inflaton, minimally coupled to gravity, can be written as:

$$\mathcal{S} = \int d^4x\sqrt{-g}\left[\frac{M_{\rm Pl}^2}{2}R - \frac{1}{2}g_{\mu\nu}\partial^\mu\phi\partial^\nu\phi - V(\phi)\right], \tag{2.19}$$

where $V(\phi)$ is the potential energy of the inflaton ϕ, R is the Ricci scalar in the quasi-de Sitter spacetime and $M_{\rm Pl} = 1/\sqrt{8\pi G}$ is the reduced Planck mass. The tiny primordial patch of the universe at the beginning of inflation is considered to be homogeneous and isotropic. Therefore, the background inflaton field ϕ is considered to be homogeneous and evolves only with time: $\phi(t, \mathbf{x}) \equiv \phi(t)$. So, the total energy density and pressure of the inflaton are respectively:

$$\rho(\phi) = \frac{\dot{\phi}^2}{2} + V(\phi), \quad p(\phi) = \frac{\dot{\phi}^2}{2} - V(\phi). \tag{2.20}$$

The Friedman equations during inflation are therefore:

$$H^2 = \frac{1}{3M_{\rm Pl}^2}\left(\frac{\dot{\phi}^2}{2} + V(\phi)\right), \tag{2.21}$$

$$\dot{H} = -\frac{\dot{\phi}^2}{2M_{\rm Pl}^2}. \tag{2.22}$$

The equation of motion for the inflaton field is obtained by minimizing the above action in Eq. (2.19). The resulting Klein-Gordon equation (can also be derived directly from the equation of continuity (2.8)) is:

$$\Box\phi + V_{,\phi} = 0 \;\Rightarrow\; \ddot{\phi} + 3H\dot{\phi} + V_{,\phi} = 0, \tag{2.23}$$

where $\Box\phi = \frac{1}{\sqrt{-g}}\partial_\mu(\sqrt{-g}g^{\mu\nu}\partial_\nu\phi)$ and $V_{,\phi} = \partial V/d\phi$. The term $3H\dot{\phi}$ is in Eq. (2.23) is proportional to the velocity of the inflaton and is therefore known as the Hubble friction term.

The equation of state parameter for inflaton is:

$$w = \frac{p(\phi)}{\rho(\phi)} = \frac{\frac{\dot{\phi}^2}{2} - V(\phi)}{\frac{\dot{\phi}^2}{2} + V(\phi)}. \tag{2.24}$$

Now, in a perfect de Sitter universe, the strong energy condition is violated as $w = -1$, such that the energy density is exactly negative of the pressure $\rho = -p$. So, for the quasi-de Sitter inflationary universe, the violation of the strong energy condition requires $w \approx -1$. This leads to the first assumption for the background inflationary dynamics in terms of the slow roll (SR) condition. The SR assumption enables the inflaton to roll very slowly along the constant part of the potential so that the potential energy dominates of over the kinetic energy at the time of inflation (Fig. 2.5). So, from Eq. (2.24),

$$\frac{\dot{\phi}^2}{2} \ll V(\phi). \tag{2.25}$$

Now, the Friedmann equation for acceleration (Eq. (2.7)) can be written as:

$$\frac{\ddot{a}}{a} = H^2(1-\epsilon), \text{ where } \epsilon \equiv -\frac{\dot{H}}{H^2} = \frac{\dot{\phi}^2/2M_{\rm Pl}^2}{H^2}. \tag{2.26}$$

Therefore, SR inflation requires $\epsilon \ll 1$ and ϵ is conventionally termed as the first SR

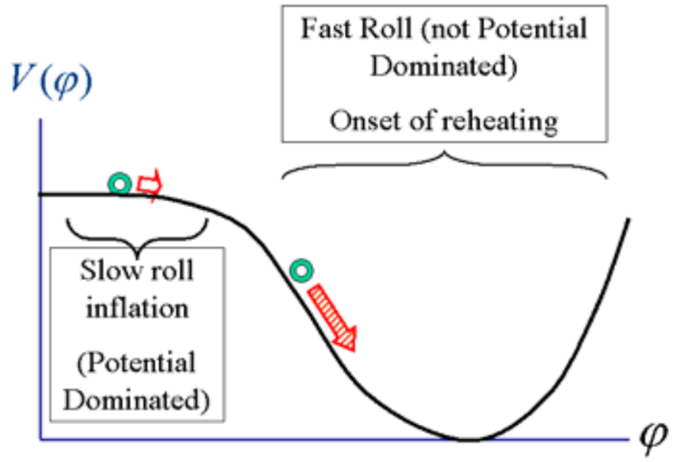

Figure 2.5: Slow Roll of the scalar field during inflation is depicted for a prototype potential. The onset of fast roll drives inflation towards the end. Figure courtesy: [25]

parameter. Moreover, to sustain such a slow rolling of the inflaton, the acceleration of the field also needs to be small which leads to the second SR condition:

$$\eta = -\frac{\ddot{\phi}}{H\dot{\phi}} \ll 1. \tag{2.27}$$

η is known as the second SR parameter. In general, the n-th SR parameters can be defined as:

$$\epsilon_n = -\frac{d\ln\epsilon_{n-1}}{dN}, \text{ and } \epsilon_1 = \epsilon = -\frac{d\ln H}{dN}, \tag{2.28}$$

where $N = \ln a = \int H dt$ is known as the number of e-folds of the inflationary expansion. ϵ and η are known as Hubble slow roll (HSR) parameters as opposed to the potential slow roll parameters ϵ_V and η_V, which represent the SR conditions in terms of the potential function. The potential SR parameters are given as:

$$\epsilon_V = \frac{M_{\rm Pl}^2}{2}\left(\frac{V_{,\phi}}{V}\right)^2, \tag{2.29}$$

$$\eta_V = M_{\rm Pl}^2 \frac{V_{,\phi\phi}}{V}. \tag{2.30}$$

ϵ_V and η_V are very useful while analysing the background dynamics for a particular model of inflation. The two kinds of SR parameters are related as:

$$\epsilon \approx \epsilon_V \;\text{ and }\; \eta \approx \eta_V - \epsilon_V. \tag{2.31}$$

Under the SR assumption $\epsilon_V, |\eta_V| \ll 1$, the EoM of inflaton and the first Friedman equation can be written as:

$$\dot{\phi} \approx -\frac{V_{,\phi}}{3H}, \tag{2.32}$$

$$H^2 \approx \frac{V}{3M_{\rm Pl}^2} \approx constant \tag{2.33}$$

2.2.4 End of Inflation

Eventually, the inflaton rolls down the potential and gains larger velocity when the slow roll conditions are violated:

$$\epsilon_V = 1, \;\text{ and }\; \eta_V = 1. \tag{2.34}$$

The number of e-folds of inflation can also be calculated as a function of ϵ_V.

$$N = \int_{t_i}^{t_e} H dt = \int_{\phi_i}^{\phi_e} \frac{H}{\dot{\phi}} d\phi = \frac{1}{M_{\rm Pl}} \int_{\phi_i}^{\phi_e} \frac{d\phi}{\sqrt{2\epsilon_V}}, \tag{2.35}$$

where t_e and ϕ_e correspond to end of inflation and t_i and ϕ_i correspond to the time and field value at which the largest observable scale at CMB exits the horizon. In general, given a model of inflation with a potential $V(\phi)$, Eq. (2.34) is used to evaluate ϕ_e and then Eq. (2.35) is used to find the initial field value ϕ_i for a given number of e-folds.

After rolling down the potential, the inflaton oscillates around the minimum of the potential. During this oscillation, the inflaton energy density is transformed into the standard fields found in the standard model theory or beyond the standard model theory of particle physics. This process of post-inflationary oscillation and decay of inflaton into other fields is known as reheating since the cold expanded universe at the end of inflation is populated by relativistic fields. The current CMB experiments have measured the number of observable e-folds of inflation to lie between 50 - 60. This observable number of e-folds depends on the inflationary dynamics as well as the reheating history of the universe. We will derive the number of e-folds in terms of inflationary observables and reheating parameters towards the end of this chapter.

2.2.5 Quantum fluctuations during inflation

In the classical analysis of the background dynamics, the inflaton is assumed to be spatially homogeneous. But a complete analysis of the inflationary picture contains quantum fluctuations in the field as well as spacetime (Fig. 2.6). Therefore, the inflaton and metric can have the following expansion in perturbations up to the linear order:

$$\phi(t, \mathbf{x}) = \phi(t) + \delta\phi(t, \mathbf{x}) \;\text{ and }\; g_{\mu\nu} = g^0_{\mu\nu} + \delta g_{\mu\nu}, \tag{2.36}$$

where $g^0_{\mu\nu}$ corresponds to the background FLRW metric given in Eq. (2.1).

Metric perturbations

The metric perturbation can be decomposed into scalar, vector and tensor components so that the full perturbed line element can be written as:

$$ds^2 = g_{\mu\nu}dx^\mu dx^\nu = -(1+2\Phi)dt^2 + 2aB_i dx^i dt + a^2[(1-2\Psi)\delta_{ij} + E_{ij}]dx^i dx^j, \tag{2.37}$$

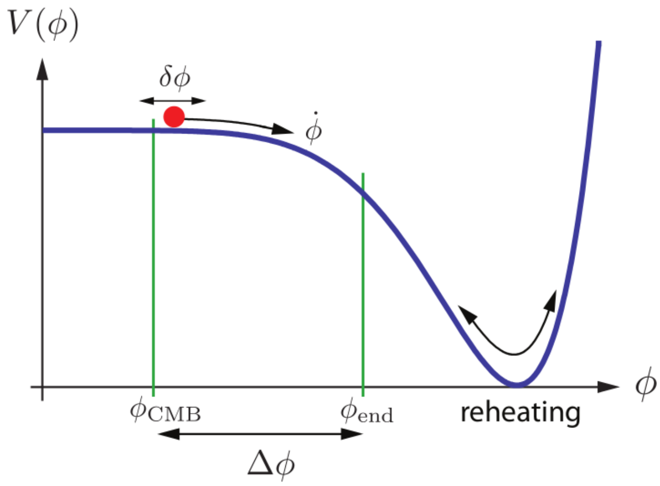

Figure 2.6: Background slow roll evolution of the inflaton field ϕ with quantum fluctuations $\delta\phi$. Figure borrowed from [26].

where

$$B_i \equiv \partial_i B - S_i \text{ where } \partial^i S_i = 0 \text{ and} \tag{2.38}$$

$$E_{ij} \equiv 2\partial_{ij} E + 2\partial_{(i} F_{j)} + h_{ij} \text{ where } \partial^i F_i = 0,\ h^i_i = \partial^i h_{ij} = 0. \tag{2.39}$$

The scalar, vector and tensor (SVT) decomposition in real space is suitable since each of these components obey distinct transformation properties on the spatial hypersurfaces. The vector components decay with the expansion of the universe and therefore, we focus only on the scalar and tensor perturbations. In general, relation between the quantities in the perturbed and the unperturbed spacetime depend on what transformation is chosen relating these two spacetimes (gauge choice). For example, under the following gauge choice:

$$t \to t + \alpha \tag{2.40}$$

$$x^i \to x^i + \delta^{ij}\beta_{,j}, \tag{2.41}$$

the scalar perturbations transform as:

$$\Phi \to \Phi - \dot{a} \tag{2.42}$$

$$B \to B + a^{-1}\alpha - a\dot{\beta} \tag{2.43}$$

$$E \to E - \beta \tag{2.44}$$

$$\Psi \to \Psi + H\alpha, \tag{2.45}$$

whereas, the tensor perturbation h_{ij} is itself gauge-invariant. Therefore, we need to look for gauge-invariant quantities as physical observables which do not depend on the choice of coordinate transformations.

Field perturbations

The perturbed stress-energy tensor in Eq. (2.3) is:

$$T^0_0 = -(\bar{\rho} + \delta\rho) \tag{2.46}$$

$$T^0_i = (\bar{\rho} + \bar{p})av_i \tag{2.47}$$

$$T^i_0 = -(\bar{\rho} + \bar{p})(v^i - B^i)/a \tag{2.48}$$

$$T^i_j = \delta^i_j(\bar{p} + \delta p) + \Sigma^i_j, \tag{2.49}$$

where the momentum density is $(\delta q)_{,i} \equiv (\bar{\rho} + \bar{p})v_i$. With the gauge choice given in Eq. (2.41), the above perturbations transform as:

$$\delta\rho \to \delta\rho - \dot{\bar{\rho}}\alpha \tag{2.50}$$

$$\delta p \to \delta p - \dot{\bar{p}}\alpha \tag{2.51}$$

$$\delta q \to \delta q + (\bar{\rho} + \bar{p})\alpha. \tag{2.52}$$

Gauge-invariant variables

• The curvature density on uniform density hypersurfaces is a gauge-invariant quantity which is defined as:

$$-\zeta \equiv \Psi + \frac{H}{\dot{\bar{\rho}}}\delta\rho. \tag{2.53}$$

For slow roll inflation, this can be written as:

$$-\zeta \approx \Psi + \frac{H}{\dot{\bar{\phi}}}\delta\phi. \tag{2.54}$$

The matter perturbations are adiabatic when they satisfy:

$$\delta p_{en} \equiv \delta p - \frac{\dot{\bar{p}}}{\dot{\bar{\rho}}}\delta\rho = 0. \tag{2.55}$$

ζ remains constant on superhorizon scales for adiabatic perturbations.

• Another gauge-invariant quantity is the comoving curvature perturbation $\mathcal{R}$ given as:

$$\mathcal{R} \equiv \Psi - \frac{H}{\bar{\rho} + \bar{p}}\delta q, \tag{2.56}$$

which, for slow roll inflationary scenario takes the following form:

$$\mathcal{R} = \Psi + \frac{H}{\dot{\bar{\phi}}}\delta\phi. \tag{2.57}$$

Eq. (2.54) and Eq. (2.57) show that ζ and $\mathcal{R}$ are equal (modulo a negative sign) during slow roll inflation. Now, the constraint relation between ζ and $\mathcal{R}$ derived from the Einstein equation is:

$$-\zeta = \mathcal{R} + \frac{k^2}{(aH)^2}\frac{2\bar{\rho}}{3(\bar{\rho} + \bar{p})}\Psi_B, \tag{2.58}$$

where $\Psi_B = \Psi + a^2 H(\dot{E} - B/a)$ is the Bardeen potential. Therefore, on superhorizon scales $k \ll aH$, $-\zeta$ and $\mathcal{R}$ are equal. On the other hand, the evolution of the comoving curvature perturbation follows:

$$\dot{\mathcal{R}} = -\frac{H}{\bar{\rho} + \bar{p}} \delta p_{en} + \frac{k^2}{(aH)^2} \bigg(\dots \bigg). \tag{2.59}$$

Therefore, $\mathcal{R}$ is conserved on superhorizon scales $k \ll aH$ for adiabatic matter perturbations. Therefore, the dynamics of quantum perturbations during inflation involves deriving the evolution equations for the scalar perturbation in terms of $\mathcal{R}$ and the tensor perturbations in terms of h_{ij}.

2.2.6 Power Spectra of inflation

We choose the comoving gauge where

$$\delta\phi = 0, \text{ and} \tag{2.60}$$

$$g_{ij} = a^2[(1 - 2\mathcal{R})\delta_{ij} + h_{ij}] \text{ with } \partial^i h_{ij} = h^i_i = 0. \tag{2.61}$$

In such a gauge, the second order action for scalar perturbations during inflation can be written in terms of the Mukhanov variable $v = z\mathcal{R}$ as:

$$S_{(2)} = \frac{1}{2} \int d\tau dx^3 \bigg[(v')^2 - (\delta_i v)^2 + \frac{z''}{z} v^2 \bigg], \tag{2.62}$$

where τ is the conformal time and primes denote derivatives with respect to τ; $z^2 = a^2 \frac{\dot{\phi}^2}{H^2} = 2a^2\epsilon$. The variable v can be expanded in the Fourier space as:

$$v(\tau, \mathbf{x}) = \int \frac{d^3k}{(2\pi)^3} v_{\mathbf{k}}(\tau) e^{i\mathbf{k}\mathbf{x}}. \tag{2.63}$$

The equation of motion for the Mukhanov variable can be obtained varying the above action:

$$v_k'' + \left(k^2 - \frac{z''}{z}\right)v_k = 0. \tag{2.64}$$

This second order differential equation can be solved exactly only when the background dynamics is completely defined so that the evolution of z is known. The first boundary condition comes from the normalization of the mode functions v_k through the quantization process. The dependence on the background dynamics is prominent again with the choice of the vacuum state for the fluctuations which is the second boundary condition. If the background dynamics is chosen to be exactly de Sitter and the vacuum is chosen to be Minkowski vacuum:

$$\lim_{\tau \to -\inf} v_k = \frac{e^{-ik\tau}}{\sqrt{2k}}, \tag{2.65}$$

then the two-point correlation function for v_k can be calculated. In this case, the two-point correlation function for the comoving curvature perturbation is:

$$\langle \mathcal{R}_{\mathbf{k}} \mathcal{R}_{\mathbf{k}'} \rangle = (2\pi)^3 \delta(\mathbf{k} + \mathbf{k}') \frac{H^2}{2k^3} \frac{H^2}{\dot{\phi}^2}. \tag{2.66}$$

Now, this correlation function can be related to the power spectrum as:

$$\langle \mathcal{R}_{\mathbf{k}} \mathcal{R}_{\mathbf{k}'} \rangle = (2\pi)^3 \delta(\mathbf{k} + \mathbf{k}') P_{\mathcal{R}}(k), \;\; \Delta^2_{\mathcal{R}}(k) \equiv \frac{k^3}{2\pi^2} P_{\mathcal{R}}(k). \tag{2.67}$$

Therefore, the dimensionless scalar power spectrum for slow roll inflation is:

$$\Delta^2_{\mathcal{R}} = \frac{H_*^2}{(2\pi)^2} \frac{H_*^2}{\dot{\phi}_*^2}. \tag{2.68}$$

The $*$ in the subscript corresponds to the horizon exit where all the relevant perturbation quantities are calculated, owing to their conservation at superhorizon scales. In a similar manner, the tensor fluctuations can be calculated using the tensor part of the second order action and the tensor power spectrum turns out to be:

$$\Delta_t^2 = \frac{2}{\pi^2}\frac{H_*^2}{M_{\rm Pl}^2}. \tag{2.69}$$

The scale dependence of the power spectra are defined in terms of *spectral indices*:

$$n_s - 1 = \frac{d\ln\Delta_{\mathcal{R}}^2(k)}{d\ln k} \tag{2.70}$$
$$n_t = \frac{d\ln\Delta_t^2(k)}{d\ln k}. \tag{2.71}$$

In a similar manner, the running (α_s) and running of running (β_s) of n_s can also be defined as:

$$\alpha_s = \frac{dn_s}{d\ln k} \text{ and } \beta_s = \frac{d\alpha_s}{d\ln k}, \tag{2.72}$$

so that the scalar power spectrum can be approximated in the following form:

$$\Delta_{\mathcal{R}}^2 = A_s(k_*)\left(\frac{k}{k_*}\right)^{n_s-1+\frac{\alpha_s}{2}(k_*)\ln(k/k*)+\frac{\beta_s}{6}(\ln(k/k_*))^2}, \tag{2.73}$$

where k_* is an arbitrary pivot scale chosen to fit the power spectrum, which varies from one CMB observation survey to another[3]. It can be shown that to the first order in Hubble slow roll parameters,

$$n_s - 1 = 2\eta_* - 4\epsilon_* \text{ and } n_t = -2\epsilon_*. \tag{2.74}$$

[3]PLANCK 2018 usually calculates pivot quantities at $k_* = 0.05\text{Mpc}^{-1}$ and $k_* = 0.002\text{Mpc}^{-1}$.

The ratio of tensor and scalar power spectra is:

$$r = \frac{\Delta_t^2}{\Delta_{\mathcal{R}}^2}, \tag{2.75}$$

which is known as the *tensor-to-scalar ratio*. r is a direct measure of the energy scale of inflation since:

$$V^{1/4} \sim \left(\frac{r}{0.01}\right) \times 10^{16}\mathrm{GeV}. \tag{2.76}$$

Slow roll results

Under the slow roll approximation, the scalar and tensor power spectra can be written in terms of the inflaton potential $V(\phi)$ as:

$$\Delta_{\mathcal{R}}^2(k) \approx \frac{1}{24\pi^2}\frac{V}{M_{\rm Pl}^2}\frac{1}{\epsilon_V}\bigg|_{k=aH} \text{ and } \Delta_t^2(k) \approx \frac{2}{3\pi^2}\frac{V}{M_{\rm Pl}^3}\bigg|_{k=aH}. \tag{2.77}$$

Furthermore, using Eq. (2.31),

$$n_s - 1 = 2\eta_V^* - 6\epsilon_V^* \tag{2.78}$$

$$n_t = -2\epsilon_V^*. \tag{2.79}$$

The tensor-to-scalar ratio is:

$$r = 16\epsilon_V^*, \tag{2.80}$$

and therefore, slow roll models of inflation satisfy the consistency relation:

$$r = -8n_t. \tag{2.81}$$

The Lyth bound

The excursion of the inflaton field during inflation can also be written in terms of the tensor-to-scalar ratio as:

$$\frac{\Delta\phi}{M_{\rm Pl}} = \mathcal{O}(1) \times \left(\frac{r}{0.01}\right)^{1/2}, \tag{2.82}$$

which is known as the Lyth bound.

2.2.7 Number of e-folds of inflation

The number of e-folds before the end of inflation when a certain mode of wavenumber k leaves the horizon is:

$$\begin{aligned} N(k) &= \ln\left(\frac{a_e}{a_k}\right) && (2.83)\\ &= \ln\left(\frac{a_e H_e}{a_{\rm reh} H_{\rm reh}}\right) - \ln\left(\frac{k}{k_*}\right) + \ln\left(\frac{H_k}{H_e}\right) + \ln\left(\frac{a_{\rm reh} H_{\rm reh}}{a_0 H_0}\right) - \ln\left(\frac{k_*}{a_0 H_0}\right), && (2.84) \end{aligned}$$

where, a_k, a_e, $a_{\rm reh}$ and a_0 correspond to the scale factors respectively at the time when the mode k leaves the horizon during inflation, at the end of inflation, at the end of reheating and today. $H_k = k/a_k$, H_e, $H_{\rm reh}$ and H_0 are the Hubble parameters $N(k)$ e-folds before the end of inflation, at the end of inflation, at reheating and at present day respectively (Fig. 2.7). Eq. (2.84) evidently shows that $N(k)$ depends on the full evolution history of the horizon $(aH)^{-1}$ from the end of inflation until today. Now, the knowledge about big bang nucleosynthesis (BBN) imply that the universe was thermalised below $\rm MeV$ temperatures. The cosmological evolution from BBN to today is well understood. But, the cosmic history before BBN is vague since no observation can extract the exact energy density of the universe at the end of reheating when the universe is completely thermalised and radiation starts to dominate. However, one can put a lower bound to the reheating temperature

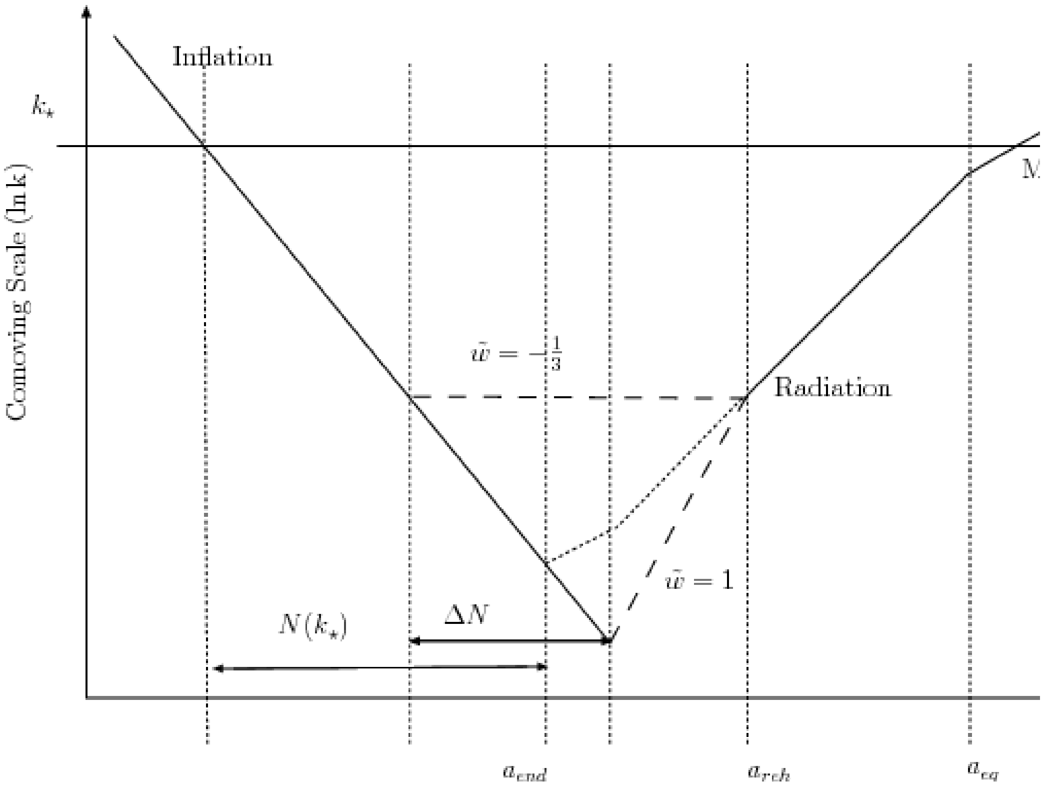

Figure 2.7: The evolution of the Hubble horizon for the inflationary universe is shown, where the x-axis describes the cosmological scale factor $a(t)$ on a logarithmic scale. The parameter $\tilde{w}$ describes the growth during the reheating epoch. For smaller $\tilde{w}$, the value of N at which the pivot leaves the horizon is decreased. Figure courtesy: [26].

from BBN. Therefore, while counting the inflationary number of e-folds $N(k)$, there is an inherent dependence on the reheating number of e-folds $N_{\rm reh}$. Due to our lack of knowledge about the reheating, the average equation of state of this epoch is parameterised as $\tilde{w}$, such that

$$\tilde{w} = \frac{1}{\Delta(\ln a)} \int w(a) d(\ln a), \tag{2.85}$$

where the integration runs from the end of inflation until the beginning of radiation domination. Therefore,

$$\ln\left(\frac{a_e H_e}{a_{\rm reh} H_{\rm reh}}\right) = -\frac{1+3\tilde{w}}{6(1+\tilde{w})}\ln\left(\frac{\rho_{\rm reh}}{\rho_e}\right) \tag{2.86}$$

$$\text{and } N_{\rm reh} = \frac{1}{3(1+\tilde{w})}\ln\left(\frac{\rho_e}{\rho_{\rm reh}}\right), \tag{2.87}$$

where ρ_e and $\rho_{\rm reh}$ are the energy densities at the end of inflation and reheating respectively.

By the end of inflation, accelerated expansion stops so that $\ddot{a} = \rho + 3p = 0$, which implies $\rho_e = 3V_e/2$, where V_e is the inflation potential at the end of inflation. Moreover, after inflation, the comoving particle horizon starts to grow so that $\tilde{w} \geq -1/3$. On the other hand, if the universe thermalized instantaneously at the end of inflation then the post-inflationary expansion starts from a radiation epoch and $\tilde{w} = 1/3$. Therefore, $\tilde{w}$ is considered to lie in the limit $-1/3 < \tilde{w} < 1/3$ in general. However, in some non-trivial post-inflationary history the reheating epoch can have an exotic equation of state so that the most generic bound is $-1/3 < \tilde{w} < 1$, where the upper bound is imposed from the SEC in GR.

Therefore, using Eq. (2.86) and with some algebraic jugglery, Eq. (2.84) can now be written as:

$$N(k) = 56.12 - \ln\left(\frac{k}{k_*}\right) + \frac{1}{3(1+\tilde{w})}\ln\left(\frac{2}{3}\right) + \ln\left(\frac{V_k^{1/4}}{V_e^{1/4}}\right) \tag{2.88}$$

$$+ \frac{1-3\tilde{w}}{3(1+\tilde{w})}\ln\left(\frac{\rho_{\rm reh}^{1/4}}{V_e^{1/4}}\right) + \ln\left(\frac{V_k^{1/4}}{10^{16}\mathrm{GeV}}\right), \tag{2.89}$$

which is famously known as the matching equation. Now, the Hubble parameter at a_k can also be written in terms of the power spectrum $H_k = \pi M_{\rm Pl}(r(k)\Delta_{\mathcal{R}(k)})^{1/2}/\sqrt{2}$. On the other hand the energy density at reheating can be written as:

$$\rho_{\rm reh} = \frac{\pi^2}{30} g_{\rm reh} T_{\rm reh}^4, \tag{2.90}$$

$$\text{where } T_{\rm reh} = \left(\frac{43}{11 g_{s,\rm reh}}\right)^{1/3} \frac{a_0}{a_{\rm eq}} \frac{a_{\rm eq}}{a_{\rm reh}} \tag{2.91}$$

$$= \left(\frac{43}{11 g_{s,\rm reh}}\right)^{1/3} \left(\frac{\rho_0}{\rho_{\rm eq}}\right)^{1/3} \left(\frac{\rho_{\rm eq}}{\rho_{\rm reh}}\right)^{1/4}. \tag{2.92}$$

Here, $T_{\rm reh}$ is the reheating temperature, $g_{\rm reh}$ and $g_{s,\rm reh}$ are the number of degrees of freedom and entropy number of degrees of freedom respectively during reheating. The subscript 0 denotes present day whereas the subscript $\rm eq$ denotes the matter-radiation equality epoch. Thus,

$$N_{\rm reh} = \frac{1}{4} \ln \rho_e + \frac{1}{4} \ln \left(\frac{30}{\pi^2 g_{\rm reh}}\right) + \frac{1}{3} \left(\frac{11 g_{s,\rm reh}}{43}\right) - \ln T_0 - \frac{1}{3} \ln \left(\frac{\rho_0}{\rho_{\rm eq}}\right) - \frac{1}{4} \ln \left(\frac{\rho_{\rm eq}}{\rho_{\rm reh}}\right). \tag{2.93}$$

Now, at pivot scale $k_* = 0.05 \mathrm{Mpc}^{-1}$, assuming $g_{\rm reh} = g_{s,\rm reh}$ and replacing the current observed values $T_0 = 2.725$ K and $\ln(10^{10} \times \Delta^2_{\mathcal{R}}) = 3.044$[4], we arrive at the following:

$$N_{\rm pivot} + \frac{1}{4}(1 - 3\tilde{w}) N_{\rm reh} \approx 55.43 + \frac{1}{4} \ln r_* + \frac{1}{4} \ln \left(\frac{\rho_k}{\rho_e}\right), \tag{2.94}$$

where r_* is the tensor-to-scalar ratio at the pivot scale. Once again, it is important to note that the pivot number of e-folds depends on the reheating history of the universe. CMB observations predict the pivot number of e-folds $50 < N_{\rm pivot} < 60$ which comes from the uncertainty in the prediction of the scalar spectral index n_s. These uncertainties in $N_{\rm pivot}$ accounts for the unknown dynamics of the reheating epoch in Eq. (2.94), known as the

[4]The quoted values are at 68% confidence level for the PLANCK 2018 data combination: TT+TE+EE + lowE + lensing.

consistency relation.

Eq. (2.89) and Eq. (2.94) are profusely used in the phenomenological studies of inflation, especially to understand post-inflationary history. Several non-trivial models of inflation and early universe predict non-standard evolution after inflation, but the low energy constraint from BBN has to be satisfied for all of them.

CHAPTER 3

PHENOMENOLOGY OF INFLATION

In the last chapter, we have derived the groundwork of inflationary dynamics, both in the background and perturbation regime. In this chapter, we will relate theoretical quantities with the observables in CMB. We will discuss the power spectra observed by CMB and how it relates to the cosmological parameters. Later in this chapter, we will mention the statistical and numerical methodology to constrain inflationary theories with CMB observations.

3.1 The Cosmic Microwave Background

In the early universe ($z > 1100$), photons were tightly coupled to the electrons by Thomson scattering process and electrons were coupled to the baryons via Coulomb interactions. This hot photon-baryon plasma was embedded upon the density fluctuations, whose primordial seeds were created by inflation. The inflationary fluctuations that grew out of the horizon during inflation, re-entered the horizon at post-inflationary times to supply initial fluctuations for structure formation. These fluctuations created potential wells and hills in regions of high and low energy density respectively. While gravity tries to compress the photon-baryon fluid in such a potential well, the radiation pressure from the fluid tries to resist the compression. Under such gravitational instabilities, the plasma executes acoustic oscillations generating the cosmological sound waves.

When the universe is cooled down to $\sim$ 3000 K, (age $378,000$ yrs) the photons are released from the plasma as the electrons combine with the protons (recombination) to produce the first neutral Hydrogen atoms. These photons travel freely almost unscattered to us and serve as a snapshot of the epoch of recombination. Due to expansion in the universe, these photons from recombination reach us now with redshifted energy in the microwave range and therefore, the snapshot of the last scattering surface of the photons is known as the Cosmic Microwave Background (CMB). At recombination, the acoustic oscillations stop due to photon decoupling and hence patterns of the cosmic sound waves is imprinted on the CMB temperature profile.

The distance traveled by the photon-baryon plasma until recombination is known as the sound horizon. Since inflation generates potential fluctuations on all scales, the general method of CMB analysis involves decomposing the fluctuations in Fourier space into plane wave modes of various wavelengths. The angular power spectrum is computed by taking two-point correlation function of the fluctuations. Since the CMB photons arrive at us from all directions, the spatial inhomogeneities at the last scattering surface are visualized as angular anisotropies in the CMB sky.

3.1.1 CMB angular power spectra

The harmonic expansion of the temperature fluctuations ΔT relative to the average temperature $T_0 = 2.725$ K in the CMB sky can be written as:

$$\Theta(\hat{n}) \equiv \frac{\Delta T(\hat{n})}{T_0} = \sum_{\ell,m} a_{\ell m} Y_{\ell m}(\hat{n}), \tag{3.1}$$

where $\hat{n}$ is a particular direction in the sky, $Y_{\ell m}(\hat{n})$ are the standard spherical harmonics, and $a_{\ell m} = \int d\Omega Y^*_{\ell m}(\hat{n})\Theta(\hat{n})$. The monopole, dipole and quadrupole moments correspond to $\ell = 0, 1, 2$ respectively and for a particular value of ℓ, the magnetic quantum number m can take the values $m = -\ell, ..., +\ell$. The rotationally invariant temperature power spectrum is given as:

$$C_\ell^{TT} = \frac{1}{2\ell+1}\sum_m \langle a^*_{\ell m} a_{\ell m}\rangle \text{ so that } \langle a^*_{\ell m} a_{\ell' m'}\rangle = C_\ell^{TT}\delta_{\ell\ell'}\delta_{mm'}. \tag{3.2}$$

On the other hand, the linear evolution relating the scalar fluctuations $\mathcal{R}_{\mathbf{k}}$ (discussed in the previous chapter) with the temperature fluctuations ΔT in Eq. (3.1) is:

$$a_{\ell m} = 4\pi(-i)^\ell \int \frac{d^3k}{(2\pi)^3}\Delta_{T\ell}(k)\mathcal{R}_{\mathbf{k}} Y_{\ell m}(\hat{\mathbf{k}}). \tag{3.3}$$

Here, $\Delta_{T\ell}(k)$ is the transfer function in the k-space, responsible for the evolution of the scalar perturbations $\mathcal{R}_{\mathbf{k}}$ from horizon re-entry up to recombination. Therefore, using the identity $\sum_{m=-\ell}^{+\ell} Y_{\ell m}(\hat{\mathbf{k}})Y_{\ell m}(\hat{\mathbf{k}}') = \frac{2\ell+1}{4\pi}P_\ell(\hat{\mathbf{k}}, \hat{\mathbf{k}}')$, the angular power spectrum can then be written as:

$$C_\ell^{TT} = \frac{2}{\pi}\int k^2 dk P_{\mathcal{R}}(k)\Delta_{T\ell}(k)\Delta_{T\ell}(k). \tag{3.4}$$

The angular power spectrum is the most important probe in the statistical analysis of CMB since it contains information about the primordial universe (through $P_{\mathcal{R}}(k)$) as well as of the late time universe (through transfer functions). C_ℓ^{TT} is a compact and effective representation of the CMB temperature fluctuation map (like Fig. 1.2). The angular power spectrum can be determined for the E and B polarizations in CMB and also for the cross correlations of T, E and B in a similar way. The general form of angular power spectrum for any two quantities X and Y is:

$$C_\ell^{XY} = \frac{2}{\pi}\int k^2 dk P(k)\Delta_{X\ell}(k)\Delta_{Y\ell}(k). \tag{3.5}$$

However, discussion of the polarization powers spectra in details in out of the scope of this thesis, since here we concentrate on the temperature power spectra C_ℓ^{TT} to understand the evolution of fluctuations from the tiny perturbations at inflationary epoch.

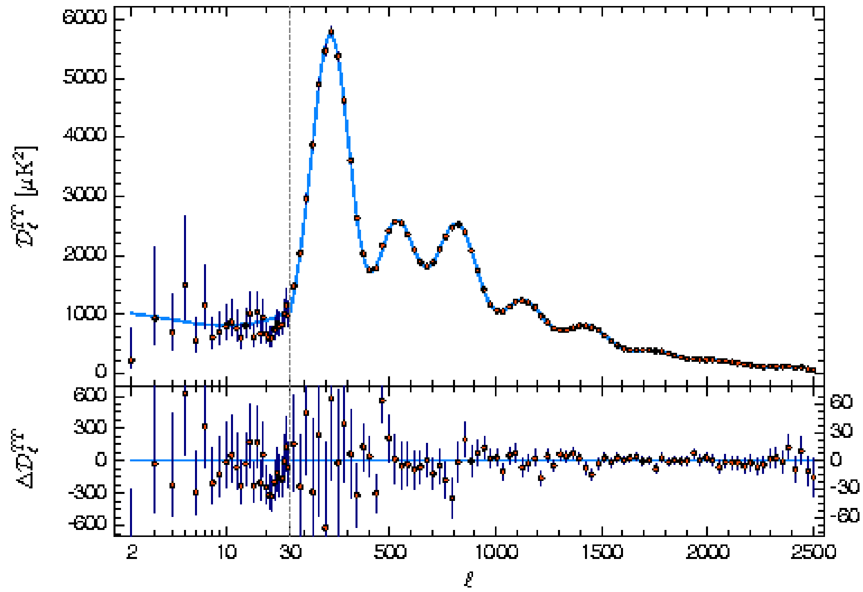

Figure 3.1: CMB angular power spectra from PLANCK 2018 [27] where $\mathcal{D}_\ell^{TT} = \ell(\ell+1)C_\ell^{TT}/2\pi$. The red data points from PLANCK TT + TE + EE + low E + lensing are plotted with error bars whereas the blue curve represents the best fit base ΛCDM value.

The positions and amplitudes of different peaks in the angular power spectra in Fig. 3.1 exhibit features that can relate to many dynamical quantities in the early universe. The fluctuation mode k_1 whose wavelength is equal to the sound horizon had the chance to compress just once after horizon re-entry and recombination and therefore is known as the fundamental mode $k_1 = 2\pi/\lambda_1$, where λ_1 is the sound horizon. Thus, the first acoustic peak of the spectrum at around $\ell \approx 220$ corresponds to the fundamental mode k_1 and acts as a measure of the sound horizon. The later peaks signify multiples of the fundamental frequency mode, e.g. the second peak corresponds to the wavenumber $k_2 = 2k_1$ and so on. Evidently, odd-numbered peaks in CMB are caught at the maxima of the oscillations (compactification of the plasma), whereas the even peaks represent minima of energy density (rarefication of the plasma).

The temperature anisotropy profile in Fig. 3.1 are distinctly related to the spatial curvature in the universe. If the curvature (κ) decreases (open universe) such that the curvature density is higher than its observed value today $\Omega_\kappa^0 = -0.0106 \pm 0.0065$, then the hot spots (potential wells) in CMB appear smaller in size[1] and the peaks shift to higher multipoles ℓ. Secondly, if the baryon density Ω_b is increased then the potential wells are deeper and as a result, the odd peaks in CMB are enhanced, but the even peaks do not change. Increasing Ω_b also slows down the acoustic oscillation and therefore peaks move to a higher ℓ value (smaller scales). The duration of the radiation dominated epoch before matter domination also influences the CMB angular power spectrum. Since the smaller length scales of perturbation re-entered the horizon before the larger scales, the potential wells at smaller scales are affected by the stretching of the modes due to radiation domination (unlike matter domination). Therefore, the relative amplitude as moving from lower to higher multipoles (ℓ) is a measure of the radiation to matter density at recombination, which also provides a measure for the age of the universe at recombination.

The higher ℓ correspond to the smaller scales in CMB, which are of the order of the mean free path of the photons engaged in Thomson scattering with the electrons before recombination. Therefore, the photons can move from maxima to minima of the smaller scale

[1] In an open universe, the paths of two photons from opposite ends of an extended object in sky bend towards each other and the object appears smaller, whereas in a closed universe, the paths move away from each other and the object appears larger.

oscillations between two consequent scatterings and therefore can smoothen the amplitude of oscillations. This results in the damping of the angular power spectrum at smaller scales (high ℓ) known as 'diffusion damping' or 'Silk damping'. Since the curvature, baryon density and matter-to-radiation density ratio are measured by the positions and peaks of the power spectrum, the damping tail provides a consistency test for the standard big bang model of cosmology.

The photons coming from the surface of recombination to us today are also affected by a few late-time cosmological effects. The presence of massive objects like galaxies and galaxy clusters at low redshifts bends the path of CMB photons through gravitational lensing [48] and what we observe through present CMB telescopes is a lensed spectrum of CMB. On the other hand, when a photon enters a gravitational potential well at its path, it gains energy, but by the time the photon leaves the well, the depth of the well changes due to the expansion of the universe. This affects the energy carried by individual photon and its effect along the full line of sight is known as the integrated Sachs-Wolfe (ISW) effect [49]. Moreover, when the photons encounter large scale structures in its path, the inverse Compton scattering with the high energy electrons in galaxies and galaxy clusters give rise to the photon energy accounting for a spectral distortion in the CMB energy spectrum. This is known as the Sunyayev-Zel'dovich (SZ) effect [50]. The recent analysis of the observed power spectra of CMB by surveys like PLANCK takes all these effects into account to recover the true power spectra at recombination. These late time effects have interesting implications for large scale structures of the universe as well, but they are out of the focus of this thesis.

3.1.2 Constraints from CMB

The latest measurement of the temperature angular power spectrum measured by PLANCK 2018 [27] is give in Fig. 3.1 where the data (red points) are fitted with the base six-parameter ΛCDM model of cosmology (blue curve). The six parameters of the minimal ΛCDM model are

A_s: amplitude of primordial scalar power spectrum,

n_s: spectral index of the primordial scalar power spectrum,

$\Omega_b h^2$: baryon density,

$\Omega_c h^2$: cold dark matter density,

θ: sound horizon and

τ: optical depth at reionization.

Table 3.1: Central values with 1σ errors of cosmological parameters by PLANCK (2018) [27].

Parameter	TT+lowE	TE+lowE	TT+TE+EE+lowE	TT+TE+EE+lowE+lensing+BAO
$\Omega_b h^2$	0.02212 ± 0.00022	0.02249 ± 0.00025	0.02236 ± 0.00015	0.02242 ± 0.00014
$\Omega_c h^2$	0.1206 ± 0.0021	0.1177 ± 0.0020	0.1202 ± 0.0014	0.11933 ± 0.00091
$100\theta_{MC}$	1.04077 ± 0.00047	1.04139 ± 0.00049	1.04090 ± 0.00031	1.04101 ± 0.00029
τ	0.0522 ± 0.0080	0.0496 ± 0.0085	$0.0544^{+0.0070}_{-0.0081}$	0.0561 ± 0.0071
$\ln(10^{10} \times A_s)$	3.040 ± 0.016	$3.018^{+0.020}_{-0.018}$	3.045 ± 0.016	3.047 ± 0.014
n_s	0.9626 ± 0.0057	0.967 ± 0.011	0.9649 ± 0.0044	0.9665 ± 0.0038

A_s and n_s are the parameters related to the primordial history of fluctuations and thus contain information about the inflationary dynamics, whereas the other four parameters are responsible for the evolution of the fluctuations after horizon re-entry in the decelerating epochs of matter domination. Therefore, recounting the definition of inflationary power spectrum from the previous chapter, the dynamics of inflation contributes to the derivation of C_ℓ^{TT} through Eq. (3.4). The extensions of this standard ΛCDM model in the inflationary sector can involve more parameters such as the tensor-to-scalar ratio (r), running and running-of-running of the spectral index (α_s and β_s), amplitude and spectral index of the tensor power spectrum (A_t and n_t) etc. The fitting of the theoretical angular power spectrum from ΛCDM model with that from CMB data provides constraints to the cosmological parameters discussed above which is the primary method of constraining models in cosmology.

The main statistical limitations in the measurement of CMB come from instrumental noise and angular resolution. The latest observation of CMB angular power spectrum by PLANCK in 2018 [27] can estimate the cosmological parameters with errors at sub-percent levels. In this era of precision cosmology, the theoretical models of inflation are extremely constrained with data. The phenomenology of inflation in this modern era is primarily based on comparing the theoretically computed scalar and tensor angular power spectra with observed C_ℓs from CMB experiments for the correlations of temperature as well as polarization. The tensor fluctuations being smaller in amplitude than scalar fluctuations do not contribute much into the angular power spectra and therefore current CMB experiments only put an upper bound on r. Upcoming CMB surveys like CORE [30], CMB-S4 [29] etc. are very hopeful as they propose to measure the inflationary observables like n_s and r with tremendous precision. Future prospects of observing primordial gravitational waves in advanced experiments with interferometry [51, 52] are very promising in understanding the primordial tensor fluctuations.

The work included in this thesis is based on constraining models of inflation using CMB observations from PLANCK 2015 [18] and 2018 [27]. The models considered in this work are inspired by particle physics or string theory. The motivation lies in accommodating these models in dynamically non-trivial scenarios like warm inflation and modified post-inflationary history.

The methodology used here in confronting the models of inflation with CMB data involves statistical and numerical analysis. Given a set of base ΛCDM parameters listed above, the CAMB (Code for Anisotropies in the Microwave Background) module [53] can generate the angular power spectra for temperature and polarizations. The default CAMB code uses the almost scale invariant inflationary power spectrum for the scalar fluctuations:

$$\Delta^2_{\mathcal{R}} = A_s(k_*)\left(\frac{k}{k_*}\right)^{n_s-1}. \tag{3.6}$$

where A_s and n_s are the input parameters and k_* is the pivot scale. The tensor power spectrum:

$$\Delta^2_t = A_t(k_{*t})\left(\frac{k}{k_{*t}}\right)^{n_t} \tag{3.7}$$

can be calculated in the extended model by one of the following ways: (i) using $A_t = r \times A_s$ with r as a parameter; (ii) using $\Delta^2_t = r \times \Delta^2_{\mathcal{R}}$ with r as a parameter, which yields same results as the previous option only if the pivot scales for scalar and tensor fluctuations are taken to be the same; (iii) using Eq. (3.7) and directly parameterizing A_t. k_{*t} is the pivot scale for calculating tensor power spectrum and in general, is equal to k_*. While calculating tensor power spectrum, n_t can either be a derived parameter using the gravitational wave consistency relation $r = -8n_t$ or can be treated as an independent input parameter.

In the works [17, 22] discussed in this thesis we have used the Cosmological Monte Carlo (CosmoMC) code [14] which is a publicly available tool that includes the CAMB module. The n number of parameters of the base or extended ΛCDM model can be varied in CosmoMC in a prior range and for each point in the n-dimensional parameter space, CAMB feeds back the temperature and polarization angular power spectra at recombination. These simulated power spectra are then compared with the observed CMB power spectra. The statistical analysis for comparing simulation to data involves Bayesian analysis technique to minimize the value of χ^2. If χ^2 at a particular coordinate in the parameter space is smaller than the χ^2 value at the previous point in the chain then the run accepts the later point, otherwise rejects it. Running the simulation until a considerable accuracy in χ^2 results in reaching the best fit values of the cosmological parameters. The method of moving across the parameter space uses Bayesian approach where a prior likelihood $\pi(\theta_i)$ is provided for each parameter θ_i, and the posterior probability for θ_i is calculated using Bayes' theorem. The posterior probability for θ_i is:

$$p(\theta_i|D) = \frac{p(D|\theta_i) \times \pi(\theta_i)}{p(D)} = \frac{p(D|\theta_i) \times \pi(\theta_i)}{\int d\theta_i p(D|\theta_i) \times \pi(\theta_i)}, \tag{3.8}$$

which uses the likelihood $p(D|\theta_i)$ for a particular set of data D. The marginal likelihood $p(D) = \int d\theta_i p(D|\theta_i) \times \pi(\theta_i)$ signifies the probability of obtaining a particular data set D given a set of priors for θ_i with $i = 1, ..., n$. The posterior probabilities for the cosmological parameters can be plotted in individually for each parameter, or as cross-correlation of the posterior probabilities for two parameters with 1σ and 2σ confidence levels marked distinctly.

In work [17], we have used COSMOMC while modifying the module for computing inflationary power spectra inside CAMB into a subroutine for calculating the warm inflationary power spectra given in Eq. (5.22) and Eq. (5.29) in terms of the parameters of the model under consideration. In work [22], we have used an additional module MODECODE with COSMOMC. MODECODE is also a publicly available Fortran package that computes the primordial power spectra for a given model of inflation. Using MODECODE with COSMOMC allows for independently varying the model parameters for inflation. Additionally, MODECODE also keeps the inflationary number of e-folds as a varying parameter to be estimated via simulation, which was found very useful in [22] as this model includes a modification of the number of inflationary and post-inflationary e-folds.

Usage of advanced statistical and numerical methods of comparing inflationary models with CMB data is very appealing as it helps probe the parameter space with a tremendous level of precision. The constrained values of the model parameters can be compared with the theoretically proposed order-of-magnitude values for them to understand the underlying dynamics better. It is crucial to utilize these numerical tools phenomenologically to validate models of inflation with well-defined levels of confidence.

CHAPTER 4

ATTRACTOR MODELS IN SCALAR-TENSOR THEORIES

4.1 Introduction

The recent advances in parameter estimation in cosmology from CMB observations is extremely helpful in knowing the details about the dynamics in the early universe. The PLANCK 2015 [28] observation of CMB measures the observables of inflation very precisely: the scalar spectral index $n_s = 0.968 \pm 0.006$ and the tensor-to-scalar ratio $r < 0.11$. Interestingly, the observable predictions of Starobinsky model $R + R^2$ [10], the model with a non-minimal coupling $\xi\phi^2 R$ and $V(\phi) \sim \phi^4$ [54–57] fall into the sweet spot of the PLANCK 2-σ contour. For a large number of e-folds N, the observables for these models are given by

$$n_s = 1 - 2/N, \quad r = 12/N^2 \tag{4.1}$$

where $N = 50$-60 is the time when the CMB scales leave the horizon during inflation[1]. In terms of a canonically normalised scalar field in minimal gravity, all the above mentioned models have exponentially flat potential in large field values.

Among large varieties of potentials, the models with a plateau-like behaviour are generically favoured by the recent data [61]. Subsequently, interests renewed in understanding models that can produce little amount of gravitational waves with spectral index in the above-mentioned limit. Using Lyth bound, that relates the value of r with the field excursion $\Delta\phi$ during inflation, these type of models would require $\Delta\phi \lesssim \mathcal{O}(M_{\rm Pl})$ [62]. It has been achieved in two ways. Firstly it was noticed that a coupling between the inflaton with heavy fields can effectively flatten the inflaton potential [63]. Secondly, Kallosh and Linde discovered a class of models whose observable predictions are attracted towards the point of Eq. (4.1) when one parameter in the model is continuously modified [11]. In fact, the models with arbitrarily small r were also proposed. The predictions of the Starobinsky model just sit at this attractor point. It was found that these class of attractor models have underlying conformal symmetry structure, and their supergravity realizations have been discussed extensively in the literature [12, 64–73].

One type of attractor model, namely the α-attractor, finds its attractor nature from the second-order pole in the kinetic energy term [74]. In terms of the field variable, the potential must be smooth at the position of the pole. In this case, the potential of the canonically normalised field asymptotes to a constant value. In terms of the canonical field, the pole is shifted to infinity and so is never reached physically through its dynamical evolution during inflation. We get a nearly shift symmetric plateau asymptotically. For the case of ξ-attractor models, the gravity is non-minimally coupled to the scalar field. In this case with

[1]Unconventional post inflationary dynamics can affect the preferred number of e-folds, and thus inflationary observables. For example, see [58–60].

the proper choice of the non-minimal coupling function, the kinetic term, and the potential function, the predictions of the model quickly converge to the asymptotic value given by Eq. (4.1) as we increase ξ. Both these attractor models can be unified in the picture of kinetic formulation of the theory, where n_s is related to the order of the pole of the kinetic term in its Laurent series expansion and r primarily depends both on the leading order pole and also on the residue corresponding to that pole in the expansion.

In this work, we have studied $f(R)$ theories of gravity and Brans-Dicke theory in the context of attractor models for inflation. We show explicitly how these models can be rewritten in terms of the attractor models with an appropriate kinetic term that is suitable for attractor mechanism to work. For some particular choice of the functional degrees of freedom in these theories, one obtains Starobinsky like predictions in the n_s-r observable plane. Any choice of these functions fixes the potential in the Jordan frame or in the Einstein frame in terms of the non-canonical field. Whether any model would show attractor properties crucially depends on the asymptotic nature of these potential functions. For example, any deviation from $R+R^2$ gravity distorts the asymptotic nature of the potential and makes the potential unstable for the attractor. Our work is complementary to the approach taken by Ref [75] where the effects of the asymptotic shift symmetry breaking corrections to the potential corresponding to R^2 term have been studied. Similar studies have been also carried out in [76–84].

We also discuss the robustness of the attractor mechanism by varying conformal function in the case of the ξ-attractor, and analyzing the effect of higher order pole in the kinetic energy term. In the case of ξ attractor, even when the conformal function is changed by adding higher order monomial, for a sufficiently large value of ξ the predictions come back to the attractor point. On the other hand, when the kinetic function is changed with a higher order pole, the predictions deviate from the attractor curve. This is consistent with the conclusion of [85] where changes to the observables have been calculated in the limit of perturbative corrections to the kinetic function.

We emphasise the point that even when a model has a kinetic term with a suitable pole structure (as we will recast), the potential in the Jordan frame is fixed from the underlying structure of the model. We get the attractor behaviour only for certain functional choices. In the case of Brans-Dicke theory, we choose only these functions judiciously and show how predictions for the attractor models are guaranteed to be reproduced when certain limits of the model parameters are taken.

The motivation of this work is two-fold:

• After reviewing the explicit mechanism of the attractor dynamics, we check the robustness of this mechanism for higher order corrections in the functional degrees of freedom for α and ξ- attractors.

• We theorize how attractor mechanism can be obtained from scalar-tensor theories and explicitly show the $f(R)$ theory and Brans-Dicke theory as examples. For this, we study the allowed range of the parameters in the functional degrees of freedom in light of the observables in CMB.

We will see that the plateau nature of the effective potential for large fields values in attractors is governed by the dynamics of the functional forms of the non-minimal coupling (for ξ-attractors) and the pole-containing kinetic term (for α-attractors). Therefore, both the analyses mentioned above relate to this dynamics and its outcomes.

This chapter is organized as follows. In the next section, we summarize the attractor mechanism. In Sec. 4.3, we analyze the robustness of the attractor mechanism. In Sec. 4.4, we discuss $f(R)$ inflation models in the language of attractor models and discuss phenomenology when polynomial terms are present in the action. In section V, we discuss Brans-Dicke theory in the context of attractor models and find potentials which suitably provide attractor solutions. Finally, we conclude in Sec. 4.6.

4.2 Attractor mechanism for inflation models

A class of inflationary models has been identified whose predictions in the space of observables are not so sensitive to the specific potential function due to particular non-canonical nature of the kinetic term. The data coming from PLANCK experiment shows this coincidence amongst various inflation models like - Starobinsky model [1,45], Goncharov-Linde Model [86], supersymmetric version of non-minimal chaotic inflation with ϕ^4 potential [12, 87, 88] and Higgs inflation [54]. In the leading approximation of $1/N$, where N being the number of e-folds of inflation, the observable predictions *i.e.* scalar spectral index (n_s) and tensor-to-scalar ratio (r) of all these models are attracted to a common point given by Eq. (4.1). These models are collectively known as cosmological attractors.

The cosmological attractors broadly come into two categories, where the Lagrangian either has a non-minimal coupling to the Ricci scalar or may feature a characteristic kinetic term with a second-order pole. The former description is known as non-minimal ξ-attractor and the later one is called α-attractor, where ξ or α is a free dimensionless parameter of the theory which when varied the predictions converge to Eq. (4.1). The origin of the attractor properties of both kinds can be traced back to the pole structure of the Kinetic function in its Laurent expansion and the potential function is smooth at the position of that pole [11]. Under special condition, these models can be mapped to each other.

4.2.1 α and ξ attractors

The Lagragian for the models of cosmological attractor is given by

$$\mathcal{L} = \sqrt{-g_E}\left[\frac{1}{2}R_E - \frac{1}{2}\left(\frac{a_p}{\phi^p} + \cdots\right)(\partial\phi)^2 - V_E(\phi)\right] , \tag{4.2}$$

where the kinetic function is given by a Laurent series expansion with a pole of order p at $\phi = 0$ (without loss of generality), and the dots denote subleading terms. We approximate the potential energy by a Taylor series expansion $V_E(\phi) = V_0(1+c\phi+\cdots)$ near the vicinity of the pole. Here ϕ is the inflaton field with non-canonical kinetic energy term, and gravity is minimally coupled. The constant V_0 sets the asymptotic value of the potential in term of the canonical field.

It turns out that the observable predictions of this model are uniquely characterised by the properties of the pole. In particular, the scalar spectral index n_s and the tensor-to-scalar ratio r at leading order in $1/N$ are given by [11]

$$n_s = 1 - \left(\frac{p}{p-1}\right)\frac{1}{N}, \qquad r = \frac{8c^{\frac{p-2}{p-1}} a_p^{1/(p-1)}}{(p-1)^{\frac{p}{p-1}}} \frac{1}{N^{\frac{p}{p-1}}} \,. \tag{4.3}$$

Note that whereas the spectral index depends only on the order of the pole, the tensor-to-scalar ratio depends both on the order and the residue of the pole. For $p = 2$ and $a_p = 1$, this yields the famous Starobinsky inflation prediction for the scalar spectral index given by Eq. (4.1). Depending on the value of a_p, the tensor-to-scalar ratio can be arbitrarily small. The second-order pole with $p = 2$ is special as its origin can be traced back to some superconformal supergravity theories [12, 64–73], and to non-minimal gravity theories in the Jordan frame [89].

As mentioned earlier, there are primarily two classes of cosmological attractors. Both of them can be interpreted as having a pole in the kinetic term of order $p = 2$. The Lagrangian for the cosmological α-attractor is given by,

$$\mathcal{L} = \sqrt{-g_E}\left[\frac{1}{2}R_E - \frac{1}{2}\frac{\alpha(\partial\phi)^2}{(1-\phi^2/6)^2} - \alpha f^2(\phi/\sqrt{6})\right] , \tag{4.4}$$

where α is a dimensionless parameter of the model. If we make a field redefinition as $\phi/\sqrt{6} = (1-\rho)/(1+\rho)$, we can write the above Lagrangian as[2]

$$\mathcal{L} = \sqrt{-g_E}\left[\frac{1}{2}R_E - \frac{3\alpha}{2\rho^2}\frac{(\partial\rho)^2}{2} - \alpha f^2(\rho)\right] . \tag{4.5}$$

This is similar to what is written in Eq. (4.2) with the specified form of the kinetic function with $a_2 = \frac{3}{2}\alpha$. Therefore, the Lagrangian of an α-attractor model also features a second-order pole at $\rho = 0$.

In terms of the canonical field $\hat{\phi}$, the pole at $\rho = 0$ is shifted to large field values, and the potential is given by

$$V_E(\hat{\phi}) = \alpha f^2 \left[\tanh(\hat{\phi}/\sqrt{6\alpha})\right] \tag{4.6}$$

where $\rho = e^{-\sqrt{\frac{2}{3\alpha}}\hat{\phi}}$. For monomial functions, the potential reduces to the form of T-models of conformal attractors. For the choice of $f(x) = \frac{cx}{1+x}$, one finds the generalization of Starobinsky potential [11]

$$V_E = \frac{\alpha c^2}{4}\left(1 - e^{-\sqrt{\frac{2}{3\alpha}}\hat{\phi}}\right)^2 . \tag{4.7}$$

This potential has a long plateau at large $\hat{\phi}$. It is this particular functional form of V_E that makes the potential asymptotically flat at large values of the canonically normalized field. The predictions of this model varies from quadratic chaotic inflation model (for large α) to

[2]Instead of making this field redefinition, if we make the Laurent series expansion of the kinetic function K_E, at the leading order we get a second-order pole at $\phi = \sqrt{6}$ with a residue of $3\alpha/2$. The subleading terms in the expansion do not contribute to the observables in the large N limit.

Starobinsky model (for $\alpha = 1$) with [74]

$$n_s = 1 - 2/N, \quad r = 12\alpha/N^2 \,. \tag{4.8}$$

This model can also produce arbitrarily small r for $\alpha \ll 1$.

Note that the choice of the function $f(x)$ can be more general than what has been mentioned above. Because of the nature of $\tanh(\hat{\phi})$ function, when the argument of the function becomes of order one, the potential is stretched with a constant asymptotic plateau. But the function must be chosen appropriately such that the post-inflationary vacua are consistent with observations.

The other description for the cosmological attractor with non-minimal coupling to gravity is given by [89, 90][3]

$$\mathcal{L}_J = \sqrt{-g_J}\left[\frac{1}{2}\Omega^2(\phi)R_J - \frac{1}{2}K_J(\phi)(\partial\phi)^2 - V_J(\phi)\right] , \tag{4.9}$$

where $\Omega^2(\phi) = 1 + \xi f(\phi)$ is the conformal factor. Here the theory is defined in a Jordan frame. The corresponding Einstein frame description after a conformal transformation of the metric tensor $g^E_{\mu\nu} = \Omega^2(x^\mu)g_{\mu\nu}$ is

$$\mathcal{L}_E = \sqrt{-g_E}\left[\frac{1}{2}R_E - \frac{1}{2}\left(\frac{K_J}{\Omega^2} + 6\frac{\Omega'^2}{\Omega^2}\right)(\partial\phi)^2 - V_E\right] . \tag{4.10}$$

Here $V_E = V_J/\Omega^4$, and the prime is w.r.t the field variable ϕ. If $K_J(\phi) \ll 6\Omega'^2$, the above

[3]For multifield models of inflation with non-minimal couplings, the expressions for n_s and r in the leading approximation in $1/N$ is different [91]. Higher order correlation functions for these models are studied in [92].

Lagrangian reduces to the usual form of the attractor model.

$$\mathcal{L}_E = \sqrt{-g_E}\left[\frac{1}{2}R_E - 3\frac{(\partial\Omega)^2}{\Omega^2} - V_E(\Omega)\right]. \tag{4.11}$$

In this case, the canonically normalised field $\hat{\phi}$ is related to the conformal factor by $\Omega^2 = e^{\sqrt{\frac{2}{3}}\hat{\phi}}$. Now, with ξ being negative, $\Omega^2(\phi) = 1+\xi f(\phi)$ has a pole of order two in the kinetic term. However, with positive ξ, the pole structure is clear if we make the transformation $\Omega^2 \to 1/\rho$, and the above Lagrangian becomes

$$\mathcal{L}_E = \sqrt{-g_E}\left[\frac{1}{2}R_E - \frac{3}{4}\frac{(\partial\rho)^2}{\rho^2} - V_E(\rho)\right]. \tag{4.12}$$

Thus, at large ξ or large ϕ, the pole at $\rho \to 0$ is accessible. If $V_E(\rho)$ is smooth at the position of the pole, the potential w.r.t to the canonically normalised field is going to be flattened for large field values. Therefore both the classes of cosmological attractors are basically a realisation of the same description given in Eq. (4.2) through redefined field variables. For the case of ξ-attractor, the residue at pole is $a_2 = 3/2$, and the predictions are given by Eq. (4.1) for a suitable choice of V_J. For the particular choice of $V_J(\phi) = c^2(\Omega^2 - 1)^2$ this yields the famous Starobinsky model. On the other hand, for the choice of $V_J = \Omega^4 f^2\left(\frac{\Omega^2-1}{\Omega^2+1}\right)$, the resulting theory in the Einstein frame becomes a T-model of α-attractor [93]. See [94] for some other attractor models where the form of the potential function has to be approximately close to this form to show attractor mechanism.

In summary, any choice of the potential function of the non-canonical field having second-order pole in the Einstein frame will show attractor nature if it satisfies the following three criteria:

• Potential must be a smooth function at the location of the pole,

• the potential has to be a positive definite function, and

• at large field values, the potential must asymptotically approach to a constant (or nearly constant) value.

The second criterion is a statement about the boundedness of the potential from below. The last one is seemingly significant as this asymptotic domain of the potential is responsible for the attractor type predictions in the n_s-r plane.

We note that the way the Einstein frame scalar potential of a canonical field manifesting an asymptotically long plateau is slightly different for the two kinds of attractor models. In the case of α-attractor, the potential in the Einstein frame after canonical normalization is controlled by the canonical conversion function $\tanh\hat{\phi}$, and it causes flattening of the potential. It happens because in the defining Lagrangian of the α-attractor, the pole in the Kinetic term appears at some finite value of ϕ. Nevertheless, a suitable field redefinition can make the pole to appear at zero field value. But in that case, the potential still remains a $\tanh\hat{\phi}$ function in the canonical field. Therefore, for the α-attractor viewing the pole in the non-canonical field either at zero or at finite value does not make any difference in the argument of the potential function of the canonically normalized field. In contrast, for the ξ-attractor, the canonical conversion generates an exponential function $\Omega^2 \sim e^{\hat{\phi}}$. But in this case, a tacit choice of the potential function V_J makes the potential exponentially flat. However, in either case, the asymptotic behaviour of the Einstein frame scalar potential is similar. In summary, in addition to the pole structure in the kinetic energy term, the attractor behaviour also crucially depends on the properties of the potential functions.

In Sec. 4.4 we are going to study how the inflationary predictions of some well studied scalar-tensor theories can be reinterpreted in the language of attractor models.

4.3 Robustness of attractor mechanism

The attractor mechanism works due to the existence of a second-order pole in the kinetic term, and the potential being smooth at the position of the pole. As we have seen in the previous section, for the case of ξ-attractor, a certain condition has to be satisfied between the conformal factor and the potential function. Specifically, the order of the monomial in both these functions must be the same such that asymptotically the potential in the Einstein frame becomes constant. On the other hand, the shift symmetric potential in the asymptotic limit can be broken by including higher order poles. These higher order poles, in general, can appear when the Kinetic function is expanded in Laurent series [11, 85]. For the non-minimal ξ-attractor, higher order corrections arise when the conformal function is Taylor expanded [89]. In this section, we will analyze the robustness of the attractor mechanism by modifying the conformal factor[4] and the pole structure of the kinetic function. If the corresponding corrections arise at field values much larger than the field value ϕ_{60} when the CMB scales goes outside the horizon, the attractor prediction remains robust. For the case of perturbative corrections to the leading order pole in the kinetic function, the corrections to the inflationary observables have been shown to be universal [85]. We analyze this case when the corrections are not necessarily perturbative.

Here we would like to see how a correction term in the non-minimal coupling function is going to affect an otherwise attractor like predictions. For the purpose of our analysis we start with the Lagrangian density of Eq. (4.9). For simplicity, the non-minimal function and the potential function of this theory are taken to be

$$\Omega^2(\phi) = 1 + \xi(b_1\phi + b_2\phi^2), \qquad V_J(\phi) = m^2\phi^2, \tag{4.13}$$

[4]Note that here we modify the conformal factor perturbatively which is different from quantum corrections to the attractor models, which is studied extensively in [95].

where b_1, b_2 are arbitrary constants of the theory. Recasting the Lagrangian density into the Einstein frame through a conformal transformation we obtain for the potential function to be

$$V_E(\phi) = \frac{m^2\phi^2}{[1+\xi(b_1\phi + b_2\phi^2)]^2} \, . \tag{4.14}$$

With $b_2 = 0$ and after eliminating ϕ in terms of Ω^2, the potential can be written as $V_E = \frac{m^2}{\xi^2}(1-\Omega^{-2})^2$. This represents a ξ-type attractor model with predictions interpolating between quadratic chaotic model and Eq. (4.1) when ξ is varied from zero to large values. Here ξ is the attractor parameter when its value is increased. Without loss of generality, for the purpose of our analysis we have taken $b_1 = 1$ as it can be absorbed in the redefinition of ξ. We now want to see how this attractor like behaviour changes when we include $b_2\phi^2$ term in the non-minimal function.

Let us now investigate the predictions of this potential in the light of PLANCK 2015 data. With the form of the Einstein frame potential specifield, one can calculate the scalar spectral index and the tensor-to-scalar ratio from the following expressions respectively,

$$n_s = 1 - 6\epsilon_E + 2\eta_E, \qquad r = 16\epsilon_E$$

where ϵ_E and η_E are the inflationary slow roll parameters which are given as,

$$\epsilon_E = \frac{1}{2}\left(\frac{V_E'(\hat{\phi})}{V_E}\right)^2, \qquad \eta_E = \frac{V_E''(\hat{\phi})}{V_E} \tag{4.15}$$

These parameters have to be calculated when observable CMB modes go outside the horizon.

The theory now contains three free parameters m, ξ and b_2. But m gets fixed from the amplitude of curvature perturbation, and ξ and b_2 remain free parameters that we vary. For several representative values of b_2, we change ξ from zero to 10^4 and calculate the scalar spectral index and the tensor-to-scalar ratio. The observable predictions, in this case, are shown in Fig. 4.1a. In this figure, the various colored curves correspond to fixed values of the b_2 parameter. All of them approach to the attractor point in the n_s-r plane from their $\xi = 0$ limit of quadratic chaotic inflation limit. The rightmost black curve with $b_2 = 10^{-4}$ goes directly into the attractor point. But the way other two curves with larger values of b_2 (red, blue) approaches towards the attractor point is quite different from the first. With the increasing value of the ξ-parameter they initially deviate from the attractor point. Thereafter, for a further increase of ξ, the curves once again return to the attractor point. To understand this behaviour let us have a close look at the expression for the Einstein frame potential in Eq. (4.14). There is a maximum of the potential at $\phi = \phi_0 = \frac{1}{\sqrt{b_2\,\xi}}$ when the effect of $b_2\phi^2$-term in the denominator is comparable to ϕ-term. Note that this is true for any non-zero value of b_2 with $\phi_0 \to \infty$ when $b_2 \to 0$. The potential now develops two branches. For values of $\phi > \phi_0$, it asymptotes to zero while it acquires a flat part for $\phi < \phi_0$. For viable inflation, we must have $\phi_{60} < \phi_0$, and necessary inflation can proceed in the flat part of the potential.

Now the value of ϕ_{60} depends on both ξ and b_2. For smaller values of $b_2 \sim \mathcal{O}(10^{-4})$, the value of $\phi_{60} \gtrsim 1$, but due to the smallness of b_2 parameter the effect of the quadratic term is negligible, and the curve directly moves towards the attractor point. On the other hand for $b_2 \sim \mathcal{O}(10^{-3})$, the curve initially moves away from the attractor point for up to a certain value of ξ. In this case, up to the turning point, even though $\phi_{60} \gtrsim 1$, the effects of larger b_2 in the quadratic correction term is appreciable. With further increasing value of ξ, the potential distorts and inflation happens with $\phi_{60} \lesssim 1$ in an asymptotic flat part. In this case, the quadratic term becomes negligible in the region where inflation proceeds

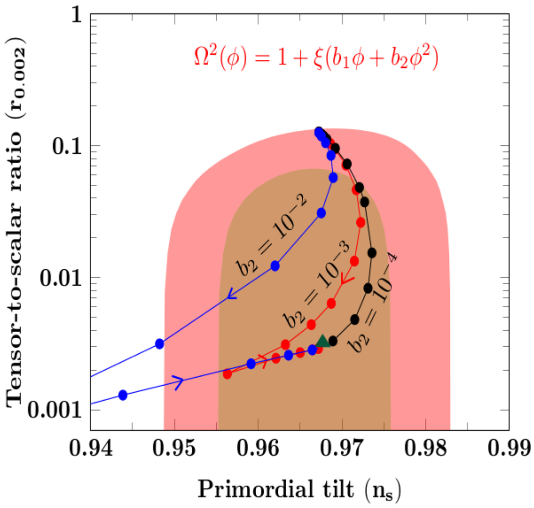

(a)

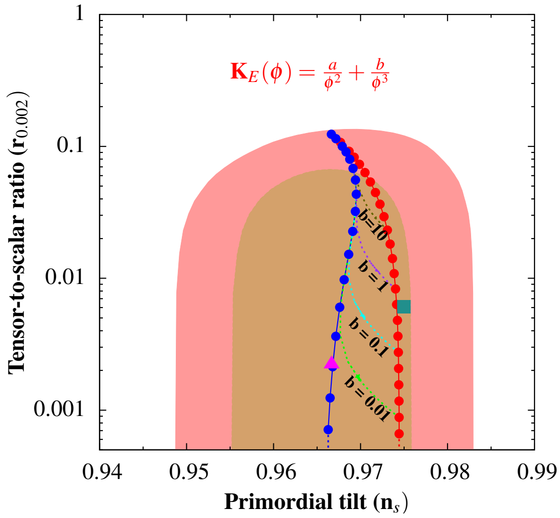

(b)

Figure 4.1: Plots show the variations of n_s-r with the 68% and 95% confidence contours from 2015 PLANCK data. In Fig. (a) the arrow in each line shows the direction of increasing ξ. The green triangle in the plot shows the attractor point given by Eq. (4.1). In Fig. (b) the blue dots correspond to the quadratic pole only, and the red dots correspond to the cubic pole. The arrow in each dotted lines shows the direction of decreasing a for various b values. The magenta triangle and the blue square correspond to Eq. (4.3) with $p = 2$ and $p = 3$ respectively for $a_p = 1$.

and the attractor point is reached. In conclusion, we find that if we increase the value of ξ sufficiently, we regain the attractor behaviour even with the correction term with $b_2 \sim \mathcal{O}(1)$ in the conformal factor. Therefore, we conclude that the attractor behaviour is very robust to the perturbations in the functions that define the attractor Lagrangian as long as the attractor parameter is increased sufficiently.

We now would like to understand how an attractor theory is sensitive with respect to the variations in its kinetic function. For this analysis, we pick up the Einstein frame Lagrangian density given in Eq. (4.2). The kinetic and the potential functions are taken as[5]

$$K_E(\phi) = \frac{a}{\phi^2} + \frac{b}{\phi^3}, \qquad V(\phi) = V_0(\phi - 1)^2 \,. \tag{4.16}$$

[5]For a general discussion on poles of higher orders in relation to attractor models, see [85, 96]

From Eq. (4.3), we know that the attractor point in n_s vs. r space is reached for a pole of order two with $b = 0$. We are now going to study what happens to the curve reaching to the attractor point when a third order pole is additionally present. In the absence of third order pole term, the attractor parameter is a when its value is decreased. For $a = 1$, we reach Starobinsky point.

Here both a and b are free parameters of the theory, and V_0 will be fixed from the amplitude of scalar curvature perturbations. To perform the analysis we have kept the parameter b fixed at some representative values. For each fixed value of b we change a from large values of order $\sim 10^4$ to small values and calculate the inflationary observables. The predictions of this model are shown in Fig. 4.1b. In this figure, the blue curve on the left represents the prediction when $b = 0$ *i.e.,* there is only second-order pole in the kinetic function. The curve approaches the attractor point (magenta triangle) with decreasing value of a (from top to bottom), and it is consistent with general predictions of Eq. (4.3). The red curve on the right shows the predictions for having only the third order pole $(a = 0)$ in the kinetic function. Between these two curves, the various (dotted) curves show how inflationary predictions are changing when poles of both orders are present in the theory. For $b = 0.01$ (dotted green curve) the value of $\phi_{60} \sim \mathcal{O}(10^{-3})$, and in this case initially the effect of b/ϕ^3-term is subdominant compared to a/ϕ^2-term. But with a gradual lowering of attractor parameter a, ϕ_{60} remains constant and the third order pole starts to affect the observables. Finally, with a sufficiently small value of a, the predictions finally hit the line for only having third order pole in K_E. For other values of b, this behaviour remains the same.

In all these dotted curves, it turns out that after a certain critical value $a \lesssim a_0$ (say), when the curves start to deviate from the blue line, the value of ϕ_{60} at first decreases. After that with further decreasing a, ϕ_{60} practically becomes unchanging. Therefore, the strength of the cubic pole becomes dominant over the quadratic pole. For certain non-zero values of b, even though some curves pass through the attractor point, they never come back to the same point with further decreasing the attractor parameter a. In summary, it is the dependence of ϕ_{60} upon the attractor parameter (ξ for the case modifying the conformal factor, and a for modifying the kinetic term) that determines whether the predictions will approach back to the attractor point or not.

4.4 $f(R)$ theory as attractor models

The modification of Einstein's theory of gravity is an interesting avenue in exploring physics beyond the standard picture of Big Bang cosmology. Because of high curvature in the early universe during inflation, the corrections to the Einstein-Hilbert gravity turns out to be generic [10]. In general, these corrections are such that either the geometry can be non-minimally coupled to some scalar field or higher derivative term in the metric can appear. Study of these higher derivative theories are important when gravity is quantized in a curved spacetime background and the issue of renormalization is addressed [97, 98]. Moreover, they also appear in studies of inflation in early universe [76–78].In its simplest version, the corrections may take the form of some arbitrary function of the Ricci scalar R. The action for this modified theory of gravity is given by [99],

$$S = \frac{1}{2\hat{\kappa}^2} \int d^4x \sqrt{-g} f(R), \tag{4.17}$$

where $\hat{\kappa}^2 = 8\pi G = 1/M_{\rm Pl}^2$ and the Ricci scalar $R = g^{\mu\nu} R_{\mu\nu}$ is the contracted version of Ricci Tensor $R_{\mu\nu}$. Each choice of the function $f(R)$ corresponds to a different theory and a large number of viable theories exist in the literature for both late time and early universe cosmology. Out of the diverse possibilities of $f(R)$, from the standpoint of inflationary cosmology the form $f(R) = R+R^2$, proposed by Starobinsky, grew with alluring attention for its remarkable agreement with PLANCK observations.

By a conformal transformation $g^E_{\mu\nu} = \Omega^2(x^\mu)g_{\mu\nu}$ of the metric tensor, the above theory can be recasted in the form of a scalar field minimally coupled to gravity. For the following *choice* of the conformal factor

$$\Omega^2 = F(R) = \frac{\partial f(R)}{\partial R} > 0\,, \tag{4.18}$$

the Eq. (4.17) becomes

$$\mathcal{L}_E = \sqrt{-g_E}\left[\frac{1}{2\hat{\kappa}^2}R_E - \frac{1}{2}g_E^{\mu\nu}\partial_\mu\hat{\phi}\partial_\nu\hat{\phi} - V_E(\hat{\phi})\right]\,, \tag{4.19}$$

where,

$$\hat{\phi} = \frac{1}{\hat{\kappa}}\sqrt{\frac{3}{2}}\ln F. \tag{4.20}$$

In Eq. (4.19), we have dropped a surface term that vanishes at the boundaries. Now the potential function for the field is given by

$$V_E(\hat{\phi}) = \frac{FR - f(R)}{2\hat{\kappa}^2F^2}\,. \tag{4.21}$$

Eq. (4.19) and Eq. (4.21) show that any $f(R)$ theory is dynamically equivalent to a minimally coupled scalar field with a potential function determined by the form of $f(R)$. This scalar field is responsible for driving inflation. In the next subsections, we are going to demonstrate that any $f(R)$ theory can be reformulated with the desired pole structure in the kinetic term of the scalar degree of freedom. But whether the theory shows attractor behaviour or not depends on the potential function, that is uniquely determined by the $f(R)$ function.

4.4.1 Relating $f(R)$ Theories to ξ-attractor

Let us now investigate when attractor properties exists for an $f(R)$ theory in its Jordan frame description. For our purpose, we can write the action of Eq. (4.17) as [99]

$$S = \frac{1}{2\hat{\kappa}^2} \int d^4x \sqrt{-g} \Big[F(\phi)(R-\phi) + f(\phi) \Big] \, . \tag{4.22}$$

The equation of motion of the scalar field ϕ yields $R = \phi$, and it is clear that the above action describes the same theory given by Eq. (4.17). With the identification of $\Omega^2 = F(R)$, the action becomes

$$S = \int d^4x \sqrt{-g} \left[\frac{\Omega^2(\phi) R}{2\hat{\kappa}^2} - \left(\frac{F(\phi)\phi - f(\phi)}{2\hat{\kappa}^2} \right) \right] . \tag{4.23}$$

Comparing this theory with what has been defined earlier in Eq. (4.9), we find that the resulting structure of the theory is analogous to a ξ-attractor with $K_J(\phi) = 0$ and $V_J = (F(\phi)\phi - f(\phi))/(2\hat{\kappa}^2)$ in the Jordan frame. So the behaviour of the resulting potential in this theory is now dependent upon the functional form of $f(R)$. The important difference of this theory with the corresponding ξ-attractor is that whereas for the cosmological ξ-attractor some particular choices of the Jordan frame potential show attractor like predictions, here the attractor property will rely upon the choice $f(R)$.

To have a more clearer picture, we go to the Einstein frame. In this frame, in terms of the variable Ω (conformal factor) we obtain

$$S = \int d^4x \sqrt{-g_E} \left[\frac{1}{2\hat{\kappa}^2} R_E - 3\frac{(\partial\Omega)^2}{\Omega^2} - \frac{V_J(\Omega(R))}{\Omega^4} \right] . \tag{4.24}$$

As we are interested in the nature of the potential at large positive field values, the variable Ω^2 also becomes large. By using the simple transformation $\Omega^2 \rightarrow 1/\rho$, the above Lagrangian transform to Eq. (4.12) with pole at $\rho = 0$. Thus in terms of Ω^2, the kinetic term in the Einstein frame has a second-order pole. However, now we can not simply choose $V(\Omega)$ so as to make it, for an example, $V_J \propto (\Omega^2 - 1)^2$. Let us investigate some specific form of $f(R)$ that leads us to attractor like predictions. As we are only interested in understanding the asymptotic behaviour of the potential, here we will not be explicitly careful about dimensionful constants except for one case. The following analysis is complementary to the discussion in Ref [75] where an investigation has been done to see how functional form $f(R)$ changes when small distortions are made to the case of asymptotic flat potential.

Case (a): $f(R) \sim R + R^2$

This is the famous Starobinsky model [10]. Here we are not careful about the exact coefficients as we we are interested in finding the asymptotic behaviour of the potential. The predictions of this model indeed show attractor nature of Eq. (4.1). Here we are looking at this model through the non-canonical structure in the Lagrangian density in the Einstein frame. Solving for the Ricci scalar from Eq. (4.18) and expressing the potential function in terms of the canonical field we get $R = \frac{\Omega^2-1}{2}$, and it gives

$$V(\phi) \simeq (1 - \Omega^{-2})^2 \simeq (1 - \rho)^2 \tag{4.25}$$

In terms of the non-canonical field ρ, the Lagrangian has a second-order pole in the kinetic term, and the potential is finite positive at the position of the pole $\rho \rightarrow 0$. When written in terms of the canonical field as Eq. (4.7), the potential asymptotes to the constant value which is equal to the value at the position of the pole. In terms of $\hat{\phi}$ however this pole shifts to infinity and at large $\hat{\phi}$, $V(\hat{\phi})$ approaches to an exponentially flat plateau. The form of the potential remains the same as in the standard case.

Case (b): $f(R) \sim R + R^3$

In this case, we get $R = \sqrt{\frac{\Omega^2-1}{3}}$ and the potential function

$$V(\rho) \simeq \left(\frac{1}{\Omega^{2/3}} - \frac{1}{\Omega^{8/3}}\right)^{3/2} \simeq \left(\rho^{1/3} - \rho^{4/3}\right)^{3/2} \tag{4.26}$$

We see that both at the position of $\rho = 0(\Omega \to \infty)$, and $\rho = 1(\Omega = 1)$, the potential vanishes, and in this case, the potential makes a local maximum that is unsuitable for asymptotically flat potential. In fact, the potential in terms of the canonically normalized field looks like

$$V \simeq e^{-2\sqrt{2/3}\hat{\kappa}\hat{\phi}}(e^{\sqrt{2/3}\hat{\kappa}\hat{\phi}} - 1)^{3/2} \tag{4.27}$$

For $\rho \to 0$ or at large value of the canonical field $\hat{\phi}$, the potential vanishes because of an overall exponential factor - no suitable vacuum energy to drive inflation. Hence no attractor solution is possible.

Case (c): $f(R) = R + aR^2 + bR^3$

Here by solving for R in terms of Ω we get,

$$R = \frac{-1 + \sqrt{1 + 3\frac{\epsilon}{a}(\Omega^2 - 1)}}{3\epsilon} \tag{4.28}$$

The potential now depends upon two dimensionful parameters a and ϵ, where $\epsilon = b/a$. We here want to investigate the manner in which the predictions of this model are going to be affected due to presence of the correction term bR^3. The Einstein frame potential for this $f(R)$ theory is,

$$V_E = a\frac{\left(1-\sqrt{1+3\frac{\epsilon}{a}(\Omega^2-1)}\right)^2\left(1+2\sqrt{1+\frac{\epsilon}{a}(\Omega^2-1)}\right)}{54\epsilon^2\Omega^4} \tag{4.29}$$

It is easy to check that in the limit $\epsilon \to 0$ we get back to the results of Eq. (4.25) of *Case (a)*. The Fig. 4.2a shows how the nature of the potential with respect to the canonical field $\hat{\phi}$ changes as we vary the parameter ϵ for a given value of the parameter a. The potential

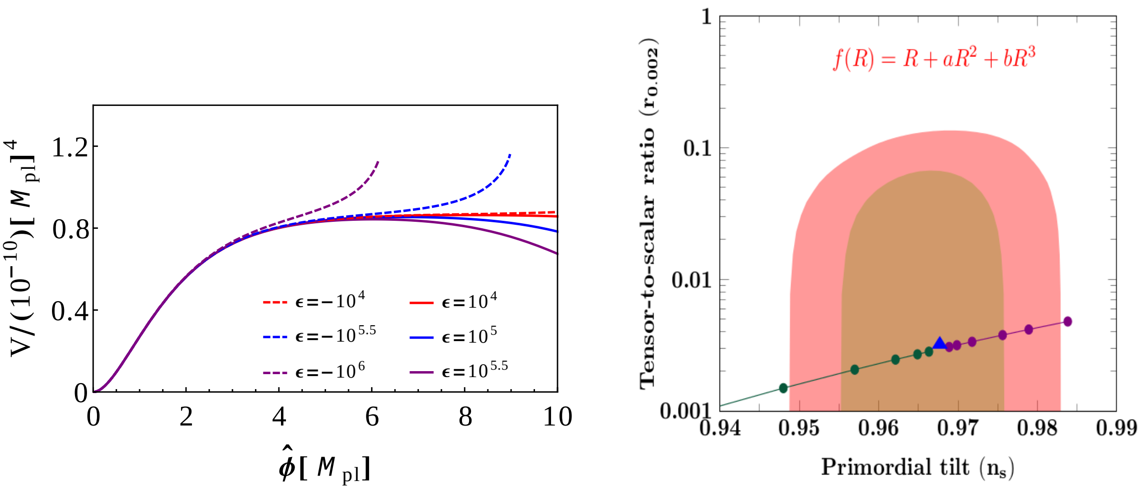

(a) (b)

Figure 4.2: Fig. (a) shows Einstein frame potential with respect to the canonically normalized field $\hat{\phi}$ for various choices of the parameter ratio $\epsilon = b/a$, taking $a \sim 10^9$. Fig. (b) is the plot showing the variations of n_s-r with the 68% and 95% CL contours from 2015 PLANCK data. With decreasing b predictions approaches to Starobinsky model shown here by blue triangle.

depicts different behaviour according to the sign of the ϵ parameter. We can see that as we keep on increasing $|\epsilon|$ beyond 10^4 the strength of R^3-term begins to dominate. For $\epsilon > 0$ the asymptotic behaviour of the potential is such that it gradually looses its height at large field values. This is in contrast to what is found in case of attractor type potentials. However, for $\epsilon < 0$ the potential is real only if $\Omega > \sqrt{1 - \frac{a}{3\epsilon}}$. Moreover for negative values of ϵ the potential develops a steep rising branch [100]. As we lower the value of ϵ the steep branch appears at lower values of $\hat{\phi}$. It turns out that in this case decreasing ϵ beyond -10^6 would not allow to have 60-efolds of inflation.

Observable predictions of this model are shown in Fig. 4.2b. The above figure shows variations of the spectral tilt n_s and tensor-to-scalar ratio r with respect to the parameter ϵ. The plot consists of two branches. In the left branch, the green coloured dots indicate points for ϵ ranging from 10^4 to about 10^6 (right to left). The diamond indicates the usual attractor point. It turns out that keeping $a \sim 10^9$ (fixed by the amplitude of scalar curvature perturbation) the predictions lie within the PLANCK 2σ contours as long as $\epsilon \sim 10^5$. Beyond that value of ϵ, the strength of R^3 term is such that it will violate the spectral index constraint. In the right branch of the plot the violet data points correspond to the range $-10^6 < \epsilon < -10^4$. The requirement of real potential restricts ϵ being larger than -10^6 and hence constrains the range of e-folds.

Case (d): $f(R) \sim R + R^n$

Here n is a finite integer and $R = \left[\frac{\Omega^2-1}{n}\right]^{\frac{1}{n-1}}$. Therefore, in terms of the Ω variable the potential function can be written as,

$$\begin{aligned} V(\Omega) &= \frac{(n-1)\left(\frac{\Omega^2-1}{n}\right)^{\frac{n}{n-1}}}{\Omega^4} \\ &\simeq (1-\rho)^{\frac{n}{n-1}} \rho^{\frac{n-2}{n-1}} \end{aligned} \tag{4.30}$$

The above form of the potential function is a generalization of the Starobinsky model when $n = 2$, for which it approaches to a constant at at smaller values of ρ (or equivalently at asymptotically large values of Ω). However, for $n > 2$ the potential has an overall ρ-dependence due to the $\rho^{\frac{n-2}{n-1}}$ factor. Hence at large values of $\hat{\phi}$ the potential vanishes.

In summary, we can think of the corrections to Einstein gravity in a $f(R)$ theory as equivalent to the higher order corrections in the conformal factor of the theory. For $f(R)$ theory, the conformal factor term is appearing like $\Omega^2(\phi)R = F(R)R = (1 + c_0\phi + c_1\phi^2 + \ldots)R$, since $\phi = R$ following from Eq. (4.22). Therefore any modification in the $f(R)$ function amounts to a likewise modification in the non-minimal function of Sec. 4.3 . Hence the robustness of attractor model investigated in Sec 4.3 can be directly correlated with the various $f(R)$ models envisaged here. Similar analysis in [101] also shows that the modifications to potential function give corrections which are suppressed for power $n > 3$ in $f(R)$.

4.4.2 Relating $f(R)$ theories to α-attractor

In the previous subsection we have written down $f(R)$ gravity in terms of conformal factor variable Ω^2, and that clearly spells out the speciality of R^2 in terms of its asymptotic nature. Now we will recast the $f(R)$ Lagrangian directly in the form of α-attractor given by Eq. (4.4). It can be easily done if instead of the choice given by Eq. (4.18) we *choose*

$$F = \frac{\sqrt{6} + \hat{\kappa}\,\phi}{\sqrt{6} - \hat{\kappa}\,\phi}\,. \tag{4.31}$$

Then the kinetic term becomes

$$\frac{6\hat{\kappa}^2}{(6 - \hat{\kappa}^2\phi^2)^2}(\partial\phi)^2\,.$$

Note that this choice does not affect the expression for the potential function in Eq. (4.21). For a given $f(R)$ one solves for R in terms of ϕ using Eq. (4.31). The Lagrangian density for this choice turns out to be,

$$\mathcal{L} = \sqrt{-g}\Big[\frac{R_E}{2\hat{\kappa}^2} - \frac{1}{2}\frac{g_E^{\mu\nu}}{\big(1-\frac{\phi^2\hat{\kappa}^2}{6}\big)^2}\partial_\mu\phi\partial_\nu\phi - V(\phi)\Big]. \tag{4.32}$$

Thus the theory now has a non-canonical field with a pole of order two in the coefficient of its kinetic term. One can also describe the same theory through a canonically normalized scalar field

$$\hat{\phi} = \frac{\sqrt{6}}{\hat{\kappa}}\tanh^{-1}\frac{\phi\hat{\kappa}}{\sqrt{6}} \tag{4.33}$$

One can easily verify that the two canonical description given by Eq. (4.20) and Eq. (4.33) are exactly equivalent. To feature the attractor properties in the n_s-r plane we require in addition a smooth potential function at the location of the pole.

4.5 Brans-Dicke theory as attractor models

In this section we will analyze Brans-Dicke models of inflation explicitly. A Brans-Dicke model is an example of $f(R)$-theory. In fact, $f(R)$-theory in metric formalism can be reformulated to the Brans-Dicke theory with Brans-dicke parameter $w = 0$. We will study here the attractor properties of the generalised Brans-Dicke theory defined by the following Lagrangian density,

$$\mathcal{L}_J = \frac{1}{2}\phi\, R - \frac{1}{2}\frac{\omega}{\phi}\, g^{\mu\nu}(\partial_\mu\phi)(\partial_\nu\phi) - U(\phi)\ , \tag{4.34}$$

where $U(\phi)$ is the potential function. Because of the presence of non-minimal coupling term, the description here is in Jordan frame. Now comparing this Lagrangian with the general conformal attractor in Eq. (4.9), we see that $\Omega^2(\phi) = \phi$ and $K_J(\phi) = \frac{\omega}{\phi}$. Switching to the Einstein frame we obtain

$$\mathcal{L}_E = \sqrt{-\tilde{g}}\left[\frac{1}{2}\tilde{R} - \frac{1}{2}\frac{(2\omega+3)}{2\phi^2}(\partial\phi)^2 - \frac{U(\phi)}{\phi^2}\right]. \tag{4.35}$$

The above equation has second-order pole in the kinetic term. It is clear that with the proper choice of the potential function $U(\phi)$, we can always construct models whose predictions are converged to the attractor point. For the kinetic term in the Einstein frame to be canonical we define,

$$\frac{d\hat{\phi}}{d\phi} = \sqrt{\frac{(2\omega+3)}{2\phi^2}} \tag{4.36}$$

Now we want to see for which choice of the potential function $U(\phi)$, the Brans-Dicke theory gives rise to the attractor like predictions. From our previous discussion in Sec. 4.2, we know that the choice of the potential must satisfy the three conditions mentioned there to show attractor properties. As the Lagrangian in Eq. (4.34) is exactly equivalent to that of the ξ-attractor, choice of potential in the Jordan frame can be either of the two forms: $f\left[(\phi-1)^{2n}\right]$ or $f\left[\left(\frac{\phi-1}{\phi+1}\right)^{2n}\right]$. In the Brans-Dicke case, the attractor mechanism is highly sensitive to the form of the higher order corrections to the potential. Even if we add these higher order corrections, the corrections have to take the forms as $a_m e^{-c\hat{\phi}}$ to preserve the attractor behaviour of the Lagrangian. See [89] for more discussion about the forms of the correction terms in the potential.

We make two following choices:

4.5.1 $\mathbf{U(\phi) = U_0(\phi-1)^2}$

where U_0 is a potential parameter that is to be fixed from the value of the scalar power spectrum. Even though there is a second-order pole at $\phi = 0$ in the kinetic term, however in terms of the canonical field obtained from Eq. (4.36), this pole shifts to infinity. In this case, the potential in terms of the canonical field in the Einstein frame is given by

$$V_E(\hat{\phi}) = U_0(1 - e^{-c\hat{\phi}})^2, \tag{4.37}$$

where $c = \sqrt{\frac{2}{2\omega+3}}$.

Let us now investigate the predictions of this potential in the light of PLANCK 2015 data. The observable predictions for this potential are shown in Fig. 4.3. The black dots

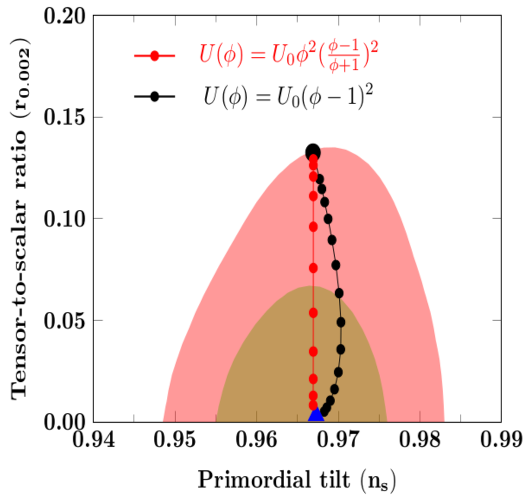

Figure 4.3: The variaton of n_s-r with the 68% and 95% CL contours from 2015 PLANCK data is shown here. The predictions asymptotically approaches to Starobinsky model (blue triangle) with decreasing ω .

indicate variations in the inflationary predictions with respect to the Brans-Dicke parameter ω ranging from 1 to about 10^6. The plot depicts that with decreasing the value of ω (top to bottom) the predictions of this model interpolates between quadratic chaotic inflation and Starobinsky model. Taking amplitude of scalar curvature perturabtions, A_s to lie within the 99.7% CL of the PLANCK data we fix $U_0 \sim 10^{-10}$. We now turn to a different choice of the potential function:

4.5.2 $\mathbf{U}(\phi) = \mathbf{U_0}\phi^2\left(\frac{\phi-1}{\phi+1}\right)^2$

In this case the potential function in the Einstein frame in terms of the canonically normalized inflaton field is given by

$$V_E(\hat{\phi}) = U_0 \tanh^2 \frac{\hat{\phi}}{\sqrt{4\omega+6}} \tag{4.38}$$

This potential is nothing but the simplest generalization of the T-model of α-attractor with the identification $\alpha = \frac{2}{3}\omega + 1$ [93]. Therefore, in the leading order approximation in the inverse efolds the inflationary predictions are

$$n_s = 1 - \frac{2}{N}, \qquad r = \frac{12(1+\frac{2\omega}{3})}{N^2}\,. \tag{4.39}$$

We numerically solve the dynamics in the above potential, and the observable predictions are plotted in Fig. 4.3.

4.6 Conclusions and Discussions

PLANCK 2015 data prefers inflation models with plateau-like potential with asymptotic flatness [28, 61]. Among many models, the modified gravity model proposed by Starobinsky has attracted a lot of attention due to its observational predictions that are nearly in the middle of 2-σ contours of spectral index and tensor-to-scalar ratio plane. A class of cosmological models has been found subsequently whose observational predictions in the n_s-r plane are attracted to this Starobinsky value when a parameter of the model is changed continuously. These models termed as attractor models, draw their attractor properties from certain pole structure of the kinetic term.

In this work, we have analysed the scalar-tensor theories of gravity in the light of the attractor models. In particular, we work with $f(R)$ gravity models and recast the models in the form of attractor models. Any particular choice of $f(R)$ automatically fixes the form of the scalar potential function. Therefore, even though any $f(R)$ model can be recast with the desired form of the kinetic energy with a certain pole structure, only for a certain case it satisfies the required condition for the scalar potential. This behaviour singles out R^2 gravity models from any other modifications. Any higher order term does not satisfy the desired asymptotic properties of the potential. We have analysed inflationary phenomenology when higher order terms in the action are also present. We also look at the Brans-Dicke theory of inflation and find suitable potential functions that automatically provides the attractor predictions when the Brans-Dicke parameter w is varied appropriately.

We also analyzed the stability of the attractor mechanism. Only for a certain choice of the potential function in the Jordan frame, the potential is asymptotically flat with constant vacuum energy. Any higher order term in the conformal function makes the potential asymptotically zero. But, if the attractor parameter ξ is increased sufficiently, the field range where observable inflation happens remains sufficiently flat, and the predictions return to the Starobinsky attractor point. This shows the robustness of the attractor mechanism. We also discuss how the predictions change when higher order poles are simultaneously present in the kinetic function. In this case, the existence of higher order pole always makes the predictions away from the usual attractor curve for second-order pole. If we decrease the residue of the second-order pole sufficiently, the effect of the second-order pole term becomes subdominant as ϕ_{60} remains almost constant.

The analysis can be extended to different generalised versions of scalar-tensor theories. In particular, it would be interesting to find attractor type solutions for theories with derivative couplings [102], and non-local modifications of gravity [103]. In these cases, the crucial point is to find a suitable conformal transformation that can recast the kinetic energy term with a certain pole structure in the Einstein frame and then design the proper functional form for attractor solutions. Further exploration along this line is interesting and we hope to come back to this later.

CHAPTER 5

WARM INFLATION

5.1 Introduction

Cosmological observations are in very good agreement with a universe that is expanding, spatially flat, homogeneous and isotropic on large scales, and where the large scale structure originated from primordial perturbations with a nearly Gaussian and scale-invariant spectrum [104–106]. On the theoretical side, in the standard paradigm of slow roll inflation, the inflaton quantum fluctuations are stretched out of the horizon due to the expansion and transferred to the curvature perturbation with constant amplitude spectrum on super-horizon scales.

However, since the Cosmic Microwave Background (CMB) radiation spectrum can be well explained with just a power-law primordial spectrum [28], we have information on the amplitude and the spectral index, but so far not much more than that. For example, there is as yet no detection of a primordial tensor component, which translates in an upper limit on the energy scale at which inflation took place. For single field models, where the dynamics during inflation is just controlled by a potential energy density, this seems to favor plateau-like potentials [10,54,55,107] or small field models [45,108,109], as opposed to large field models [9,110,111] for which the potential energy (and the tensor-to-scalar ratio) is larger.

This is the situation in the standard scenario of slow-roll inflation, which we can call "Cold Inflation" (CI), given that any other component of the energy density, and in particular radiation, will be quickly redshifted away even if present initially. However, inflation has to be followed by a radiation dominated period to allow for the synthesis of primordial nuclei (BBN), which requires the conversion of the inflaton energy density into radiation during the so-called (p)reheating period [112–115]. This necessarily implies interactions among the inflaton field and other light degrees of freedom, which may already play a role during inflation. Thus, the transfer of energy between the inflaton and radiation may start during inflation. This is the warm inflation (WI) scenario [15,116], where the energy transfer translates into extra friction or dissipative term Υ in the field EOM. The extra friction, therefore, favours slow-roll inflation, slowing down even further the evolution of the inflaton. Inflation can last for longer, and the relevant part of inflation when the primordial spectrum originates can happen at a smaller energy density value, which gives rise to a suppressed tensor-to-scalar ratio. The nature of the primordial spectrum can be completely different in WI due to the influence of the thermal bath fluctuations on the inflatons, such that the fluctuations will have now a thermal origin [117,118].

The specific functional form of the dissipative coefficient Υ with the inflaton field ϕ and the temperature T of the plasma will depend on the pattern of the inflaton interactions with other degrees of freedom [119–121]. Dissipation for example, may originate from the coupling of the inflaton and a heavy field mediator, which in turn decays into relativistic particles. This pattern does not introduce any thermal correction in the inflaton potential, the contribution of the mediators with mass $m_\chi > T$ being Boltzmann suppressed. Therefore, it does easily overcome the main difficulty faced originally to build viable warm inflation models [122, 123], i.e, preserving the required flatness of the potential to allow slow-roll inflation. However, the dissipative coefficient is only power law suppressed and one gets $\Upsilon \propto T(T/m_\chi)^\alpha$, where the power α of the ratio $T/m_\chi \lesssim 1$ depends on the bosonic/fermionic nature of the mediator and its decay products. Although it can give rise to viable models of inflation consistent with observations[1] [129, 130], it typically requires a large number of mediator fields for the effects of dissipation to be sizeable.

When the mediators are light, for example, fermions directly coupled to the inflaton, one has to check that the induced thermal corrections to the inflaton potential are under control, while still having strong enough interactions to allow the thermalization of the light degrees of freedom, and giving rise to enough dissipation. A scenario fulfilling these conditions has been recently proposed in [16]. In the same spirit as "Little Higgs" models, the inflaton is a pseudo-Nambu Goldstone boson (PNGB) of a broken gauge symmetry, its $T = 0$ potential being protected against large radiative corrections by the symmetry. Similarly, in order to avoid large T corrections due to the light fermions, a discrete (exchange) symmetry is imposed in the inflaton and fermionic sectors. This ensures that the leading field dependent thermal mass correction cancels out, leaving only the subleading T-dependent logarithmic one. This leads to a dissipative coefficient just linear in T, and to enough dissipation without the need of large no. of fields.

Given the possibilities for inflationary model building open up by the combination of symmetries and interactions/dissipation with a linear T coefficient, it is worth exploring the observational consequences and in particular, confront directly the model with CMB data. We will use the CosmoMC package to perform a multi-dimensional Markov Chain Monte Carlo (MCMC) analyses and derive constraints directly on the model parameters. We will focus on the simpler potential, the quartic chaotic potential $\lambda\phi^4$ model, which

[1]See Refs. [124–128] for consistent models of warm inflation with other dissipative coefficients.

although excluded in its CI version[2], it is compatible with data once the effects of the interactions are included [16]. Therefore the inflationary dynamics and the spectrum will be given by three parameters: the coupling λ in the inflaton potential; the combination of couplings C_T leading to linear dissipation $\Upsilon = C_T T$; and the effective no. of light degrees of freedom contributing to the thermal bath, g_*. The amplitude of the primordial spectrum and its scale dependence can be derived as a function of these parameters, and the prediction compared directly with the data without the need a priori of assuming a power-law parametrization. The scale dependence, given in terms of the comoving k scale at which perturbations exit the horizon during inflation, can be related to the no. of efolds N but implies some assumption about the (p)reheating period [26]. Typically one gets $N \in [50, 60]$ for the no. of efolds at which the largest observable scale crosses the horizon, and predictions are quoted varying N in this range. Our choice of the potential allows us to avoid this uncertainty in the predictions, given that the quartic potential will behave as radiation once inflation ends.

Recently in Ref. [134] the authors performed a thorough analysis of the different popular models of inflation in both the low and high-temperature regimes. The low-temperature regime is defined by the cubic dissipative coefficient whereas the high-temperature regime is described by a linear dissipative coefficient. In this work, our focus is on this high-temperature regime which has been first described in [16]. Ref. [134] did a statistical analysis of the models using CMB data and showed the viability of the scenario for different models which are excluded in CI scenario from present and (projected) future observations. Their work, besides the predictions for the spectral index and the tensor-to-scalar ratio, is largely motivated to accommodate the latest observed values of the running and

[2]Although it has been pointed out that 1-loop radiative corrections due to the interactions with other species can render the potential flat enough to lower the tensor-to-scalar ratio below the observable upper limit [131–133].

the running of the running of the spectral index[3]. Instead, in [17], we have chosen to work only with a particular, well motivated model as the quartic chaotic model, and study how well the data can constrain the parameters of the model. Some of the main differences in approach between Ref. [134] and our work are that, firstly, they fixed the potential parameters with the observable value of the amplitude of the spectrum, and g_* depending on the model; while we have kept both the model parameter (λ) and g_* as variables. Secondly, they chose to work with a fixed no. of e-folds, $N = 55$, while we vary the number of e-folds of infation because of its implicit dependence on the model dynamics. Moreover, they focus on the dependence with respect to the dissipative ratio, $Q = \Upsilon/(3H)$, i.e, the dissipative coefficient normalized to the Hubble parameter H. This would be equivalent to our choice of parameter C_T. And more crucially, they always consider the inflaton to be included in the thermal bath which is equivalent to the thermal case discussed in our work, but we additionally analysed the case where the inflaton does not have a thermal distribution (non-thermal case).

The plan of the chapter is as follows. In Sec. 5.2 we describe the basic mechanism of the warm inflation dynamics and the validity of slow-roll approximation during inflation. In Sec. 5.3 we give the expression for the primordial spectrum as a function of the parameters of the model, and how to get its scale dependence. Using the analytical expressions, we explore the parameter dependence of the predictions in Sec. 5.4. In Sec. 5.5 we describe the technical details of the analyses done with the MCMC and the CMB data, while in Sec. 5.6 we present the main results. Finally, a summary and the conclusions of this work are given in Sec. 5.7.

[3]General consistency relations for WI including the scale dependence of the spectral index were first considered in [135].

5.2 Basics of Warm Inflation

In warm inflation, the transfer of energy between the inflaton scalar field ϕ and the plasma leads to an additional friction term in the inflaton equation of motion [116, 136], described by the damping coefficient $\Upsilon(\phi, T)$. When dissipation leads to the production of light degrees of freedom which thermalize in less than a Hubble time, then a radiation fluid ρ_r is produced, continually replenished by the effective decay of the inflaton field. The background evolution equations for the inflaton-radiation system are given by:

$$\ddot{\phi} + (3H + \Upsilon)\dot{\phi} + V_{,\phi} = 0, \tag{5.1}$$

$$\dot{\rho}_r + 4H\rho_r = \Upsilon\,\dot{\phi}^2\,, \tag{5.2}$$

where a "dot" denotes time derivatives, $V_{,\phi} = dV/d\phi$, V is the potential energy density, and H the Hubble parameter:

$$3H^2 = \frac{\rho}{M_{\rm Pl}^2}\,, \tag{5.3}$$

ρ being the total energy density of both field and radiation, and $M_{\rm Pl}$ is the reduced Planck mass. The radiation fluid is made of g_* relativistic degrees of freedom at temperature T, with:

$$\rho_r = \frac{\pi^2}{30} g_* T^4 = C_R T^4\,. \tag{5.4}$$

Prolonged inflation requires the slow-roll conditions $|\epsilon_X| \ll 1$, where $\epsilon_X = -d\ln X/Hdt$, and X is any of the background field quantities. The background equations at leading order in the slow-roll approximation of small ϵ_X become

$$
\begin{aligned}
3H(1+Q)\dot{\phi} &\simeq -V_{,\phi}\,, && (5.5)\\
4\rho_r &\simeq 3Q\dot{\phi}^2\,, && (5.6)\\
3H^2 &\simeq \frac{V}{M_{\rm Pl}^2}\,, && (5.7)
\end{aligned}
$$

where $Q = \Upsilon/(3H)$ is the dissipative ratio.

We will consider a linear T dissipative coefficient like in Ref. [16]. Dissipation comes from the coupling of the inflaton field to a pair of fermions with coupling g, while the latter interacting with a light scalar field with coupling h. We stress that the calculation of the dissipative coefficient is done in the adiabatic and quasi-equilibrium approximation, which impose some restrictions on the values of the parameters. First, once the inflaton excites the fermions to which it directly couples, they decay into scalars which have to thermalize in less than a Hubble time, i.e., the decay rate must be larger than H. In addition, we require $T > H$, such that dissipation can be computed in the limit of flat spacetime with the standard tools of Thermal Quantum Field Theory [137]. Under those restrictions, the dissipative coefficient is then given by $\Upsilon = C_T T$, with C_T being a function of the couplings:

$$
C_T \simeq \frac{3g^2/h^2}{1-0.34\ln h}\,. \tag{5.8}
$$

For the inflaton potential, we work with the single-field chaotic quartic potential,

$$
V(\phi) = \lambda\phi^4\,, \tag{5.9}
$$

which is not excluded by observations once dissipation is taken into account [16, 129]: the extra friction slows down the motion and effectively “flattens” the potential seen by the inflaton, and therefore it tends to lower the predicted tensor-to-scalar ratio. The slow-roll parameters are given by:

$$\epsilon_\phi = \frac{M_{\rm Pl}^2}{2}\left(\frac{V_\phi}{V}\right)^2 = 8\left(\frac{M_{\rm Pl}}{\phi}\right)^2 , \tag{5.10}$$

$$\eta_\phi = M_{\rm Pl}^2\left(\frac{V_{\phi\phi}}{V}\right)^2 = 12\left(\frac{M_{\rm Pl}}{\phi}\right)^2 , \tag{5.11}$$

$$\sigma_\phi = M_{\rm Pl}^2\left(\frac{V_\phi/\phi}{V}\right) = 4\left(\frac{M_{\rm Pl}}{\phi}\right)^2 . \tag{5.12}$$

Notice that, given the extra friction term Υ, to have slow-roll inflation we now require:

$$\epsilon_\phi < 1+Q\,, \quad \eta_\phi < (1+Q)\,, \quad \sigma_\phi < (1+Q)\,. \tag{5.13}$$

From the slow-roll equations (Eq. (5.5)-Eq. (5.7)), one can get the relation between Q and ϕ:

$$Q^3(1+Q)^2 = \frac{4}{9}\left(\frac{C_T^4}{C_R\lambda}\right)\left(\frac{M_{\rm Pl}}{\phi}\right)^6 . \tag{5.14}$$

Similarly, one can write directly the evolution equation for the dissipative ratio Q, with respect to the no. of e-folds $dN = Hdt$:

$$\frac{dQ}{dN} \simeq \frac{Q}{3+5Q}\left(6\epsilon_\phi - 2\eta_\phi\right) , \tag{5.15}$$

which for the quartic potential, and using Eq. (5.14) reduces to:

$$\frac{dQ}{dN} \simeq C_Q\frac{Q^2(1+Q)^{2/3}}{3+5Q} , \tag{5.16}$$

where:

$$C_Q = 24 \left(\frac{4C_T^4}{9C_R\lambda} \right)^{-1/3} . \tag{5.17}$$

Eq. (5.16) can be integrated in terms of hypergeometric functions:

$$\begin{aligned} C_Q N &= f(Q_e) - f(Q_*) \,, \\ f(x) &= -3 \left(\frac{(1+x)^{1/3}}{x} + \frac{3}{x^{5/3}} \, {}_2F_1[2/3, 2/3, 5/3, -1/x] \right) . \end{aligned} \tag{5.18}$$

By Q_* we denote the value at horizon crossing of observable modes at CMB at N e-folds before the end of inflation, and by Q_e the value of the dissipative ratio at the end of inflation. We take the condition $\eta_\phi = 1 + Q_e$ signaling the end of inflation, and using this condition in Eq. (5.14) we have:

$$\frac{Q_e^3}{(1+Q_e)} = \frac{C_T^4}{2^4 \times 3^5 \times C_R\lambda} . \tag{5.19}$$

Given a value of N, Eq. (5.18) can be inverted (numerically) to get the value of Q_* (and then ϕ_*), needed to evaluate the amplitude of the primordial spectrum. We will revise this in the next section.

5.3 Warm inflation: primordial spectrum

The general expression for the amplitude of the primordial spectrum, independent of the nature of the dissipative coefficient, is given by [117, 118]:

$$P_{\mathcal{R}} = (P_{\mathcal{R},diss} + P_{\mathcal{R},vac}) = \left(\frac{H_*}{\dot{\phi}_*} \right)^2 \left(\frac{H_*}{2\pi} \right)^2 \left[\frac{T_*}{H_*} \frac{2\pi Q_*}{\sqrt{1+4\pi Q_*/3}} + 1 + 2\mathcal{N}_* \right] , \tag{5.20}$$

where all variables are evaluated at horizon crossing. The first term is the contribution due to the effect of dissipation on the inflaton fluctuations. In the limit of no dissipation, we would recover the standard expression for the primordial spectrum, but allowing the inflaton fluctuations to be in a statistical state other than the vacuum; for example being in a thermal excited state with $\mathcal{N}_* = n_{BE}(a_* H_*) = (e^{H_*/T*} - 1)^{-1}$. The standard Bunch-Davies vacuum is given by $\mathcal{N}_* = 0$. The latter case will be called in the following as "non-thermal" inflaton fluctuations, while we use "thermal" for the $\mathcal{N}_* = n_{BE}(a_* H_*)$ case. In [118] it has been checked that indeed the analytic solution of Eq. (5.20) reproduces the spectrum of warm inflation up to values $Q_* \lesssim 0.1$, by numerically integrating the equations for the fluctuations.

For larger dissipation at horizon crossing, the spectrum gets enhanced due to the coupling between inflation and radiation fluctuations. This effect depends on Q_*, and can be accounted for by multiplying the spectrum in Eq. (5.20) by a a function $G[Q_*]$ [118],

$$G[Q_*] \simeq 1 + 0.0185 Q_*^{2.315} + 0.335 Q_*^{1.364} \,. \tag{5.21}$$

This parametrization however depends on both the inflaton potential and the T dependence of the dissipative parameter. We quote in Eq. (5.21) the values obtained for a quartic potential with a linear T dependent Q [16].

In the above expression for the spectrum, one can replace T_*/H_* by $3Q_*/C_T$ and the field dependence (in H_* and $\dot{\phi}_*$) in terms of Q_* using Eq. (5.14):

$$P_{\mathcal{R}} = \frac{C_T^4}{4\pi^2 \times 36 C_R} Q_*^{-3} \left[\frac{3Q_*}{C_T} \frac{2\pi Q_*}{\sqrt{1 + 4\pi Q_*/3}} + 1 + 2\mathcal{N}_* \right] \times G[Q_*] \,. \tag{5.22}$$

Therefore, the spectrum is given implicitly as a function of the parameters of the model, C_T, $C_R(g_*)$ and λ, and the no. of e-folds N through Eq. (5.18). In the case of having a thermal spectrum for the inflaton fluctuations, we also have:

$$1 + 2\mathcal{N}_* = \coth \frac{H_*}{2T_*} = \coth \frac{C_T}{6Q_*} \,. \tag{5.23}$$

The no. of e-folds can be related to the scale at which the fluctuation exits the horizon $k = a_* H_*$ so that finally we have the spectrum as a function of the comoving scale k. However, the relation between N and k depends on the details of reheating [26, 138–140], the period between the end of inflation and a radiation dominated universe [58–60]. Modeling our ignorance about reheating with an effective equation of state $\tilde{w}$, the relation between the no. of efolds and the comoving wavenumber is given by [26]:

$$N(k) = 56.12 - \ln \frac{k}{k_0} + \frac{1}{3(1+\tilde{w})} \ln \frac{2}{3} + \ln \frac{V_k^{1/2}}{V_{\rm end}^{1/2}} + \frac{1-3\tilde{w}}{3(1+\tilde{w})} \ln \frac{\rho_{\rm reh}^{1/4}}{V_{\rm end}^{1/4}} + \ln \frac{V_{\rm end}^{1/4}}{10^{16}\,{\rm GeV}} \tag{5.24}$$

where $k_0 = 0.05\,{\rm Mpc}^{-1}$ is the pivot scale for PLANCK, V_k and $V_{\rm end}$ the potential values at the end and $N(k)$ e-folds before the end of inflation respectively, and $\rho_{\rm reh}$ the energy density at the end of reheating when the universe becomes radiation dominated. Typically the no. of efolds at which the largest observable scale leaves the horizon lies between $50 - 60$. But this intrinsic uncertainty in the inflationary predictions on the no. of e-folds is avoided in warm inflation with a quartic potential. In this case the dissipative ratio Q increases during inflation, such that the radiation by the end becomes comparable to the inflaton energy density (signalling also the end of inflation). And for a quartic potential, once the field starts oscillating around the minimum of the potential, the average energy density behaves as radiation. It does not matter when the inflaton finally decays after inflation, because the universe is already radiation dominated. This is equivalent to having instant reheating (i.e., and instant transition between inflation and the radiation dominated epoch), with $\tilde{w} = 1/3$ and $\rho_{\rm reh} = V_{\rm end}$ in Eq. (5.24):

$$N(k) \;=\; 56.02 - \ln \frac{k}{k_0} + \ln \frac{V_k^{1/2}}{V_{\rm end}^{1/2}} + \ln \frac{V_{\rm end}^{1/4}}{10^{16}\,{\rm GeV}} \,. \tag{5.25}$$

Therefore, instead of taking a certain N interval to derive the observable predictions of the model, like in other studies [134], we will compute directly the k-dependent power spectrum using Eq. (5.25). The value of the potential at the end of inflation can be obtained with the value of Q_e in Eq. (5.19) and

$$12\frac{M_{\rm Pl}^2}{\phi_e^2} = \frac{12\lambda}{V_{\rm end}^{1/2}} = 1 + Q_e \,. \tag{5.26}$$

And for the ratio $(V_k/V_{\rm end})^{1/2} = (\phi_k/\phi_e)^2$ we have:

$$\left(\frac{\phi_k}{\phi_e}\right)^2 = \frac{Q_e(1+Q_e)^{2/3}}{Q_k(1+Q_k)^{2/3}} \,. \tag{5.27}$$

Through the field dependence in V_k and $V_{\rm end}$, the relation between the scale k and the no. of efolds depends on the parameters of the model C_T, λ and $C_R(g_*)$.

The primordial tensor spectrum is not affected by dissipation, so we have the standard prediction:

$$P_T = 8\left(\frac{H_*}{2\pi M_{\rm Pl}}\right)^2 \,, \tag{5.28}$$

which for a quartic potential is just given by:

$$P_T = \frac{8\lambda}{4\pi^2}\left(\frac{\phi_*}{M_{\rm Pl}}\right)^4 = \frac{8\lambda^{1/3}}{4\pi^2}\left(\frac{4C_T^4}{9C_R}\right)^{2/3}\frac{1}{Q_*^2(1+Q_*)^{2/3}} \,, \tag{5.29}$$

where we have used Eq. (5.14). Finally, the tensor-to-scalar-ratio in terms of the parameters of the model (and Q_*) is given by:

$$r = \frac{P_T}{P_{\mathcal{R}}} = 32\left(\frac{16C_T^4}{9\lambda C_R}\right)^{-1/3} Q_*^3 \left[\frac{3Q_*}{C_T}\frac{2\pi Q_*}{\sqrt{1+4\pi Q_*/3}} + 1 + 2\mathcal{N}_*\right]^{-1} \times G[Q_*]^{-1}\,. \quad (5.30)$$

In the next section, we will calculate the scalar and tensor power spectrum as a function of k and will determine its parameter dependence followed by the the best fit parameter estimation in the following section.

5.4 Analysing parameter dependence on observables

In this section, we will analyse the parameter dependences of warm inflation model on inflationary observables. In particular, we will consider the scalar spectral index n_s and the scalar amplitude A_s as observables, which are functions of the parameters C_T, λ and g_*. For the choices of the parameters, the upper bound on the tensor amplitude r would be trivially satisfied, and for that purpose, we do take it as a constraint in this section. But, for parameter estimation in the next section, the tensor amplitude would be incorporated accordingly. For our consideration, we will see that the running of the spectral index would be very small (being consistent with recent observations [134, 141]), and we will not consider it as a constraining observable. The analysis of this section would be useful in determining the range of parameters as priors for the CosmoMC simulations and parameter estimation later.

Our first goal is to calculate the scalar amplitude given by Eq. (5.22) as a function of comoving wavenumber k. Other than the model parameters, the expression depends on the dissipative ratio Q that needs to be calculated at horizon crossing for each wavenumber. The k dependence of the scalar amplitude is implicit via its dependence in Q. For a particular set of C_T, λ and g_*, the value Q_e (the value at the end of inflation) is determined from Eq. (5.19), and ϕ_e can be calculated using Eq. (5.14). Note that, Eq. (5.14) gives one to one relation between ϕ and Q. On the other hand, using Eq. (5.18) and Eq. (5.25), Q can be solved as a function of k. But instead of inverting the hypergeometric function of Eq. (5.18), we solve Eq. (5.16) and Eq. (5.25) iterataively (numerically) and find $Q(k)$. We plug it in Eq. (5.22) to find the scalar amplitude as a function of k/k_0 for both the non-thermal ($\mathcal{N}_* = 0$) and thermal ($\mathcal{N}_* \neq 0$) cases. We follow the same procedure in calculating the tensor amplitude from Eq. (5.29). This algorithm is incorporated in the CAMB code [142] in the form of a subroutine in calculating the C_ℓ s for the two-point correlation functions. The pivot scale is taken at usual $k = 0.05$ Mpc^{-1} throughout the analysis.

The results for the spectrum as a function of the scale k/k_0 are shown in Fig. 5.1. We have done an example for the parameter values: $\lambda = 10^{-14}$, $g_* = 12.5$, and different values of C_T as indicated in the figure. The lowest value of C_T included in the plot gives a value $Q_* \sim 10^{-7}$, whereas for $C_T \sim 10^{-1}$, $Q_* \sim 10$. The minimum allowed value of Q_* can be calculated from the condition $T_*/H_* \simeq 1$. We note that increasing the value of C_T increases the scalar amplitude, and for the non-thermal case, the amplitude reaches to an asymptotic lower value when C_T becomes very small. To inspect the nature of the parameters better, it is judicious to compare the warm inflation power spectrum given by Eq. (5.22) to the standard power law power spectrum defined as:

$$P_{\mathcal{R}}(k) = P_{\mathcal{R}}(k_0) \left(\frac{k}{k_0}\right)^{n_s - 1} . \tag{5.31}$$

The spectral index is plotted as a function of the model parameters in Fig. 5.2. The dependence is shown for three different values of λ as indicated in the figure. In Fig. 5.2a, the variation is over C_T with $g_* = 12.5$ and in Fig. 5.2b, the variation is over g_* with

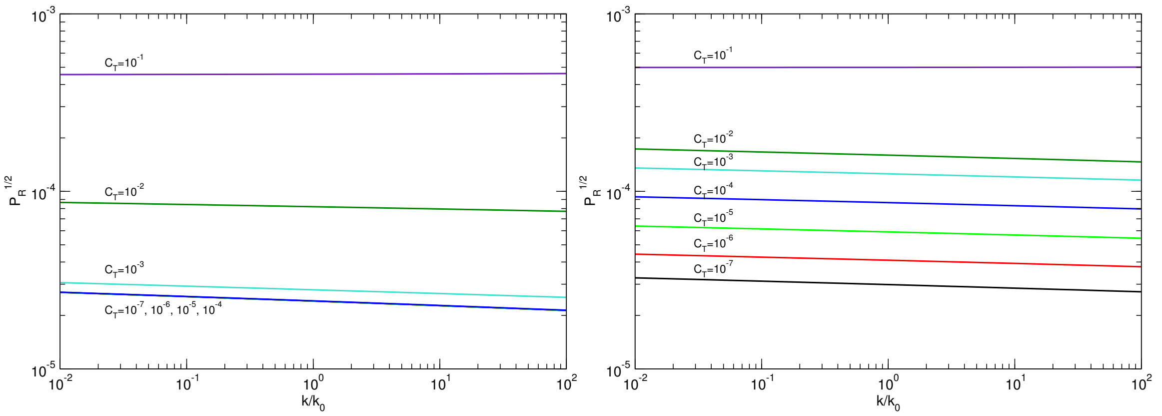

(a) (b)

Figure 5.1: Primordial spectrum as a function of k/k_0, for different values of the parameter $C_T = 10^{-7}$, 10^{-6}, ...10^{-1} and for fixed $\lambda = 10^{-14}$, $g_* = 12.5$. Fig. (a) is for a non-thermal inflaton, i.e, $\mathcal{N}_* = 0$ and Fig. (b) is for a thermal inflation, i.e., $\mathcal{N}_* \neq 0$.

$C_T = 0.004$. For warm inflation with $\mathcal{N}_* = 0$, the C_T-n_s plot in Fig. 5.2a shows that for small values of $C_T \lesssim \mathcal{O}(10^{-4})$, well in the weak dissipative regime with $Q_* \ll 1$, the first term within the brackets in Eq. (5.22) is negligible. Therefore, one recovers the standard expression in cold inflation where the spectrum is red-tilted and hardly depends on[4] λ. As C_T (Q_*) increases, the dissipative contribution tends to make the spectrum less red-tilted, and for values $C_T \gtrsim 0.1$, the growing mode will render the spectrum blue-tilted. In the intermediate regime, the spectral index shows oscillatory behaviour while being roughly consistent with PLANCK 2-σ limits. In the case $\mathcal{N}_* \neq 0$, the spectral tilt has a little higher value than the non-thermal case for small C_T due to non-zero value of $\mathcal{N}_*$ in Eq. (5.22) where the contribution depends on C_T as Eq. (5.23). For $C_T \gtrsim 1$, the contribution from growing mode makes the spectrum blue-tilted in a similar way as in the non-thermal case. The observational bounds on n_s exclude the blue-tilt part. The Fig. 5.2b shows that for both non-thermal and thermal warm inflation scenarios, the variation of n_s with g_* is small.

[4] The mild dependence on λ comes from the relation between the no. of e-folds and k in Eq. (5.25).

From this observation, we can anticipate that in the process of parameter estimation to be done in the next section, g_* might not be well constrained from the limits of the spectral index.

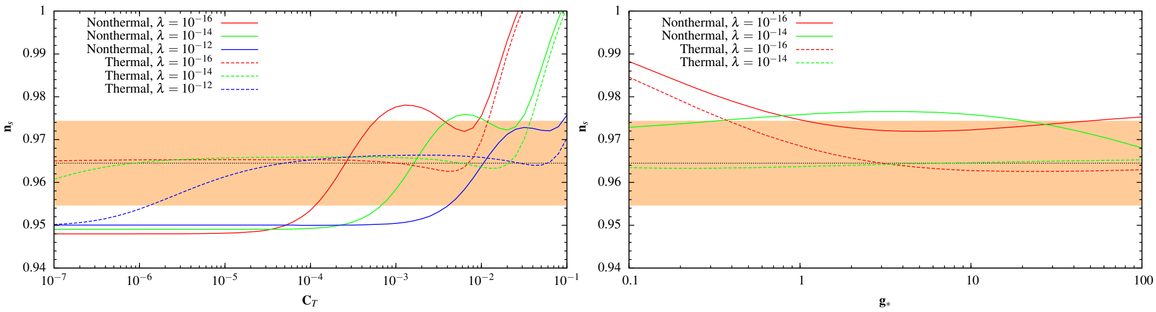

(a) (b)

Figure 5.2: Spectral index as a function of C_T with $g_* = 12.5$ in Fig. (a) and as a function of g_* with $C_T = 0.004$ in Fig. (b) for different values of λ as indicated in the plot. The solid lines are for $\mathcal{N}_* = 0$ and the dashed lines are for $\mathcal{N}_* \neq 0$. The horizontal black line denotes the marginalised central value for PLANCK TT,TE,EE+lowP data and the light brown band represents the observational 2-σ bounds on n_s from the same data combination.

In Fig. 5.3 we fit $P_{\mathcal{R}}(k_0) = A_s$ for the same specification of the parameters mentioned in the previous paragraph. Both Fig. 5.3a and Fig. 5.3b show that the observed range for A_s allows the parameter ranges for C_T and g_* with tighter constraints. It is important to note that in contrast to the cold inflation scenario with a quartic potential, the amplitude of scalar perturbations in the case of warm inflation depends substantially on other parameters, namely C_T and g_*. Analysis from Figs. 5.2 and 5.3 helps us to choose prior ranges for the parameters to be inserted in the COSMOMC run for parameter estimations in the next section.

In all the above discussions, we have neglected the running of the spectral index. Instead of a simple power law, we could include the running $(\alpha_s(k_0) = \frac{dn_s}{d(\ln k)})$ or other higher

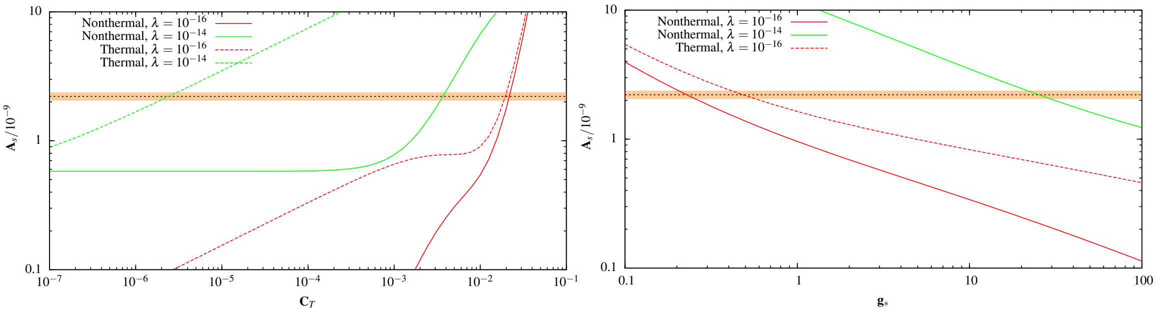

(a) (b)

Figure 5.3: Amplitude of spectrum A_s as a function of C_T with $g_* = 12.5$ in Fig. (a) and as a function of g_* with $C_T = 0.004$ in Fig. (b) for different values of λ as indicated in the plot. The solid lines are for $\mathcal{N}_* = 0$ and dashed lines are for $\mathcal{N}_* \neq 0$. The horizontal dotted black line denotes the marginalised central value for PLANCK TT,TE,EE+lowP data and the light brown band represents the observational 2-σ bounds on A_s from the same data combination. In Fig. (b), the thermal case with $\lambda = 10^{-14}$ is not inlcuded because it gives an amplitude larger than $A_s \sim 10^{-8}$ for $g_* \lesssim 10^3$.

order derivatives of the spectral index in the fit as well,

$$P_{\mathcal{R}}(k) = P_{\mathcal{R}}(k_0)\left(\frac{k}{k_0}\right)^{n_s(k)-1}, \tag{5.32}$$

$$n_s(k) = n_s(k_0) + \frac{1}{2}\alpha_s(k_0)\ln\frac{k}{k_0} + \cdots . \tag{5.33}$$

However, as shown in Fig. 5.4 this is always small with $|\alpha_s| \lesssim 10^{-4}$, as it was also found in [134]. And again, the change from negative to positive values of α_s when increasing C_T is due to the growing mode. Nevertheless, given that the estimated value of the running in this model is below the sensitivity of current and future CMB experiments [141] and assuming that higher order contributions will be lesser, we will not include the running or other higher order terms in our current analysis.

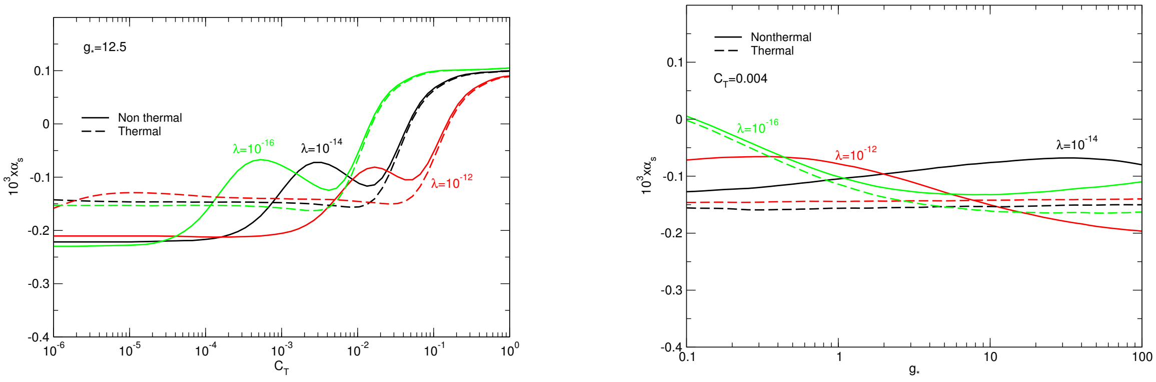

(a)

(b)

Figure 5.4: Running of the spectral index as a function of C_T with $g_* = 12.5$ in Fig. (a), and as a function of g_* with $C_T = 0.004$ in Fig. (b), for different values of λ as indicated in the plot. The solid lines are for $\mathcal{N}_* = 0$ and dashed lines are for $\mathcal{N}_* \neq 0$.

5.5 Methodology of analysis

From the analysis of the previous section, we know the range for which we expect to find the best fit parameters. In our case, inflationary power spectrum, both scalar and tensor, are known in terms of three parameters: (i) C_T, the proportionality constant for the dissipative coefficient, (ii) λ, the quartic coupling constant for the inflaton scalar potential, and (iii) g_*, the total number of relativistic d.o.f in radiation bath. These three parameters can be thought equivalent to the usual parameterization by the scalar spectral amplitude A_s, scalar spectral index n_s, and tensor-to-scalar ratio r representing the amplitude of tensor fluctuations. In addition to these primordial parameters, the spatially flat background cosmology is described by four other parameters, namely $\Omega_b h^2$ and $\Omega_c h^2$ (h is related to the present Hubble parameter) representing baryon and dark matter densities respectively, the acoustic peak angular scale θ, and the reionization optical depth τ. Effectively, we have exactly the same number of parameters as like the usual ΛCDM+r model. Although our goal is to constrain the model parameters C_T, λ and g_*, for convenient comparison with the data we will quote values of n_s and r for the marginalised and best fit values of the parameters with the usual assumption of power spectrum given by Eq. (5.31) with flat tensor spectrum.

We analyse the warm inflation scenario using a multi-dimensional Markov Chain Monte Carlo (MCMC) simulation provided by the publicly available COSMOMC package [14] coupled to the PLANCK 2015 data [106] and BICEP2/KECK array data [31]. This analysis uses Bayesian parameter estimation to constrain the model parameters C_T, λ and g_* and find respective posterior probability distributions. As outlined in the previous section, we calculate the primordial scalar and tensor spectrum for all wave vectors required by CAMB that calculate C_ℓs using the following relation [143]:

$$C_\ell = \int d(\ln k) P_{\mathcal{R}}(k) T_l^2(k), \tag{5.34}$$

where $T_l(k)$ is the transfer function that evolves the power spectrum from the end of inflation to the last scattering surface, and it depends only on the background parameters. These C_ℓ values are fed into COSMOMC for different points in the multi-dimensional parameter space. These theoretically calculated C_ℓ's are then compared to the data using Bayesian analysis, given the prior probability distributions for the parameters that are varied. COSMOMC code analyses the parameter spaces, provides posterior probability distributions for the parameters and determines a marginalised χ^2 for these distributions. We emphasise that we have modified only the inflationary sector by plugging in the power spectrum $P_{\mathcal{R}}(k/k_0)$ for the warm inflation as a function of the model parameters instead of a usual power-law expression.

While doing the MCMC analysis for the warm inflation case, instead of C_T we have constrained $\ln(C_T \times 10^{10})$ in COSMOMC so that we can simply use the standard parameters already defined in the CAMB code. The parametrisations of λ and g_* are different for the non-thermal and thermal cases which are discussed later. The prior ranges for the warm inflation parameters are chosen after analysing the dependence of the parameters on the pivot scalar amplitude and spectral index (see Figs. 5.2, 5.3). But, even then, there are multiple sets of values in the parameter space (λ, C_T, g_*) that correspond to the same value of χ^2 when compared to the CMB data. We have checked it explicitly. This degeneracy is shown in Fig. 5.5 for the case of non-thermal warm inflation ($\mathcal{N}_* = 0$), where the scattered points are plotted in the 3-dimensional parameter space $\ln(C_T \times 10^{10})$, $\sqrt{\lambda} \times 10^7$ and g_*, with $\log(\chi^2)$ represented in the colour spectrum. The points with the darkest blue colour in the parameter space are the degenerate points for minimum or near-to-minimum value of χ^2. The lack of clustering of these dark blue points around a single point in this plot implies that multiple degenerate points can be sampled while minimising χ^2 using a typical MCMC procedure. Therefore, the posterior probability distribution of these parameters can have multiple peaks and subpeaks (multimodal systems). This was practically encountered many times while performing the MCMC analysis. Similar degeneracy can be observed in the parameter space for thermal warm inflation scenario also. For this reason, the warm inflation COSMOMC sampling faced the challenge of slow mixing and therefore slow convergence.

For the non-thermal case ($\mathcal{N}_* \neq 0$), this problem was statistically dealt with the use of higher *temperature* (t) of the MCMC chains with the default sampling algorithm. The *temperature* (t) defines how likely it is to sample from a low-density part of the target distribution. The advantage of low t system is more precise sampling but on the other hand, it can get trapped in a local region of the phase space. Especially, in case of a theory with multiple modes, keeping low t would mean definite entrapment in local modes. Though high t-analysis is less precise in sampling with respect to those with low t, it ensures sampling of a large volume of the phase space. Thus, increasing the *temperature* of the chains saved computation time without making too much compromise. The standard procedure is to set *temperature* $t = 1$ in CosmoMC, and we have taken $t = 2$ to serve our purpose[5].

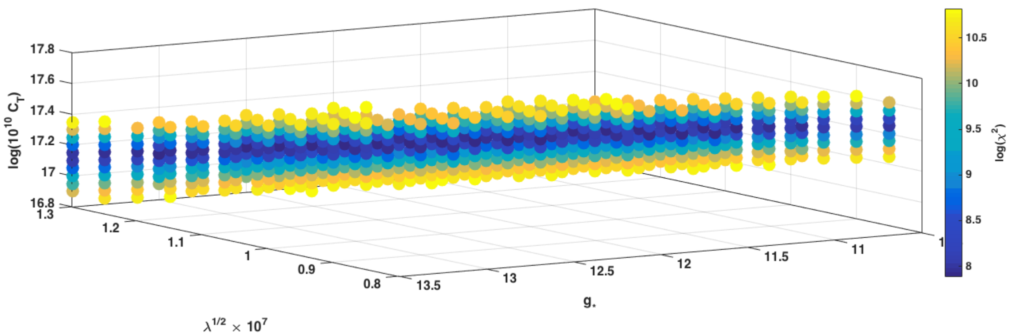

Figure 5.5: Scattered points in the 3-dimensional parameter space with different values of $\log(\chi^2)$ for warm inflation with non-thermal fluctuations. The points with colour in the extreme blue end of the spectrum correspond to minimum χ^2. Instead of centred around a region, multiple dark blue points along a strip represent multiple modes in the probability space.

For the thermal case, careful reparametrisation is needed due to the presence of non-zero $\mathcal{N}_*$ in the expression for the power spectrum given by Eq. (5.20). Through the term $\mathcal{N}_*$, there is an overall factor of $C_T^4/C_R\lambda$. Therefore, the dependence on g_* is different from the non-thermal case. For our convenience we have reparametrised g_* as $19 - \log(30C_T^4/\pi^2 g_*\lambda)$. This reparametrisation is done following hierarchical centering [144] which is an algorithm to replace original parameters in a model with modified parameters that are less correlated with each other in the joint posterior distribution. The multimodality in the posterior distribution becomes more cumbersome in this case due to more mixing between the model parameters. Therefore the sampling method for the MCMC chains was also changed to Wang-Landau sampling algorithm[6] [145, 146] which is

[5]Note that this *temperature*(t) is merely a technical term used in the MCMC statistics and is to be distinguished from the warm inflation temperature (T) defined in Eq. (5.4). The temperature of the chains can be changed in the common.ini file in CosmoMC. If the temperature is modified, the corresponding post-processing can be taken care of in GetDist by modifying the cool parameter.

[6]sampling method=6 in the CosmoMC package

better sampling to tackle unknown target distributions. In addition, the *temperature* of the chains is also increased to 2. All these statistical tweaks help to deal with the secondary peaks and long tails in the posterior distributions and lead to faster and better convergence as well.

5.6 Results and Discussions

In this section, we present our results both for the thermal and non-thermal case. The COSMOMC code constrains the model parameters as well as the late time cosmological parameters for warm inflation and estimates the posterior probability distribution with marginalised central values and standard deviations.

The following Figs. 5.6 and 5.8 show the posterior distributions for the model parameters. The parametrisation is done as $(\ln(C_T \times 10^{10}), \sqrt{\lambda} \times 10^7, g_*)$ for the non-thermal case (Fig. 5.6) and as $(\ln(C_T \times 10^{10}), \sqrt{\lambda} \times 10^7, 19 - \log(30C_T^4/\pi^2 g_* \lambda))$ for the thermal case (Fig. 5.8) respectively as mentioned in the earlier section. The likelihoods used here are PLANCK TT+TE+EE, PLANCK lowP, estimated using commander, PLANCK lensing and BICEP2/KECK array and PLANCK joint analysis likelihood [18, 31, 35]. These plots show both one-dimensional and two-dimensional marginalised posterior distributions for these parameters. The marginalised central values are determined by post-processing using GETDIST package included in COSMOMC.

In Table 5.1, the marginalised values for the model parameters along with the late time cosmological parameters in ΛCDM model are quoted with their respective 1-σ errors. In the case of the non-thermal warm inflation, it can be seen from Fig. 5.6 that the posterior probability for g_* has a long tail and is far from a Gaussian distribution. This can be interpreted as an effect of the degeneracy in the parameter space as mentioned earlier in

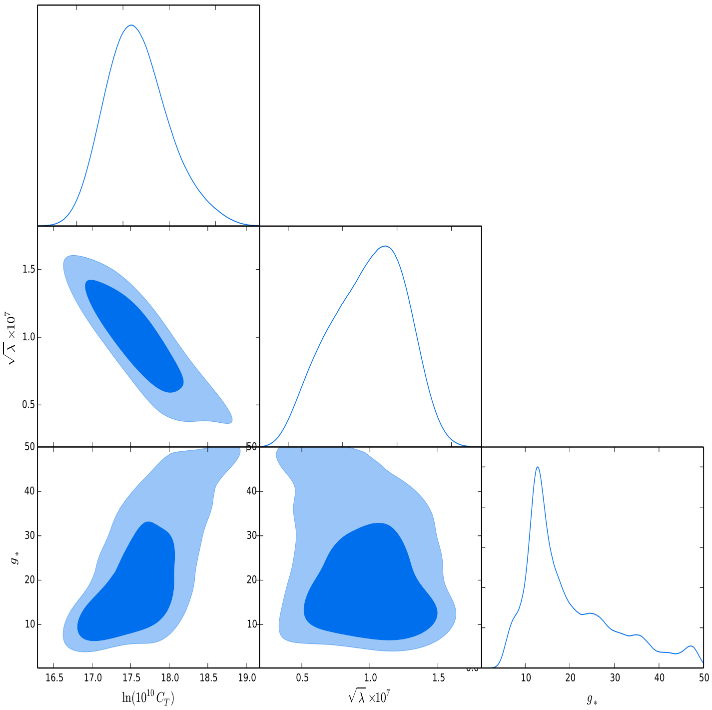

Figure 5.6: Triangle plot for the model parameters C_T, λ and g_* when $\mathcal{N}_* = 0$. Diagonal plots are the marginalised probability densities for these parameters and off diagonal plots represent 68% and 95% confidence limits for the variation of two sets of model parameters.

Table 5.1: Constraints on cosmological parameters for non-thermal and thermal case compared with ΛCDM $+r$ using PLANCK 2015+BICEP2/KECK Array [18, 31, 35] observations .

Warm Inflation					Cold Inflation		
	$\mathcal{N}_* = 0$		$\mathcal{N}_* \neq 0$			ΛCDM$+r$	
parameters	mean value	1σ	mean value	1σ	parameters	mean value	1σ
$\Omega_b h^2$	0.02233	0.00022	0.02224	0.00019	$\Omega_b h^2$	0.02224	0.00017
$\Omega_c h^2$	0.1178	0.0015	0.1194	0.0013	$\Omega_c h^2$	0.1192	0.0016
$100\theta_{MC}$	1.04097	0.00046	1.04088	0.00038	$100\theta_{MC}$	1.04085	0.00034
τ	0.077	0.019	0.068	0.021	τ	0.064	0.018
C_T	0.0043	0.0018	0.0104	0.0077	$\ln(A_s \times 10^{10})$	3.06	0.031
λ	9.77×10^{-15}	5.41×10^{-15}	9.74×10^{-16}	6.78×10^{-16}	n_s	0.966	0.0052
g_*	20.03	10.39	139.91	487.98	r	< 0.07	

Sec. 5.5. Therefore, the marginalised mean value and standard deviation for g_* in Table 5.1 is not completely conclusive as marginalisation is done by fitting the posterior distribution as a Gaussian. The marginalised mean value for the inflationary parameters are as follows:

$C_T = 0.0043$, $\lambda = 9.77 \times 10^{-15}$, and $g_* = 20.03$. Looking at the 1-σ values, the current set of data along with the default algorithm [147] that we use for the MCMC analysis cannot constrain the g_* parameter stringently. On the other hand, C_T and λ are well constrained. To have a better understanding of this, we also quote the best-fit values of the warm inflation parameters for the non-thermal case: $\lambda \sim 1.38 \times 10^{-14}$, $C_T \sim 0.0030$, $g_* \sim 12.32$. It is interesting to note that the most likely value of g_* is close to the particle content proposed in the model in Ref. [16]. These values denote the positions of the maximum posterior probability in the triangle plot of Fig. 5.6. We note that for the case of g_*, the position of the maximum posterior probability and the mean value from the marginalised one-dimensional plot differs by 1-σ. The marginalised mean values for other background cosmological parameters in Table 5.1 are consistent up to 1-σ confidence level for ΛCDM+r model for the same data combinations.

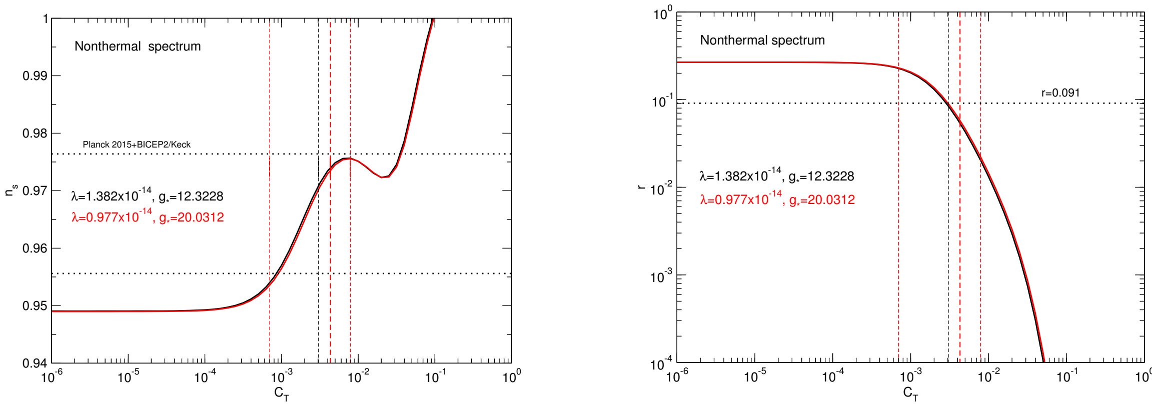

(a) (b)

Figure 5.7: The predictions for the spectral index and tensor-to-scalar ratio for the best-fit (black) and mean value (red) of parameters for non-thermal case. The vertical black dotted line corresponds to the best-fit value of C_T, whereas dotted red lines corresponds to the mean value (central), and its 2-σ limit as given in Table 5.1. In Fig. (a), the horizontal lines correspond to the 2-σ constraints for different data combinations, whereas horizontal line in Fig. (b) corresponds to the current upper limit on r.

To understand the consistency of the model, it is instructive to find the inflationary observables for the best-fit parameters and compare those with bounds from the recent data. We show this in Fig. 5.7 where we plot the scalar spectral index n_s and the tensor-to-scalar ratio r as a function of C_T for both the best-fit parameter and marginalised mean values for λ and g_*, and those are not much different from each other. The best-fit parameters are $n_s = 0.9709$, $r = 0.09$ with running $\alpha_s = -6.7 \times 10^{-5}$, whereas parameters for the marginalised mean values are $n_s = 0.9736$, $r = 0.06$ with $\alpha_s = -7.2 \times 10^{-5}$. For the marginalised mean value of the parameters, we find $Q_* = 0.031$ with $T/H_* = 21.3$, and the pivot scale exits the horizon $N_* = 58$ e-folds before the end of inflation, whereas for the case of best-fit values, we find $Q_* = 0.019$ with $T/H_* = 19.3$, and the horizon exit scale happened $N_* = 58$. As we have argued earlier, the running is always negligible. The vertical lines in Fig. 5.7 correspond to the mean value for C_T and their 2-σ error bars, and the best fit value. The horizontal lines correspond to the observational constraints. We see that smaller values of $C_T \lesssim 10^{-3}$ are excluded as it predicts larger tensor amplitude and too small scalar tilt. C_T in the range of 10^{-3} and 10^{-2} could have been consistent with both the constraints from n_s and r, but in that range, it predicts too large scalar amplitude as can be seen in Fig. 5.3a. Therefore, we see that for the non-thermal case, the preferred values of the parameters predict r that is close to the current upper limit, and further constraint on r would either validate or exclude the set-up. In particular, non-observation of $r \sim 0.01$ would strongly constrain the scenario.

Now, we turn to the discussion of the thermal case with $\mathcal{N}_* \neq 0$. In thermal warm inflation scenario, the marginalised mean values of the parameters are (see Table 5.1): $C_T = 0.0104$, $\lambda = 9.74 \times 10^{-16}$, and $g_* = 139.91$. Here, we note that the observations are unable to tightly constrain the number of thermal degrees of freedom g_* as compared to the non-thermal case, and this was anticipated from the analyses in Sec. 5.4. Both C_T and λ values are well constrained in this case, and C_T is larger by one order of magnitude

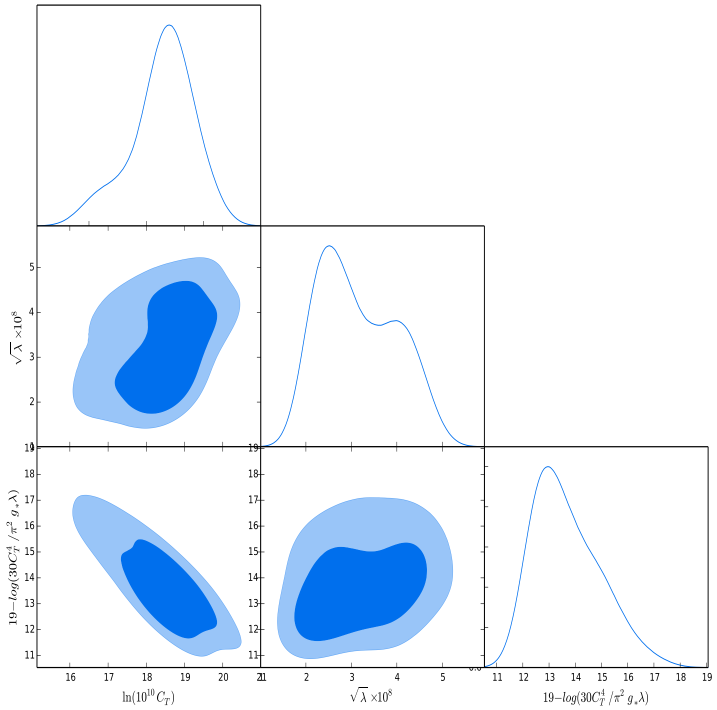

Figure 5.8: Triangle plot for the model parameters C_T, λ and g_* when $\mathcal{N}_* \neq 0$. Diagonal plots are the probability density for these parameters and off diagonal plots represent 68% and 95% confidence limits for the variation of two sets of model parameters

compared to the non-thermal case, whereas λ is smaller by a similar amount. We also quote the best-fit values of the parameters here: $C_T = 0.0032$, $\lambda = 9.6145 \times 10^{-16}$, and $g_* = 126.7637$. The marginalised mean values of the background cosmological parameters are consistent with those from the ΛCDM+r run up to $1-\sigma$ confidence level for the same set of data combinations.

We also find the inflationary observables for the mean and best-fit values of the model parameters for comparison with recent observations. Fig. 5.9 shows n_s and r as a function of C_T for mean and best-fit values of λ and g_*, and these two curves are almost overlaps. The vertical dashed red and black lines correspond to the mean and best-fit values of C_T whereas the thin red dotted lines correspond to the 2-σ error in C_T. Horizontal lines are the bounds from recent PLANCK observations. The marginalised mean values of the parameters predict $n_s = 0.9631$, $r = 0.03$ with running $\alpha_s = -1.6 \times 10^{-4}$ whereas, for the best-fit values of the parameters, the observables are $n_s = 0.9648$, $r = 0.06$ with running $\alpha_s = -1.6 \times 10^{-4}$. The running is very small as discussed earlier. The marginalised mean values of the parameters predict $Q_* = 0.14$ with $T/H_* = 40.70$ and $N_* = 58.5$ for the horizon exit of the pivot scale. The best-fit values of the parameters give $Q_* = 0.24$ with $T/H_* = 22.5$ and $N_* = 58.07$. We note that the thermal scenario predicts lower values of the tensor-to-scalar ratio r than that predicted in non-thermal warm inflation case and r for thermal warm inflation is well within the bounds of the present observations.

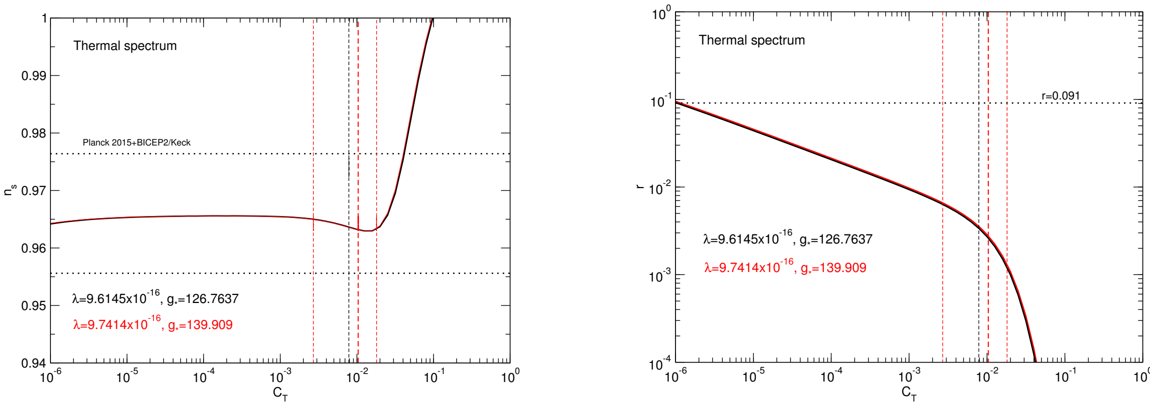

(a) (b)

Figure 5.9: The predictions for the spectral index and tensor-to-scalar ratio for the best-fit (black) and mean value (red) of parameters for thermal case. The vertical black dotted line corresponds to the best-fit value of C_T, whereas dotted red lines corresponds to the mean value (central), and its 1-σ limit as given in Table 5.1. In Fig. (a), the horizontal lines correspond to the 2-σ constraints for different data combinations, whereas horizontal line in Fig. (b) corresponds to the current upper limit on r.

In Fig. 5.10, the difference in the temperature power spectrum for non-thermal and thermal warm inflation cases with the ΛCDM+r model is plotted for the best-fit values of the model parameters quoted above in the corresponding cases for the data combination PLANCK 2015+BICEP2/KECK Array.

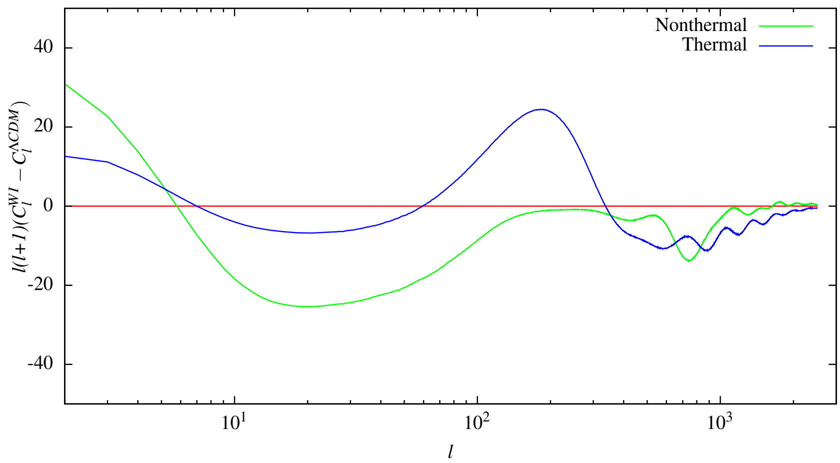

Figure 5.10: Temperature power spectrum residual plots for the best-fit values of the model parameters for both non-thermal (green) and thermal (blue) cases with respect to the ΛCDM+r model for the data combination same as Table 5.1

Although Ref. [134] did a similar MCMC analysis, there are considerable differences between our methodology of analysis with respect to theirs. Here, the complete power spectra $P_{\mathcal{R}}$ and P_T are calculated numerically using Eq. (5.22) and Eq. (5.29) while feeding them inside CAMB rather than a power-law fitting approximation in [134]. Moreover, [134] used Bound Optimization BY Quadratic Approximation (BOBYQA) algorithm which is not the case in our MCMC methodology. Finally, n_s is calculated as a function of the marginalised (and best-fit) values of the model parameters and corresponding r values are also quoted in this section which is different from the approach in [134] where all the observables are calculated for $n_s = 0.9655$, the mean value from PLANCK TT+low P [106]. Therefore, the values of Q_* at the pivot scale are different in our case than that mentioned in [134]. This explains the difference in observables such as r and α_s in our thermal case from that of quartic potential with linear dissipation in [134]. Recently ref. [148] analysed warm inflation model with $\Upsilon \propto T^3$ whereas we concentrated on the linear dissipative regime.

The difference in the mean (and best-fit) values of g_* for non-thermal and thermal cases is due to the difference in effective thermalisation in these two cases. The minimum number of d.o.f. required to get this kind of linear dissipation is $g_* = 11.5$ for the non-thermal case. For the thermal case, the inflaton, having a thermal (BE) distribution, contributes to g_* and increases the minimum required g_* to be 12.5 [16]. Whether or not SM or BSM fields are present in the thermal bath depend on how the inflaton+dissipation sector couples to those fields. Incomplete thermalization of the (B)SM fields due to weak coupling can result in a suppressed value of effectively thermalized d.o.f. g_* ($< O(100)$). The marginalised values of g_* from Table 5.1 imply that for a warm non-thermal inflation, the preference is for a thermal bath made of the dissipative sector, but not yet thermalised (B)SM sector; whereas, for warm thermal inflation, more d.o.f. are included in the thermal bath than the minimal sector. Whether those are SM or BSM fields is a question of model building.

It is worth mentioning here, there are some of the other features in the observables that can help to distinguish between WI from CI. One feature as discussed in [134] is the sign of the running of the running of the spectral index (β). The recent observations by PLANCK [28] hint that β ($\beta = 0.025 \pm 0.013$) could be positive, which contradicts the expectation from the standard CI models, whereas a quartic potential in WI scenario can predict a positive β. Another way to distinguish is by studying the non-Gaussianities as WI have some distinct features in the shapes of the bispectrum when compared to the CI picture [149].

5.7 Conclusions

In this work, we have explored the possibility of constraining parameters of the warm inflationary scenario when comparing its predictions directly with the latest CMB data. Warm inflation just takes into account possible dissipative effects induced by the interactions of the inflaton field with other species; interactions needed anyway in order to be able to reheat the universe after inflation ends. But given the variety of possibilities when combining inflationary models with patterns of dissipation, we have chosen to work (a) with a simple model of inflation, a chaotic model with a quartic coupling λ; (b) a linear T dissipative coefficient, given by the interactions of a few fermions and scalars with the inflaton. Consistency of the model with observations has been already established studying its background dynamics and the primordial spectrum [16], by varying the parameters of the model. Indeed, for chaotic models dissipation helps in sustaining inflation for longer, lowering the value of potential at horizon crossing, and therefore the tensor-to-scalar ratio.

We have used COSMOMC to get the parameter estimation. As parameters of the model we have: the combination of coupling constants giving rise to dissipation, C_T in Eq. (5.8), the effective number of relativistic degrees of freedom contributing to the thermal bath g_*, and the quartic coupling in the inflaton potential λ. We work directly with the scale-dependent primordial spectrum, $P_{\mathcal{R}}(k)$. In principle, the calculation of the primordial spectrum is done as a function of the no. of e-folds, Eq. (5.22), and to get the relation with the scale k one needs to assume something about reheating: at least an effective equation of state during reheating $\tilde{w}$, and how long it will take for the universe to become radiation dominated. However, these extra assumptions are avoided in our case given that (a) we already have radiation produced during inflation, (b) the quartic chaotic model behaves as radiation once the field starts oscillating after inflation so that $\tilde{w} = 1/3$. Therefore we have used Eq. (5.25) to convert the N dependence into k-dependence.

In warm inflation, the presence of the thermal bath and its fluctuations can affect also the statistical state of the inflaton fluctuations, and this is taken into account with the term $\mathcal{N}_*$ in Eq. (5.22). We have considered in our analyses that either the inflaton remains in its standard Bunch-Davies vacuum, with $\mathcal{N}_* = 0$ (nonthermal case), or that it is in a thermally excited state with $\mathcal{N}_* = n_{BE}$ (thermal case). The main results of our analyses are given in

Fig. 5.6 for the nonthermal case and Fig. 5.8 for the thermal case. The constraints on the model parameters are given in Table 5.1. Notice that we have the same no. of parameters in our analyses than in the standard cold inflation one, but we have traded the three parameters related to the primordial spectrum with our model parametrisation: C_T, λ and g_*. While studying the parameter dependence of the observables in Sec. 5.4, we checked that in this model the running of the spectral index is always small: $|\alpha_s| \lesssim O(10^{-4})$, so the power spectrum can be well fitted by a simple power law.

In both cases, thermal and non-thermal, the less constrained parameter is the effective no. of relativistic degrees of freedom g_*; mainly because this parameter always appears in the combination $C_T^4/(\lambda C_R)$, with $C_R = \pi^2 g_*/30$. Still, in the non-thermal case the behaviour of the spectral index with C_T (see Fig. 5.2a) selects a preferred range for this value, the amplitude of the spectrum do the same for λ, and therefore $g_* \simeq O(20)$. This is of the same order as the minimum no. of degrees of freedom needed to get this kind of linear dissipation, $g_* = 12.5$ [16]. The Monte Carlo analyses indeed returns values for the parameters such that the spectral index is as close as possible to the ΛCDM + Cold Inflation analyses mean value, i.e., $n_s \simeq 0.966$, which in this case implies a slightly larger value for the tensor-to-scalar ratio than in Cold Inflation, close to the upper limit. Future data providing a more restrictive upper limit on r may then disfavor this scenario.

In the thermal case, the problem of the degeneracy among the parameters is stronger. In addition, the behavior of the spectral index with C_T is rather flat (until it does increase owing to the growing mode), as can be seen in Fig. 5.2a, which does not help with the parameter estimation. This is the reason for which we have explored different parametrisations and method in order to get the best possible estimation. Still, we hardly get any constraint on g_*. Nevertheless, the typical value for the spectral index is again very close to the ΛCDM + CI, whereas in this scenario the tensor-to-scalar ratio is further suppressed with $r \simeq 0.006$. Still, it may be within the range of next generation CMB experiments.

CHAPTER 6

KÄHLER MODULI INFLATION

The most commonly adopted method to constrain models of inflation is to express the primordial perturbations in terms of empirical parameters such as A_s (the amplitude of the scalar power spectrum), n_s (the scalar spectral tilt), r (the tensor-to-scalar ratio), f_{nl} (the non-Gaussianity parameter) etc. The most likely values of these parameters are determined by evolving the initial fluctuations (as expressed in terms of these parameters) and then comparing with the observed CMB fluctuations. Given a model of inflation, its theoretical prediction for the empirical parameters are computed as a function of model parameters, and a model is considered successful if the predicted values match the constraints on the empirical parameters from the observations. This indeed is the general procedure followed by the PLANCK collaboration to obtain constraints on several inflation models [28]. The next generation of CMB experiments is very promising in improving the accuracy in determining the observables of cosmological inflation. For example, it is expected that the scalar spectral index n_s is going to be measured with an accuracy of $\Delta n_s \sim 0.002$ (1-σ) by forthcoming ground-based CMB-S4 experiment [29], and satellite-based experiment

CORE [30]. If approved, it is expected that these experiments are going to be operational within ten years.

The slow-roll conditions require the inflationary potential to be flat in Planck units. Any inflation model is sensitive to ultraviolet degrees of freedom, and therefore, inflation models should be embedded in ultraviolet complete theories. String theory being our best hope for an ultraviolet complete theory, inflationary models obtained from string theory deserve to be analysed in detail. The central input for obtaining predictions of an inflationary model is the number of e-foldings between horizon exit and the end of inflation $(N_{\rm pivot})$. This, in turn, depends on the entire post-inflationary history of the universe (including reheating). A generic feature of the post-inflationary history of models of inflation constructed in string theory (and supergravity) is an epoch in which the energy density of the universe is dominated by cold moduli particles (which arises as a result of vacuum misalignment during the inflationary epoch) - See [150] for a recent review. Thus, in order to obtain precise theoretical predictions, it is necessary to incorporate the effect of this epoch along with the reheating epoch.

In [21] and [22], we have analysed a particular model of this sort, namely the Kähler moduli inflation [20] in details. Kähler moduli inflation is a model of inflation in the Large Volume Scenario (LVS) for moduli stabilisation [19, 151] in IIB flux compactifications [152]. Recently, a 'global' embedding of the model in compact oreintifold was provided in [153]. The post-inflationary history of this model was analysed in [60] – in particular the dynamics of the epoch in which the energy density is dominated by cold moduli particles was studied in detail; the effect of this epoch on the value of $N_{\rm pivot}$ was computed.

Although in general the precise microscopic details of reheating can be complicated, in [21], we followed the usual approach of parameterizing the effect of the reheating epoch on $N_{\rm pivot}$ by the number of e-foldings during reheating $(N_{\rm re})$ and the effective equation of state $(w_{\rm re})$ during the epoch (see for e.g. [154]). With this the inflationary predictions can be expressed in terms of $N_{\rm re}$ and $w_{\rm re}$. Interesting constraints arise from the fact that $w_{\rm re}$ cannot be arbitrary; physical arguments and simulations constrain the range of $w_{\rm re}$. Overall our analysis is similar in spirit to [26, 140, 155, 156], subsequent analysis along these lines using PLANCK data has been carried out in in [154, 157–161]. Recently, an analysis similar to ours has been carried out for the fibre inflation model in [162]. We note that fibre inflation does not lead to an epoch of modulus domination in the post-inflationary history. In the case of Kähler moduli inflation, this epoch plays a crucial role.

Moreover, if one is interested in confronting a particular model of inflation with data, then a robust approach can be taken, as developed in [23, 139, 140]. One takes the coefficients of the inflaton potential and the parametrization of the reheating epoch as the 'model inputs'. Observational predictions are examined directly in terms of the coefficients of the potential; estimates and errors for the coefficients of the potential are directly obtained. One of the ways, this can be achieved is by making use of MODECHORD[1] [23] which provides a numerical evaluation of the inflationary perturbation spectrum (even without relying on the slow-roll approximation) taking the potential coefficients as input; which is then used as a plug-in for CAMB [142] and COSMOMC [14]. The parameters are then estimated using a nested sampling method [163]. The importance of reheating effects in constraining inflation models using current cosmological data was first discussed in [140], and was subsequently applied to the WMAP data in [164] and to the PLANCK data in [8].

Given the dependence of $N_{\rm pivot}$ on the model parameters, it is crucial to also determine inflationary observables with precision. With this motivation, a complete numerical analysis for Kähler moduli inflation using MODECHORD+COSMOMC [14, 23] is carried out in [22]. We note that Kähler moduli inflation in light of Bayesian model selection was dis-

[1] MODECHORD is publicly available at www.modecode.org

cussed in [7, 165, 166], but the key difference between those analysis and the present one is the incorporation the effects of the epoch (exact duration) of modulus domination in the post-inflationary history, that depends on the model parameters.

This chapter, which contains the work of both [21] and [22], is organized as following: we first review some basic aspects of Kähler moduli inflation and briefly outline the post-inflationary history of the model in Sec. 6.1. We then mention the duration of modulus dominated epoch at the end of inflation $N_{\rm mod}$ for the model in Sec. 6.2 and analyse the dependences of $N_{\rm pivot}$ on the dynamics of post-inflationary modulus domination and modulus reheating. In Sec. 6.2.1, we obtain the expression for the spectral tilt n_s in terms of the reheating parameters and compare the model predictions to observational data. Our results are summarized in the plots in the same section. Given the number of e-foldings during the reheating epoch, the temperature at the end of reheating $T_{\rm re}$ of the Standard Model is determined; thus predictions for the spectral tilt in terms of $N_{\rm re}$ and $w_{\rm re}$ can be parametrized in terms of $T_{\rm re}$ and $w_{\rm re}$. As in [154], we also present our results in terms of the later parametrization. The analysis and estimations of the Sec. 6.2 and Sec. 6.2.1 are based on theoretically inspired values for the parameters of the inflationary model. In Sec. 6.3 we discuss the methodology for analysing the model parameters and how the required modification in $N_{\rm pivot}$ can be implemented in ModeChord. In Sec. 6.3.1, we analyse and discuss the results for Generalised Reheating (GRH) scenario where $N_{\rm pivot}$ is varied between 20 and the number corresponding to the instantaneous reheating case. This analysis is independent of average equation of state parameter $w_{\rm re}$ during reheating. The case for specific values of $w_{\rm re}$ with the requirement of $T_{\rm re} > T_{BBN}$ is analysed in Sec. 6.3.2. We conclude in Sec. 6.4.

6.1 A brief review of Kähler moduli inflation

We begin by briefly reviewing Kähler moduli inflation, the reader may consult [20] for further details. Kähler moduli inflation is set in the Large Volume Scenario (LVS) [19,151] for moduli stabilisation of IIB flux compatifications [152]. The complex structure moduli of the underlying Calabi-Yau are stabilised by fluxes. The simplest models of LVS are the ones in which the volume of the Calabi-Yau takes the Swiss-cheese form: $\mathcal{V} = \alpha\Big(\tau_1^{3/2} - \sum_{i=2}^{n} \lambda_i \tau_i^{3/2}\Big)$. Note that the overall volume is set by τ_1; the moduli $\tau_2, ..., \tau_n$ are blow-up modes and correspond to the size of the holes in the compactification. Incorporating the non-perturbative effects in the superpotential, the leading α' correction to the Kähler potential and an uplift term (so that a nearly Minkowski vacuum can be obtained), the potential for the scalars in the regime $\mathcal{V} \gg 1$ and $\tau_1 \gg \tau_i$ (for $i > 1$) is

$$V_{\rm LVS} = \sum_{i=2}^{n} \frac{8(a_i A_i)^2 \sqrt{\tau_i}}{3\mathcal{V}\lambda_i} e^{-2a_i\tau_i} - \sum_{i=2}^{n} \frac{4a_i A_i W_0}{\mathcal{V}^2} \tau_i e^{-a_i\tau_i} + \frac{3\hat{\xi} W_0^2}{4\mathcal{V}^3} + \frac{D}{\mathcal{V}^\gamma}. \tag{6.1}$$

Here A_i, a_i are the pre-factors and coefficients in the exponents of the non-perturbative terms in the superpotential and W_0 is the vacuum expectation value of flux superpotential. The uplift term is $V_{\rm up} = \frac{D}{\mathcal{V}^\gamma}$ with $D > 0$, $1 \le \gamma \le 3$ (see [167–173] for mechanisms that can lead to such as term).

In Kähler moduli inflation, one of the blow-up moduli (τ_n) acts as the inflaton. For simplicity, we will focus on Calabi-Yau's of the Swiss Cheese form (although the analysis can be carried out in more general settings, [174]). Inflation takes place in region $e^{a_n\tau_n} \gg$

$\mathcal{V}^2$, here the potential is well approximated by:

$$V_{\rm inf} = \sum_{i=2}^{n-1} \frac{8(a_iA_i)^2\sqrt{\tau_i}}{3\mathcal{V}\lambda_i} e^{-2a_i\tau_i} - \sum_{i=2}^{n-1} \frac{4a_iA_iW_0}{\mathcal{V}^2}\tau_i e^{-a_i\tau_i} + \frac{3\hat{\xi}W_0^2}{4\mathcal{V}^3} + \frac{D}{\mathcal{V}^\gamma} - \frac{4a_nA_nW_0}{\mathcal{V}^2}\tau_n e^{-a_n\tau_n}\,. \tag{6.2}$$

It is exponentially flat in the inflaton direction (τ_n). The other directions ($\mathcal{V}, \tau_i$ with $i = 2, .., n-1$) in field space are heavy during inflation. Integrating out the heavy directions and canonically normalising the inflaton (we denote the canonically normalised field by σ), one finds its potential (in Planck units) to be

$$V = \frac{g_s}{8\pi}\left(V_0 - \frac{4W_0a_nA_n}{\mathcal{V}_{\rm in}^2}\left(\frac{3\mathcal{V}_{\rm in}}{4\lambda_n}\right)^{2/3}\sigma^{4/3}\exp\left[-a_n\left(\frac{3\mathcal{V}_{\rm in}}{4\lambda_n}\right)^{2/3}\sigma^{4/3}\right]\right), \tag{6.3}$$

where

$$\frac{\sigma}{M_{\rm Pl}} = \sqrt{\frac{4\lambda_n}{3\mathcal{V}_{\rm in}}}\,\tau_n^{\frac{3}{4}} \quad \text{with} \quad V_0 = \frac{\mathrm{W}_0^2}{\mathcal{V}_{\rm in}^3}\,. \tag{6.4}$$

$\mathcal{V}_{\rm in}$ is the value of the volume during inflation and $\beta = \frac{3}{2}\lambda_n a_n^{-3/2}(\ln\mathcal{V})^{3/2}$. Phenomenological considerations put the volume at $\mathcal{V}_{\rm in} \approx 10^5 - 10^7$, and we will discuss cosmological constraints on it in the next section. We note that 'gobal embedding' of the model (realisation in a compact Calabi-Yau with a semi-realistic Standard Model sector) was carried out in [153].

Vacuum misalignment and the resulting post-inflationary moduli dynamics in this model was studied in detail in [60], here we summarise its conclusions. During inflation, the volume modulus gets displaced from its global minimum. The displacement of the canonically normalised field in Planck units is:

$$Y = 2R\left(\frac{\hat{\xi}}{2P}\right)^{2/3}$$

with

$$R = \frac{\lambda_n a_n^{-3/2}}{\left(\sum_i^n \lambda_i a_i^{-3/2}\right)}, \quad P = \sum_i^n \lambda_i a_i^{-3/2}, \quad \text{and } \hat{\xi} = \frac{\chi}{2(2\pi)^3 g_s^{3/2}}, \tag{6.5}$$

where χ is the Euler number of the Calabi-Yau and g_s is the vacuum expectation value of the dilaton. For typical values of the microscopic parameters, $Y \approx 0.1$ which is consistent with effective field theory expectations. This leads to an epoch in the post-inflationary history in which the energy density is dominated by cold particles of the volume modulus. The number of e-foldings that the universe undergoes in this epoch is [60]

$$N_{\text{mod}} = \frac{2}{3} \ln \left(\frac{16\pi a_n^{2/3} \mathcal{V}^{5/2} Y^4}{10\lambda_n (\ln \mathcal{V})^{1/2}} \right). \tag{6.6}$$

The presence of this epoch reduces the number of e-foldings between horizon exit of the pivot mode and the end of inflation by an amount $\frac{1}{4} N_{\text{mod}}$. The spectral index can be calculated by using the usual slow-roll formula $n_s \approx 1 - 2/N_{\text{pivot}}$, but at the reduced value of N_{pivot}. For typical values of the volume $\mathcal{V} \sim 10^5 - 10^6$ and other parameters in this model, N_{mod} can be calculated. In Kähler moduli inflation, the inflaton decays to relativistic d.o.f at the end of inflation, the energy density of these relativistic degrees of freedom becomes subdominant quickly in comparison with the energy density of the oscillating volume modulus (which arises as a result of vacuum misalignment). For typical values of the model parameter parameters, this epoch of between inflation and modulus domination has a small duration and hence a negligible effect on N_{pivot} [60]. Therefore, we neglect this epoch in our analysis. After the decay of the volume modulus, the universe has a thermal history.

6.2 Post-inflationary History and Reheating

Phenomenological considerations, including the constraints from the strength of the amplitude of scalar perturbations, require $\mathcal{V}_{\text{in}} \approx 10^5$ to 10^6 [60]. In this region of the parameter space, the spectral tilt (n_s) can be expressed in terms of the number of e-foldings between horizon exit and the end of inflation by the formula

$$n_s \approx 1 - \frac{2}{N_{\text{pivot}}}. \tag{6.7}$$

The tensor-to-scalar ratio is rather insensitive to N_{pivot}; $r \approx 10^{-10}$ to 10^{-11} is in the phenomenologically viable range. Of course, the above expression of Eq. (6.7) for the spectral index is not exact, and in principle can be evaluated by solving for the evolution of the inflation field numerically. The tensor to scalar ratio, r also has mild dependence on the model parameters. Therefore, theoretical predictions are sensitive to the global embedding of the model in a compactification and given a global embedding, numerical evolution of the fields has to be performed to obtain the predictions as in [153]. For the present analysis we will take a phenomenological approach (as in [60]) – we will use the expression of Eq. (6.7) for n_s whereas r will be taken to be in the above range. Finally, we note that the above expression for the spectral index and the value of the tensor-to-scalar ratio are also essentially independent of the post-inflationary history of the universe.

As mentioned in the introduction, the key feature of the post-inflationary history of the model that is relevant for our analysis is the epoch in which the energy density is dominated by cold moduli particles. This arises as a result of vacuum misalignment; the volume modulus is displaced from its post-inflationary minimum during the inflationary epoch. This displacement was computed explicitly in [60] by analysing the scalar potential in the inflationary epoch. The displacement of the canonically normalised field in Planck units was found be $\mathcal{O}(0.1 M_{\text{Pl}})$, in keeping with generic expectations from effective field theory. At the end of inflation, with the expansion of the universe, the Hubble friction term can no longer keep the volume modulus away from its post-inflationary minimum; the volume modulus begins to perform coherent oscillations about its post-inflationary minimum. The energy density associated with this falls off as $a^{-3}(t)$, thus it quickly dominates over the energy density associated with radiation produced from the decay products of the inflaton which falls off as $a^{-4}(t)$. This epoch of modulus domination lasts until the decay of the moduli particles.

Now, let us come to the determination of $N_{\rm pivot}$ for the model. In any cosmological model, $N_{\rm pivot}$ is determined by tracking the evolution of the energy density of the universe from the point of horizon exit of the CMB modes to the present epoch. The formula for the strength of density perturbations

$$A_s = \frac{2}{3\pi^2 r}\left(\frac{\rho_*}{M_{\rm Pl}^4}\right)$$

gives the energy density of the universe at the time of horizon exit (ρ_*); demanding that this energy density evolves to the energy density observed today gives the equation that determines $N_{\rm pivot}$. For the standard cosmological timeline (consisting of inflation, reheating, epoch of radiation domination, epoch of matter domination and finally the present epoch of dark energy domination) this yields

$$N_{\rm pivot} + \frac{1}{4}(1-3w_{\rm re})N_{\rm re} \approx 57 + \frac{1}{4}\ln r + \frac{1}{4}\ln\left(\frac{\rho_*}{\rho_{\rm end}}\right).$$

For Kähler moduli inflation (or any cosmological model with a non-standard post-inflationary history), the equation determining $N_{\rm pivot}$ gets modified. The equation determining $N_{\rm pivot}$

for Kähler moduli inflation was obtained in [60] (using the analysis of [58, 59])[2]

$$N_{\text{pivot}} + \frac{1}{4}N_{\text{mod}} + \frac{1}{4}(1 - 3w_{\text{re}})N_{\text{re}} \approx 57 + \frac{1}{4}\ln r + \frac{1}{4}\ln\left(\frac{\rho_*}{\rho_{\text{end}}}\right) . \tag{6.8}$$

Here N_{mod} is the number of e-foldings that the universe undergoes during the epoch in which the energy density is dominated by the volume modulus. The R.H.S of the above equation is entirely determined by the details of inflation. We note that the dependence on r is mild, but the size of the term involving r is appreciable as Kähler moduli inflation has a very small value of r $(r \approx 10^{-10})$. Also, since the potential for Kähler Moduli inflation is exponentially flat, it is a good approximation to take $\frac{\rho_*}{\rho_{end}} \approx 1$. Our ignorance about the detailed mechanism of the reheating epoch is parametrised by the effective equation of state parameter w_{re}, and the number of e-folding during the epoch N_{re}. Of course, for a model in which all the couplings between the modulus field with the Standard Model degrees of freedom are known, the mechanism for reheating can be determined and N_{re} and w_{re} can be computed. In [60], post inflationary dynamics of the volume modulus was discussed in detail, and it was found that $N_{\text{mod}} \approx 25$. Taking these inputs, Eq. (6.8) becomes

$$\frac{2}{1 - n_s} + \frac{1}{4}(1 - 3w_{\text{re}})N_{\text{re}} \approx 45 . \tag{6.9}$$

The above equation will be central for our analysis to confront the model with the data in the next section. Before proceeding to this analysis, let us discuss some points which will play an important role.

Firstly, the range of the equation of state parameter w_{re}. The simplest model for reheating is the canonical reheating scenario – the scalar field oscillates coherently around a

[2]In addition to the terms in Eq. (6.8), reference [60] found a term associated with the number of e-foldings in which cold inflaton particles dominate the energy density. This term was found to be small in comparison with the other; we will drop it in our analysis.

quadratic minimum producing a cold gas of particles, these decay to the Standard Model sector producing a thermal bath of temperature $T_{\rm re} \sim \sqrt{\Gamma M_{\rm Pl}}$ (where Γ is the total decay width). This has $w_{\rm re} = 0$. More generally, if the oscillations take place around a minimum of the form ϕ^n (with n even), the equation of state parameter is given by $w_{\rm re} = (n-2)/(n+2)$. Thus $w_{\rm re} > 0$ requires higher dimensional operators dominating the minimum. More exotic possibilities for the physics of reheating involve resonant production of particles, tachyonic instabilities, inhomogeneous modes, and turbulence (see [175] for a review). Recent numerical studies indicate that for all these cases $0 \lesssim w_{\rm re} \lesssim 1/4$ [176]; we will mainly focus on this range while carrying out our analysis. We note that instant thermalisation to radiation corresponds to $w_{\rm re} = 1/3$, and this is hard to achieve in practice. For the sake of completeness, we will take a very broad range $-1/3 \leq w_{\rm re} \leq 2/3$ (recall that $w \leq -1/3$ gives an inflationary epoch) for the analysis in the next section.

As discussed in the introduction, it is possible to trade the parameter $N_{\rm re}$ for the last reheat temperature $T_{\rm re}$ in Eq. (6.9). For a fixed value of $w_{\rm re}$, the equation then relates the last reheating temperature to the spectral index. The relationship between $N_{\rm re}$ and $T_{\rm re}$ for Kähler moduli inflation can be easily obtained from the analysis in [60]. Sec. 4.2 of [60] provides expressions for the energy density at the beginning and end of each epoch of the post-inflationary history of Kähler moduli inflation. Using these and incorporating the effect of the reheating epoch we find the Hubble constant at the end of the reheating epoch to be

$$H(\hat{t}) = \frac{M_{\rm Pl} W_0^3}{16\pi \mathcal{V}^{9/2} (\ln \mathcal{V})^{3/2}} \exp\left(-\frac{3}{2}(1+w_{\rm re}) N_{\rm re} \right) . \tag{6.10}$$

Here the exponential factor takes care of the effects of reheating, and $N_{\rm re} = 0$ corresponds to the instant reheating case. Combining this with the usual relationship between the associated energy density and the reheating temperature, $3M_{\rm Pl}^2 H^2(\hat{t}) = \rho(\hat{t}) \approx \frac{\pi^2}{30} g_* T_{\rm re}^4$ (where g_* is the effective number of degrees of freedom of the Standard Model sector); and taking $\mathcal{V} \approx 10^5$, $g_* \approx 100$ (the exact value of g_* has only logarithmic dependence) we find

$$T_{\rm re} \simeq 10^3 \ \exp\bigg(-\frac{3}{4}(1+\mathrm{w}_{\rm re})\mathrm{N}_{\rm re}\bigg) \ \ \mathrm{GeV}\,. \tag{6.11}$$

In the next section, we will present our main results by analysing the dependence of $N_{\rm re}$ and $T_{\rm re}$ on scalar spectral index n_s.

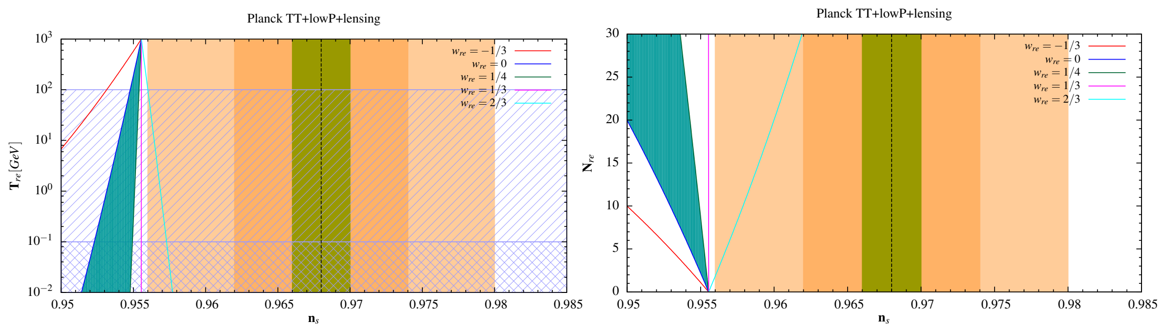

(a) (b)

Figure 6.1: Fig. (a) shows $T_{\rm re}$ as a function of n_s for different values of the equation of state parameter $w_{\rm re}$: $w_{\rm re} = -1/3$ red, $w_{\rm re} = 0$ blue, $w_{\rm re} = 1/4$ green, $w_{\rm re} = 1/3$ magneta and $w_{\rm re} = 2/3$ cyan. These lines meet each other at the point corresponding to $N_{\rm re} = 0$. The vertical dashed black line shows the PLANCK central value ($n_s = 0.968$) for TT+lowP+lensing data [28]. The dark brown band corresponds to the 1-σ region ($\Delta n_s \sim 0.006$) and the light brown band to the 2-σ region. The green band marks the projected future 1-σ sensitivity region with $\Delta n_s \sim 0.002$; assuming that the central value remains unchanged [29, 30]. The blue region corresponds to the parameter space for a physically well motivated reheating scenario with $0 < w_{\rm re} < 1/4$. The horizontally marked mesh region is excluded from BBN constraints; $T_{\rm re} \gtrsim 10\mathrm{MeV}$. On the other hand, the region with right slanted lines requires a non-standard scenario for cosmology at the electroweak scale, $T_{\rm EW} = 100\mathrm{GeV}$. Fig. (b) shows $N_{\rm re}$ as a function of n_s with lines and regions marked with the same colour coding as Fig. (a).

6.2.1 Comparison to Observations

We now have all the ingredients necessary to compare the model predictions with the observational data. For fixed values of the equation of state parameter $w_{\rm re}$, we plot $T_{\rm re}$ and $N_{\rm re}$ as a function of the spectral index n_s (using Eq. (6.9) and Eq. (6.11)) in Fig. 6.1a and Fig. 6.1b respectively. We choose five benchmark values for $w_{\rm re}$ in the range discussed in the previous section ($-1/3 \leq w_{\rm re} \leq 2/3$). Recall that canonical reheating corresponds to $w_{\rm re} = 0$, and $w_{\rm re} = 1/3$ corresponds to instantaneous thermalisation to radiation. Although the region $w_{\rm re} > 1/3$ is not very well motivated physically, we also present plots for $w_{\rm re} = 2/3$ for the purposes of illustration. Numerical simulations of reheating suggest $0 < w_{\rm re} < 1/4$ [176]; we explicitly mark this range in the plots.

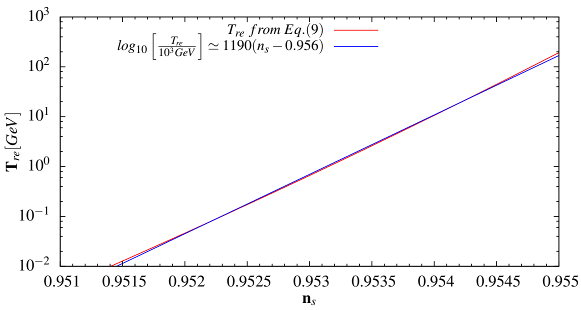

Figure 6.2: Fitting the reheating temperature in terms of the spectral tilt n_s for $w_{\rm re} = 0$ case.

Fig. 6.1a and Fig. 6.1b are based on observational data from PLANCK 2015 TT+lowP+lensing for the ΛCDM + r model; $n_s = 0.968 \pm 0.006$ at 1-σ [28]. It is clear from the plots that the predicted value of n_s is outside the PLANCK 2-σ lower bound for the physically well motivated range of $w_{\rm re}$. It is only for $w_{\rm re} = 2/3$ that the predicted n_s can become consistent with the 2-σ limit; but this requires an extended reheating epoch with $N_{\rm re} \gtrsim 30$. If we demand $T_{\rm re} \gtrsim 100$ GeV so as to have a standard scenario for electroweak phase transition, even this comes under a lot of tension. The only way the model can be viable with a realistic reheating scenario is if the observed value of n_s shifts to become further red tilted in future observations[3]. For comparison with various data sets, it is useful to obtain a simple relationship between n_s and $T_{\rm re}$, and this can be done using least square fitting method. For canonical reheating ($w_{\rm re} = 0$) we find: $\log_{10}(T_{\rm re}/10^3 \text{ GeV}) \simeq 1190(n_s - 0.956)$ (see Fig. 6.2). This clearly exhibits the difficultly in matching with data since the reheating temperature in the model is bounded by 10^3 Gev.

Next, let us consider PLANCK TT,TE,EE+lowP data for which the central value for n_s becomes smaller $n_s \simeq 0.965$, but the associated error also decreases. Our analysis is summarised in Fig. 6.3a and Fig. 6.3b. It is easily seen that the conclusion is unchanged.

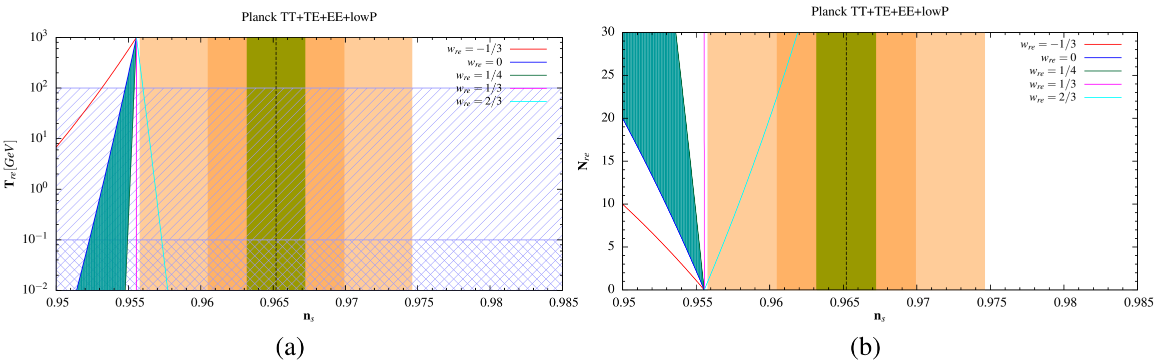

Figure 6.3: Plots for PLANCK TT,TE,EE+lowP data with the same colour specifications as Fig. 6.1.

Dark radiation is a generic feature of string models. In LVS, the axionic partner of the volume modulus is a natural candidate for dark radiation [177]. Comparison to PLANCK data TT+lowP+lensing+r+$N_{\rm eff}$ with dark radiation[4] included in the post-inflationary history is presented in Fig. 6.4a and Fig. 6.4b. Note that with this the predicted value of n_s is within the 2-σ bound for $N_{\rm re} = 0$ (this was previously noted in [153]), and remains within it for large values of $N_{\rm re}$. But we note that for this data set, the 2-σ range is large compared to the other sets.

[3]We would like to emphasise that the statements being made are for the theoretical predictions being made on the basis of the analysis of [60], global embeddings of the model can potentially change these.

[4]In this case, the central value of the marginalised $\Delta N_{\rm eff} = 0.24$.

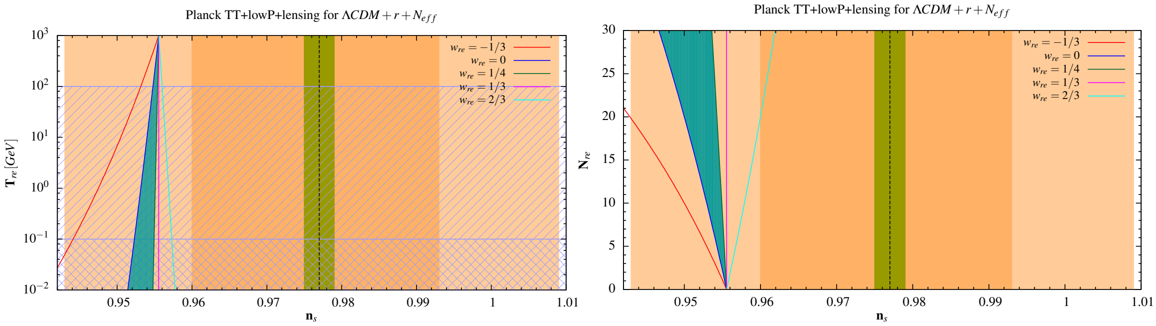

(a) (b)

Figure 6.4: Plots for PLANCK data TT+lowP+lensing+r+N_{eff} with dark radiation incorporated, the colour specifications are same as Fig. 6.1.

Future experiments will bring down Δn_s, and might as well shift the central value of n_s. But with the current measurement of the spectral index, we see that the model can be viable only for an exotic reheating scenario or with dark radiation. We stress that due to the existence of a matter-dominated post-inflationary epoch, the predicted value n_s becomes smaller as we measure the cosmologically relevant modes at a smaller number of e-folds. The effect of reheating just exacerbates the problem further. If the background cosmological model is extended from ΛCDM + r, the constraint can be relaxed in certain cases, but that is highly dependent on what extra physics is added.

6.3 Methodology of precision analysis

The analysis is dependent on the exact definition of the number of e-foldings N_{pivot}. The correctly measured number of e-foldings at the horizon exit is crucial to constrain models of inflation with an additional epoch of post-inflationary moduli domination. This analysis is devised to see how the change in the predicted number of e-foldings during inflation due to the secondary moduli dominated epoch effects the observables and therefore constrains the model parameters. But, even though the modulus dominated epoch is considered carefully, there are inherent uncertainties with the exact value of N_{pivot} due to our poor knowledge about the details of reheating/preheating at the end of modulus domination. With a better understanding in future of the several couplings between the inflation/modulus with Standard Model d.o.f, we will possibly find the total duration of the thermalization process $N_{\rm re}$ with its average equation of state parameter $w_{\rm re}$. Until this is available, it is practical to consider the reheating parameters $w_{\rm re}$ and $N_{\rm re}$ as variables when analysing the model in light of the recent CMB data.

The analysis is carried out using the publicly available COSMOMC [14] and MODECHORD [23] plugged together through MULTINEST [163]. Given a typical model of inflation, MODECHORD numerically computes the primordial scalar and tensor power spectra. These primordial spectra are fed to the CAMB in the COSMOMC package with the help of the plug-in software MULTINEST to evolve through transfer functions. The theoretically calculated perturbations at the CMB redshift is then compared to the observed fluctuations using COSMOMC. COSMOMC is a multi-dimensional Markov Chain Monte Carlo simulator which in this case compares the C_ℓ values computed numerically for the given inflationary model with the observed C_ℓ values by PLANCK and BICEP-KECK array [18, 31, 178]. In general, all the model parameters of inflation and late time cosmological parameters (e.g. Ω_b, Ω_c, θ and τ) are variables in this MODECHORD+COSMOMC set up. In addition, the number of e-folds of inflation can also be set as a variable due to our lack of knowledge of the (p)reheating epoch. In this work, we have varied all the late time cosmological parameters in the six-parameter ΛCDM model as well as the number of e-folds during inflation. The ranges of the inflationary model parameters which are varied in the simulation are chosen carefully and explained in the following paragraphs.

For the generic inflation scenario with instantaneous reheating (IRH) where the universe thermalizes instantly after inflation and makes a quick transition to the radiation dominated epoch, the number of e-foldings at the pivot scale is given by [23]:

$$N_{\rm pivot}^{\rm IRH} = 55.75 - \log\left[\frac{10^{16}{\rm Gev}}{{\rm V}_{\rm pivot}^{1/4}}\right] + \log\left[\frac{V_{\rm pivot}^{1/4}}{V_{\rm end}^{1/4}}\right]. \tag{6.12}$$

Here, $V_{\rm pivot}$ is the value of the inflation potential at which the pivot scale leaves the horizon and $V_{\rm end}$ is the potential at the end of inflation. From the observational upper limit of the strength of the gravitational wave ($r < 0.11$ [28]), the second term in the above equation is negative, whereas the third term is positive definite, but it can be very small for observationally favoured flat inflaton potential. In the usual implementation of ModeChord, the cosmological perturbations are evaluated without assuming slow-roll conditions, and the best-fit potential parameters can be estimated using CosmoMC. But this also requires that the uncertainties associated with reheating are accounted for, and this can be done by varying $N_{\rm pivot}$ between $20 < N_{\rm pivot} < N_{\rm pivot}^{\rm IRH}$. This is termed as the general reheating (GRH) scenario [23]. The upper limit is motivated from the assumption that the average dilution of energy density during the reheating epoch is not faster than radiation, i.e $w_{\rm re} \leq 1/3$. The lower limit comes from the requirement that at the end of inflation, all the cosmologically relevant scales are well outside of the horizon. The shortcoming of this approach is that the reheating scenarios with $w_{\rm re} > 1/3$ are not considered; the possibility that $N_{\rm pivot}$ can be above $N_{\rm IRH}$ is excluded in this analysis.

If there is an epoch of moduli domination in the post-inflationary history, then Eq. (6.12) gets modified. For Kähler moduli inflation $N_{\rm mod}$ is given by Eq. (6.6), and in this case $N_{\rm pivot}^{\rm IRH}$ is:

$$N_{\rm pivot}^{\rm IRH} = 55.75 - \log\left[\frac{10^{16}{\rm Gev}}{{\rm V}_{\rm pivot}^{1/4}}\right] + \log\left[\frac{V_{\rm pivot}^{1/4}}{V_{\rm end}^{1/4}}\right] - \frac{1}{6}\ln\left(\frac{16\pi a_n^{2/3}\mathcal{V}^{5/2}Y^4}{10\lambda_n(\ln\mathcal{V})^{1/2}}\right). \tag{6.13}$$

Note the additional dependence on the model parameters that arises from the last term in Eq. (6.13). In our analysis for $-1/3 < w_{\rm re} \leq 1/3$, we will vary $N_{\rm pivot}$ between 20 and $N_{\rm pivot}^{\rm IRH}$ given by Eq. (6.13).

In general, $N_{\rm pivot}$ is determined by $N_{\rm pivot}^{\rm IRH}$ (as determined by equation (6.13)), $w_{\rm re}$ and $N_{\rm re}$:

$$N_{\rm pivot} = N_{\rm pivot}^{\rm IRH} - \frac{1}{4}(1 - 3w_{\rm re})N_{\rm re}. \tag{6.14}$$

The most general reheating case for the modulus can be treated with considering $-1/3 < w_{\rm re} < 1$, where the upper bound comes from the positivity conditions in general relativity. The GRH analysis as previously discussed in this section implicitly scans the region $-1/3 < w_{\rm re} < 1/3$, where $N_{\rm pivot}$ becomes maximum when the contribution of the last term in Eq. (6.14) is minimum (vanishes) for $w_{\rm re} = 1/3$, i.e. instantaneous reheating. This allows us to put $N_{\rm pivot}^{\rm IRH}$ as the upper bound for $N_{\rm pivot}$ while varying it inside MODECHORD+COSMOMC for $-1/3 < w_{\rm re} < 1/3$. But, in the region $1/3 < w_{\rm re} < 1$, the contribution from the last term in Eq. (6.14) becomes positive which increases the value of $N_{\rm pivot}$ beyond $N_{\rm pivot}^{\rm IRH}$. Therefore, we cannot use the previous prior range for $N_{\rm pivot}$ to analyse for $1/3 < w_{\rm re} < 1$.

We note that for the case $1/3 < w_{\rm re} < 1$ the last term in Eq. (6.14) contributes maximum when $w_{\rm re}$ is maximum ($w_{\rm re} = 1$) and $N_{\rm re}$ is maximum also. Now, $N_{\rm re}$ becomes maximum for the lowest allowed reheating temperature that must be above the BBN bound, namely $T_{\rm re} > T_{\rm BBN} = 5.1\ \text{MeV}$ [179]. Therefore, we have examined the general reheating scenario by simulating with MODECHORD+COSMOMC for a few fixed values of $w_{\rm re}$ with the minimum reheating temperature with $T_{\rm re} = T_{\rm BBN}$. For particular values of $w_{\rm re}$ in the range $1/3 < w_{\rm re} < 1$, we set the upper bound on $N_{\rm pivot}$ as $\left(N_{\rm pivot}^{\rm IRH} - \frac{1}{4}(1 - 3w_{\rm re})N_{\rm re}^{\rm max}\right)$, where $N_{\rm re}^{\rm max}$ is $N_{\rm re}|_{T_{\rm re}=T_{\rm BBN}=5.1{\rm MeV}}$ for a fixed value of $w_{\rm re}$. In Sec. 6.3.2, we will discuss in detail how we find $N_{\rm re}^{\rm max}$ for $T_{\rm re} = T_{\rm BBN}$. Our methodology here differs from the previous analyses done in Ref. [7, 165, 166] since the parametrisation of the post-inflationary epoch is done in terms of the underlying model parameters and statistical techniques are used for parameter estimation.

In summary, we incorporate the effects of reheating using two different methods and carry out the analysis to obtain the preferred value of the model parameters using both the methods. These two methods are the following:

(i) Analysis using the GRH scenario: Here, we vary $N_{\rm pivot}$ from 20 up to the value of $N_{\rm pivot}^{\rm IRH}$ given (6.13).

(ii) Analysis for specific values of $w_{\rm re}$: In this case, $N_{\rm pivot}$ varies between $N_{\rm pivot}^{\rm IRH}$ and the $\hat{N}_{w_{\rm re}}$.$\hat{N}_{w_{\rm re}}$ is determined by the requirement that the reheating temperature is above the temperature needed for successful BBN.

6.3.1 Analysis and results in the GRH scenario

As described above, in the GRH scenario reheating uncertainties are accounted for by varying $N_{\rm pivot}$ between minimum value of 20 and $N_{\rm pivot}^{\rm IRH}$ given by Eq. (6.13). The model parameters (as defined in Sec. 6.1) are varied in the following ranges: $W_0 : 0.001$ to 130, $\log_{10}\mathcal{V}$: 5 to 8 and A_n : 1.80 to 1.95. We take $g_s = 0.06$ (as required for a local realisation of the Standard Model from D3 branes), $\lambda_n = 1$ and $a_n = 2\pi$. We keep these parameters fixed as its dependence on the observables is very mild, and these choices of the parameters are well motivated from the theoretical stand point. Note that among all these parameters $\log_{10}\mathcal{V}$ also determines the duration of modulus domination epoch, and therefore also affects $N_{\rm pivot}$. The likelihoods used are PLANCK TT+TE+EE, PLANCK lowP, estimated using commander, PLANCK lensing and PLANCK+BICEP2/KECK array joint analysis likelihood [18, 31, 178].

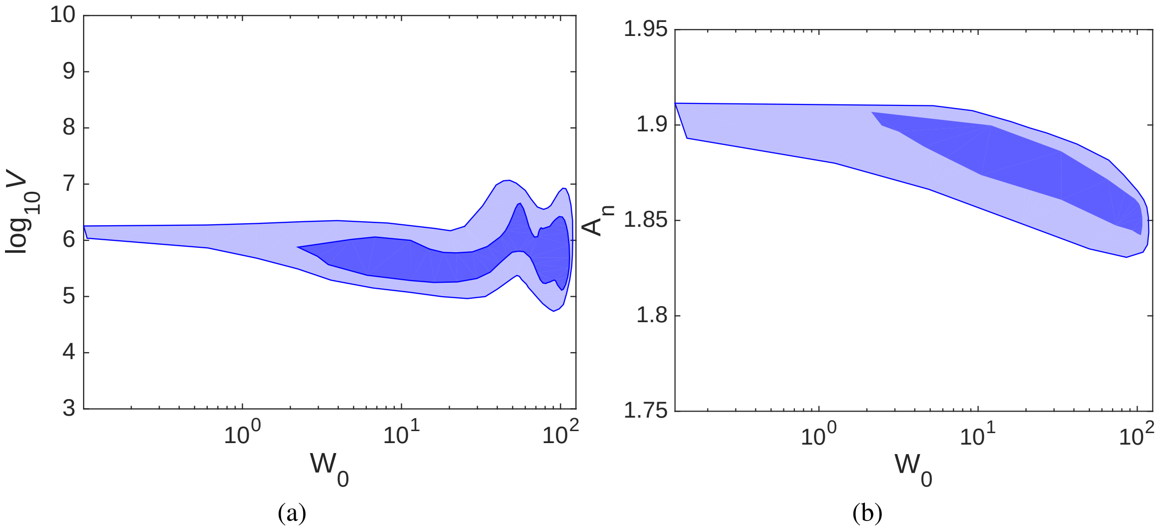

Figure 6.5: Fig. (a) represents the favoured regions in the W_0 - $\log_{10}\mathcal{V}$ plane where as Fig. (b) shows the favoured regions in the W_0 - A_n plane. The 1-σ region is shaded as dark blue, the 2-σ region is shaded as light blue, with W_0 axis is in log scale for both the cases.

In Fig. 6.5, we show the 1-σ and 2-σ bounds on the model parameters. While Fig. 6.5a shows the marginalised constraint on the parameters W_0 and $\log_{10}\mathcal{V}$, Fig. 6.5b shows the marginalised constraint on W_0 and A_n. These plots represent the most favourable region of the model parameters when $N_{\rm pivot}$ is varied between 20 to $N_{\rm pivot}^{\rm IRH}$ for this given model. The marginalised central value and the 1-σ errors are quoted in the Table 6.1. Note that W_0 is not constrained as tightly as the other two parameters. The central value of the spectral index $n_s \sim 0.953$ obtained from the simulation corresponds to number of e-folds $N_{\rm pivot} = 43$. This is in keeping with the theoretical expectation with $n_s \approx 1 - 2/N_{\rm pivot}$, derived under the slow-roll approximations.

The favoured region in the n_s-r plane is presented in Fig 6.6a. Note that the results are in agreement with earlier analytic treatments [60, 153]. But, here we would like to emphasise the difference also. In [60], the shift in the $N_{\rm pivot}$ was calculated by using Eq. (6.6)

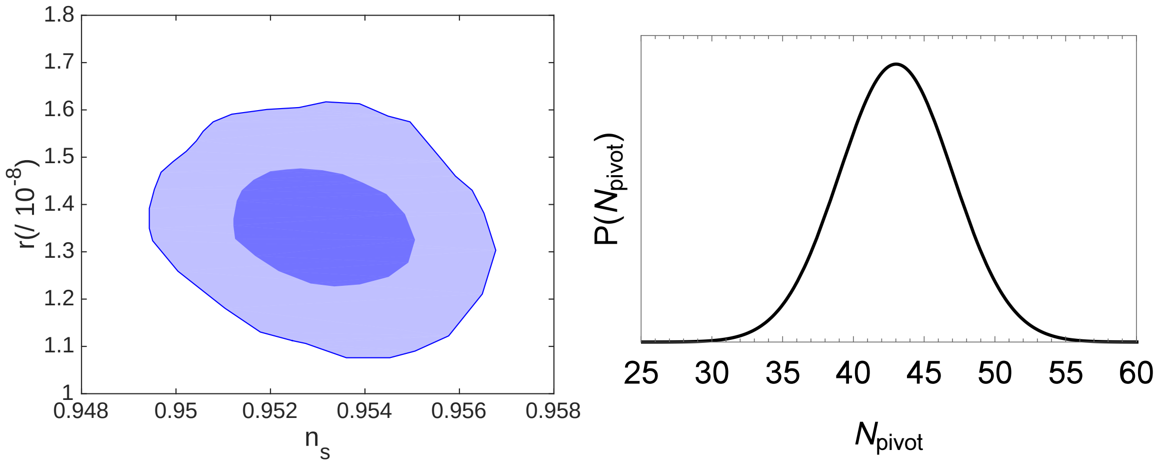

(a)

(b)

Figure 6.6: Fig. (a) shows Favoured region in the n_s-r plane. The 1-σ region is shaded as dark blue, the 2-σ region is shaded as light blue. Fig. (b) shows the 1-D probability distribution of the number of e-foldings $N_{\rm pivot}$.

Table 6.1: Constraints on the model parameters and the cosmological parameters. Data combination used: PLANCK TT+TE+EE+ low P +lensing + BKPLANCK14.

Parameters	Central Value	1σ
W_0	57	46
$\log_{10}\mathcal{V}$	5.9	0.3
A_n	1.87	0.04
n_s	0.953	0.002
$r/10^{-8}$	1.34	0.1
$N_{\rm pivot}$	43	2

where $\mathcal{V} \sim 10^5 - 10^6$, fixed by the amplitude of scalar perturbations for typical microscopic parameters. Effectively, the spectral index was calculated at $N_{\rm pivot} \sim 45$ with $n_s \sim 0.955$. But now, we have kept both $\mathcal{V}$ and $N_{\rm pivot}$ as variables under the generalised reheating scheme, and find preferred values comparing with the data. We present the distribution of $N_{\rm pivot}$ (marginalised over all other parameters) in Fig. 6.6b. We see that as an effect of precision analysis to determine exact values of the model parameters, the central value of $N_{\rm pivot}$ shifts to 43 for 45 as found in [60].

Note that the lower 2-σ bound on $N_{\rm pivot}$ is 39, which is well above 20 and closer to $N_{\rm pivot}^{\rm IRH} = 45$. As is evident from the best fit value of $n_s = 0.953 \pm 0.002$, the model is outside of the PLANCK (ΛCDM+r) 2-σ lower limit [28][5]. Our analysis also provides a χ^2 value for the model, and we find that with equal number of parameters to be varied, there is a deterioration of the fit in this case by $\Delta\chi^2 \simeq 13$ with respect to the ΛCDM+r model for the same combination of the CMB data.

6.3.2 Analysis and results for specific values of $w_{\rm re}$

In this section we carry out our analysis by making specific choices for $w_{\rm re}$ ($w_{\rm re} = 1, 2/3, 0$). As discussed earlier, we will determine the range for variation of $N_{\rm pivot}$ by using the expression for $N_{\rm pivot}^{\rm IRH}$ and the requirement of successful nucleosynthesis. Before going on to analyse the model for the various values of $w_{\rm re}$, let us first describe how we determine this range.

The Hubble parameter at the end of the reheating epoch (after the modulus decay) is given by [60]

$$H(\hat{t}) = \frac{M_{\rm Pl} W_0^3}{16\pi \mathcal{V}^{9/2} (\ln \mathcal{V})^{3/2}} \exp\left(-\frac{3}{2}(1 + w_{\rm re}) N_{\rm re} \right) . \tag{6.15}$$

Moreover, the reheating temperature is given by $3M_{\rm Pl}^2 H^2(\hat{t}) = \rho(\hat{t}) \approx \frac{\pi^2}{30} g_* T_{\rm re}^4$, where g_* is the effective number of degrees of freedom of the Standard Model sector. Thus $N_{\rm re}$ can be expressed in terms of the model parameters, the effective equation of state during reheating and the reheating temperature:

$$N_{\rm re} = -\frac{2}{3} \left(\frac{1}{1 + w_{\rm re}} \right) \ln \left[\frac{16\pi^2 g_*^{1/2} \mathcal{V}^{9/2} (\ln \mathcal{V})^{3/2} T_{\rm re}^2}{\sqrt{90} M_{\rm Pl}^2 W_0^3} \right] . \tag{6.16}$$

[5] Although the model can be consistent when the effects of dark radiation is considered [153, 177, 180].

Successful BBN requires $T_{\rm re} > T_{\rm BBN} = 5.1\ \text{MeV}$ [179]. Plugging this condition in (6.16) we find an upper bound for $N_{\rm re}$. We will denote this value by $N_{\rm re}^{\rm max}$ (note that this quantity depends on $w_{\rm re}$). Now, in general, $N_{\rm pivot}$ is determined by Eq. (6.14).

Since for a given value of $w_{\rm re}$, $N_{\rm re}$ is bounded to lie in the range $(0, N_{\rm re}^{\rm max})$, the allowed range for $N_{\rm pivot}$ is between $N^{\rm IRH}$ and $N^{\rm IRH} - \frac{1}{4}(1-3w_{\rm re})N_{\rm re}^{\rm max}$. Note that $N^{\rm IRH} - \frac{1}{4}(1-3w_{\rm re})N_{\rm re}^{\rm max}$ is greater than $N^{\rm IRH}$ for $w_{\rm re} > 1/3$, thus for $w_{\rm re} > 1/3$, $N_{\rm pivot}$ lies in the interval of

$$(N^{\rm IRH}, N^{\rm IRH} - \frac{1}{4}(1-3w_{\rm re})N_{\rm re}^{\rm max}).$$

On the other hand for $w_{\rm re} < 1/3$, $N_{\rm pivot}$ lies in the interval of $(N^{\rm IRH} - \frac{1}{4}(1-3w_{\rm re})N_{\rm re}^{\rm max}, N^{\rm IRH})$. Next, we carry out the analysis to obtain the preferred value of the model parameters for $w_{\rm re} = 1, 2/3, 0$. $N_{\rm pivot}$ is taken to lie within $N^{\rm IRH}$ and $N^{\rm IRH} - \frac{1}{4}(1-3w_{\rm re})N_{\rm re}^{\rm max}$. For all the analyses below, we vary the model parameters W_0, $\log_{10}\mathcal{V}$ and A_n in the prior ranges same as Sec. 7.4, i.e., $W_0 : 0.001\ \text{to}\ 130$, $\log_{10}\mathcal{V} : 5\ \text{to}\ 8$ and $A_n : 1.80\ \text{to}\ 1.95$. The values of the fixed parameters g_s and a_n are also same as Sec. 7.4. For the case of $w_{\rm re} = 2/3$, Fig. 6.7a and Fig. 6.7b are the 2-D marginalised plots for the model parameters, and for $w_{\rm re} = 1$, the plots are similar looking.

For the sake of completeness, we also do the analysis in this mechanism for a single $w_{\rm re} < 1/3$ case, $w_{\rm re} = 0$. Here, the lower bound to $N_{\rm pivot}$ can be specified as $N_{\rm pivot}^{\rm IRH} - \frac{1}{4}(1-3w_{\rm re})N_{\rm re}^{\rm max}$. Therefore, here, we vary $N_{\rm pivot}$ in the range $N_{\rm pivot}^{\rm IRH} - \frac{1}{4}(1-3w_{\rm re})N_{\rm re}^{\rm max} < N_{\rm pivot} < N_{\rm pivot}^{\rm IRH}$.

The best-fit values and 1-σ errors for the above three cases $w_{\rm re} = 2/3, 1, 0$ are quoted in Table 6.2. The values of the model parameters are well within 1-σ of the values quoted in Table 6.1 in Sec. 6.3.1. The 2-D marginalised plot in the n_s-r plane is given in Fig. 6.8a for the above three cases. The 1-D marginalised posterior distribution for corresponding

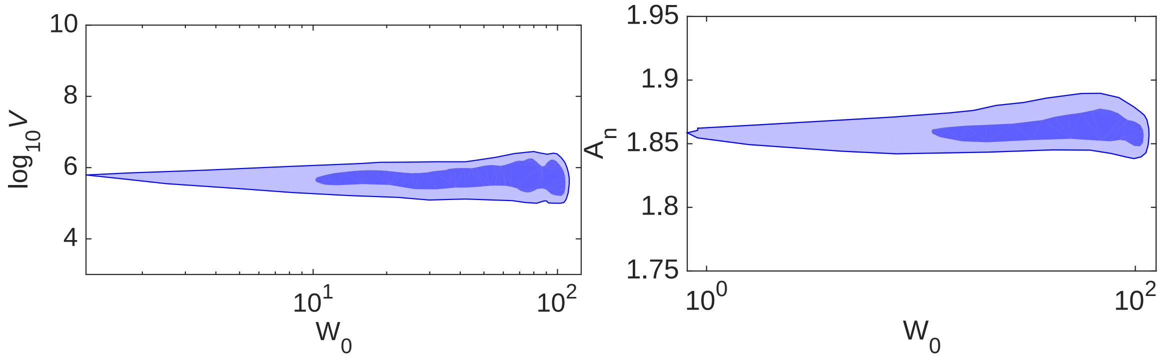

(a) (b)

Figure 6.7: Fig. (a) shows favoured regions in the W_0 - $\log_{10}\mathcal{V}$ plane for $w_{\rm re} = 2/3$. Fig. (b) shows favoured regions in the W_0 - A_n plane for $w_{\rm re} = 2/3$. The 1-σ region is shaded as dark blue, the 2-σ region is shaded as light blue in both the plots.

$N_{\rm pivot}$ are shown in Fig. 6.8b.

Table 6.2: Constraints on the model parameters and cosmological parameters for $w_{\rm re} = 2/3, 1, 0$. Data combination used: PLANCK TT+TE+EE+ low P + lensing + BKPLANCK14.

	$w_{\rm re} = 0$	$w_{\rm re} = 2/3$	$w_{\rm re} = 1$
Parameters	Best-fit$\pm 1\sigma$	Best-fit$\pm 1\sigma$	Best-fit$\pm 1\sigma$
W_0	56.9$\pm$46.5	58$\pm$45	59$\pm$48
$\log_{10}\mathcal{V}$	5.9$\pm$0.3	5.9$\pm$0.3	5.9$\pm$0.3
A_n	1.87$\pm$0.04	1.867$\pm$0.03	1.865$\pm$0.05
n_s	0.9535$\pm$0.002	0.9555$\pm$0.003	0.9575$\pm$0.003
$r/10^{-8}$	1.34$\pm$0.1	1.33$\pm$0.1	1.31$\pm$0.1
$N_{\rm pivot}$	43$\pm$2.5	45.2$\pm$2.25	47.7$\pm$2

From Table 6.2, the best-fit values of the the scalar spectral index (n_s) for the cases with $w_{\rm re} > 1/3$ is greater than n_s for $w_{\rm re} = 0$ and also greater than the value quoted in Table 6.1 for general $w_{\rm re} < 1/3$ cases. Moreover, exotic reheating scenarios produce n_s values closer to the current marginalised mean values given by PLANCK 2015 (ΛCDM+r) [28] than for the $w_{\rm re} < 1/3$ cases. For $w_{\rm re} = 2/3$, the value of n_s is just at the lower 2-σ bound given by PLANCK, whereas for the $w_{\rm re} = 1$ case, n_s is inside the PLANCK 2-σ bound[6]. Projected

[6] This is consistent to the analysis in Ref [21] presented in Sec. 6.2.

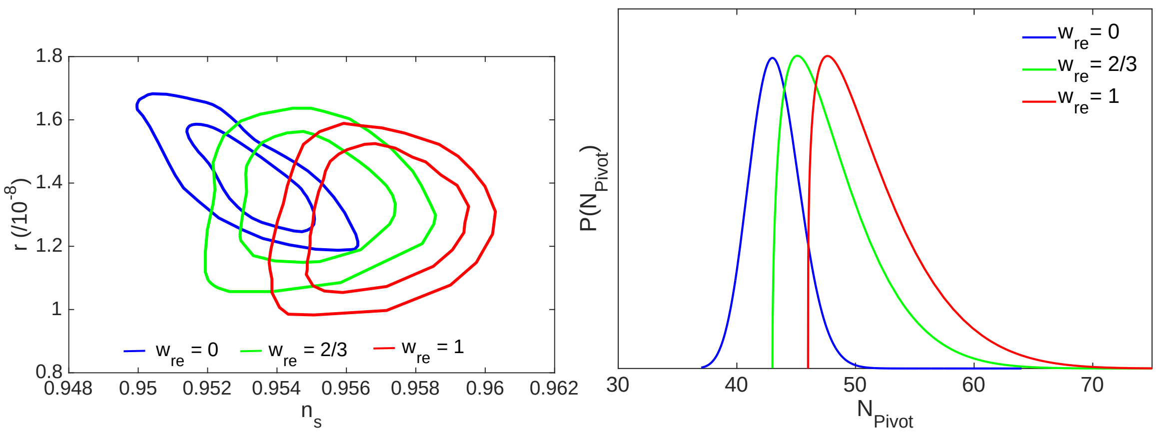

(a) (b)

Figure 6.8: Fig. (a) shows 1-σ and 2-σ confidence levels in the n_s-r plane for $w_{\rm re} = 0$ (blue contours), $w_{\rm re} = 2/3$ (green contours) and $w_{\rm re} = 1$ (red contours). Fig. (b) shows 1-D posterior probability distribution of the number of e-foldings $N_{\rm pivot}$ for $w_{\rm re} = 0$ (in blue), $w_{\rm re} = 2/3$ (in green) and $w_{\rm re} = 1$ (in red).

sensitivity of n_s in future CMB experiments [29] are expected to resolve this situation with stronger constraints. If we look at the Fig. 6.8a, we note that all possible reheating scenarios are consistent to each other at 2-σ level. But it is important to appreciate that future observations are going to measure n_s with $\sigma(n_s) \sim 0.002$ at 1-σ level, and in that case, attempts to make meaningful statements about the value of the scalar spectral index automatically requires our better understanding regarding the reheating epoch. We also note that $N_{\rm pivot}$ has a larger value in the exotic reheating cases, which is expected from the positive contribution of the last term in Eq. (6.14). The tensor-to-scalar ratio r is of the same order ($\sim 10^{-8}$) in all of the above cases.

6.4 Conclusion

We have found that for the model to be consistent with either PLANCK TT+lowP+lensing or PLANCK TT,TE,EE+lowP data, one requires an exotic epoch of reheat ($w_{\rm re} \approx 2/3$). With dark radiation PLANCK TT+lowP+lensing for ΛCDM+r+$N_{\rm eff}$, the model is within the 2-σ range even after the effects of reheating are incorporated. While we have focussed on a single model in both [21] and [22], the results exhibit the importance of carrying out a similar analysis for any model of inflation while confronting it with precision data. A crucial input for our analysis was the contribution to $N_{\rm pivot}$ from the epoch in which the energy density of the universe is dominated by cold moduli particles. To compute this contribution for a model it is necessary to embed the model in a compactification (where the masses and widths of the moduli fields can be determined). Thus to confront precision data, "global embedding" of models (as in [153]) is absolutely necessary. We note that our analysis is not limited to the case of Kähler moduli inflation. The effect is relevant for any inflation model with late decaying scalar field dominating the energy density at the end of inflation (see e.g. [181]). We would like to emphasise that future experiments like ground based CMB-S4 experiment [29], and satellite based experiment CORE [30] are going to measure the spectral index of the CMB with a projected error of $\Delta n_s \sim 0.002$ (1-σ); therefore, analysis in the spirit of the present work is going to become more and more important.

In [22], we have initiated the analysis of string models of inflation using ModeChord. Given the ultraviolet sensitivity of inflation and the fact that so far the number of inflationary models that have been obtained from string theory is not large [182], it is natural to use ModeChord when we try to confront them with data. As data becomes more and more precise $N_{\rm pivot}$ has to be determined very accurately. $N_{\rm pivot}$ itself can explicitly depend on the model parameters for string/supergravity models. Thus, analysis along the line of this work will become more pertinent as cosmological observations become more precise. Here, we constrained model parameters for Kähler moduli inflation, for which the ranges of observables are sensitive to future precision CMB measurements. The full work on Kähler moduli inflation discussed in this chapter presents a compact analysis of the model, and a similar analysis is applicable to models of inflation inspired by moduli masses in string theory.

It is known in the literature that an additional post-inflationary era (like moduli domination in our case) is completely degenerate with the re-heating from the CMB point of view [164] unless the dynamics of the reheated epoch is related to the model parameters[7]. But this is precisely what happens in the model at hand, the number of e-folds during reheating is known in terms of inflation model parameters which in turn also fixes inflationary observables (this is also the novel feature in the theoretical aspects our analysis of Kähler moduli inflation in comparison with [7, 165, 166]). We would like to emphasise that the relation between the epoch of modulus dominated and the model parameters arose from the embedding of the model our knowledge of the low energy effective action in the setting.

There are several interesting directions to pursue. The parameters in the inflationary potentials in string models themselves might have a statistical distribution, and one can try to incorporate the effect of this into the analysis. Another interesting direction is to understand degeneracies that can arise across the parameters and the model space. It will also be interesting to cross-correlate with particle physics observables (see for e.g. [185–189]) and dark radiation [177, 180] in LVS. Note that the constraints of volume and W_0 will have direct implications for the supersymmetry breaking scale. The possibility of analysing multi-field models[8] can be explored using MULTIMODECODE. [191]. Another exciting avenue is to develop a better understanding of the reheating epoch[9] in these models so that associated uncertainties can be reduced. A recent development in this direction is the possibility that the number of e-foldings during the reheat epoch is bounded [192, 193].

[7]The degeneracy can also be broken by the detection of primordial gravitational waves, see [183], [184]

[8]For Kähler moduli inflation, the single field approximation is valid for a large class of initial conditions [190].

[9]See [21, 162] for a phenomenological approach towards reheating for inflationary models in LVS.

We hope to return to these questions in near future.

CHAPTER 7

GOLDSTONE INFLATION IN THE NON-CANONICAL DOMAIN

7.1 Introduction

One of the major challenges with the standard inflationary models is that most of the textbook models are ruled out or disfavoured by the recent observations of CMB such as PLANCK and WMAP [104, 106]. In early 90's, an elegant solution was proposed by [194] from the idea of symmetry breaking to produce the inflation potential where the inflaton is a Goldstone boson (Natural inflation). Due to the shift symmetry property embedded through the symmetry breaking, the flatness of the potential is naturally maintained, which is essential for the model building of inflation. But after the recent data release by PLANCK collaboration [4], Natural inflation is almost ruled out in the standard ΛCDM model. The BIC [1] calculated for such models puts it right on the fence for getting invalidated by data.

[1]The Bayesian information criterion (BIC) is an approximate measure of the Bayes factor B, which is the ratio of the Bayesian evidence of the candidate model to that of a reference model. For details, see [195, 196]

Natural inflation is one particular limiting case of a general class of inflation models known as Goldstone inflation. To have a successful Goldstone inflation, all scales related to the theory have to be sub-Planckian, thus keeping the inflaton guarded against the UV correction from the quantum gravity effects. Now in the standard scenario of inflation, the scalar field is taken to be canonical. But, it was realised after the initial proposal of kinetic driven non-canonical inflation (NCI) in [197] that NCI's are more natural to fit with the fundamental theories like String theory.

After the proposal of tachyon inflation in [198–200], non-canonical realisation of different inflationary models have gained growing interest. Thus, in [201] we move on to study the Goldstone inflation in the non-canonical domain and check the viability of the model from direct constraints by the current observation. In this work we tried to explore the general Goldstone inflation in non-canonical domain and then studied the non-canonical natural inflation as a special case.

This chapter is based on the work [201] and is organised as follows: in the next section 7.2 we will make a brief review of the standard Goldstone inflation along with the basic ingredients to build up the non-canonical inflationary dynamics. In Sec. 7.3, we have reported the analysis part and in Sec. 7.4 we present the main results obtained through that analysis and finally the conclusions are drawn in the final section.

7.2 Revisiting the canonical Goldstone and non-canonical inflation

7.2.1 Reviewing Goldstone inflation

The originally proposed model of Natural inflation has an axion as the inflaton, which is the Goldstone of a spontaneously broken Peccei-Quinn symmetry. But, as mentioned in the previous section, it is almost ruled out in the standard ΛCDM paradigm by recent CMB observations. The model is still in the 2σ allowed region with an associated breaking scale of $10M_{\rm Pl}$ or higher. This is problematic as the effective field theory dynamics could get completely jeopardised by the effects of the Quantum Gravity(QG) which should robustly kick into the picture in the super-Planckian regime. QG in general does not conserve global symmetry and therefore to have a super-Planckian breaking scale in case of a vanilla natural inflation model is philosophically very disturbing.

Different exquisite models have been proposed to explain the super-Planckian breaking scale, such as Extra-natural inflation [202], hybrid axion models [203, 204], N-flation [205–207], axion monodromy [111] and other pseudo-natural inflation models in Supersymmetry [208]. Some or most of these models require a large amount of tuning or the existence of extra dimensions. But even with these theoretical explanations, with the recent release of PLANCK data, the idea of Natural inflation faces survival crisis. The vanilla model is disfavoured by the PLANCK 2018 plus BK14 data with a Bayes factor $\ln B = -4.2$ (Models are strongly disfavoured when $\ln B < -5$). Therefore, it is high time to reevaluate the original motivation and development of the models of Natural inflation where the potential is generated through the breaking of a global symmetry.

In [209], there is a proposal of a model where a generalised Goldstone inflation is developed from the idea of minimal Composite Higgs model [210, 211].

The form of the potential to obtain successful inflation is given as :

$$V(\phi) = \Lambda^4(C_\Lambda + \alpha\cos(\phi/f) + \beta\sin^2(\phi/f)) \tag{7.1}$$

In [209], it has been shown that with an appropriate amount of fine tuning, one obtains a successful model of Goldstone inflation with a sub-Planckian breaking scale related to the global symmetry breaking. Now, with the recent results from PLANCK 2018, even a canonical Goldstone inflation faces problem to survive. Since, this model is motivated by the minimal Composite Higgs model, it is expected to have a non-canonical origin in the dynamics of the inflation. It is also clear from Eq. (7.1) that, for the choice of the parameter $\alpha = 1, \beta = 0$ one gets back the standard form of the natural inflation potential.

7.2.2 Revisiting NCI

Here, we will briefly review the non-canonical inflation before introducing the Goldstone inflation in the non-canonical regime. NCI model features a single scalar field with the action [197, 212]:

$$S = \int \sqrt{-g}\, p(\phi, X) d^4x \; , \tag{7.2}$$

where ϕ is the inflaton field. Here $p(\phi, X) = K(X, \phi) - V(\phi)$, where $V(\phi)$ is the potential and $X \equiv \frac{1}{2}\partial_\mu\phi\partial^\mu\phi$. Now, it is very import to understand that the kinetic term $K(X, \phi)$ can be any arbitrary function of X and ϕ with proper dimensional attributions to the pre-factors. Here, let us write $K(X, \phi)$ as :

$$K(X, \phi) = K_{\rm nc}(\phi) K_{\rm kin}(X) \; , \tag{7.3}$$

here, $K_{\rm nc}(\phi)$ can be any arbitrary function of ϕ. On the other hand, assuming a power law function, $K_{\rm kin}(X) \equiv K_{n+1} X^n$, where n is the power. Thus for $n > 1$, we find higher order contribution of the pure kinetic term even with dimensionful constant $K_{n+1} = 1$. From Eq. (7.3), it is expected to get back the canonical picture once we set $n = 1, K_{n+1} = 1$ and $K_{\rm nc}(\phi) = 1$ respectively.

For the purpose of this work we separate the contributions of the field dependent kinetic term $K_{\rm nc}(\phi)$ and of the derivative dependent kinetic term $K_{\rm kin}(X)$. The scenario with

$K_{\rm nc}(\phi)$ switched on and $K_{\rm kin}(X) = X$ is termed as *Case- 1*. The case where we consider $K_{\rm nc}(\phi) = 1$ and $K_{\rm kin}(X)$ is non trivially switched on is called *Case- 2*.

***Case*- 1**

In this case, $K_{\rm nc}(\phi)$ is switched on and $K_{\rm kin}(X) \equiv X$. Thus, in this case there is no higher order kinetic term present and the effective Lagrangian for generic $K_{\rm nc}(\phi)$ and $V(\phi)$ can be written as:

$$\mathcal{L} = K_{\rm nc}(\phi)X - V(\phi). \tag{7.4}$$

Then the Equation of Motion (EoM) for the field ϕ turns out to be:

$$\ddot{\phi} + 3H\dot{\phi} + \frac{K_{nc,\phi}}{2K_{\rm nc}}\dot{\phi}^2 + \frac{V_{,\phi}}{K_{\rm nc}} = 0, \tag{7.5}$$

where $V_{,\phi} = dV/d\phi$ and $K_{nc,\phi} = dK_{\rm nc}/d\phi$. If the canonical field is given as ψ such that $\frac{1}{2}\partial_\mu\psi\partial^\mu\psi = \frac{1}{2}K_{\rm nc}(\phi)\partial_\mu\phi\partial^\mu\phi$ then the slow roll parameters are modified as:

$$\epsilon_V = \frac{M_{\rm Pl}^2}{2}\left(\frac{V_{,\psi}}{V}\right)^2 = \frac{M_{\rm Pl}^2}{2K_{\rm nc}}\left(\frac{V_{,\phi}}{V}\right)^2, \tag{7.6}$$

$$\eta_V = M_{\rm Pl}^2\left(\frac{V_{,\psi\psi}}{V}\right) = \frac{M_{\rm Pl}^2}{V}\left(\frac{V_{,\phi\phi}}{K_{\rm nc}} - \frac{V_{,\phi}K_{nc,\phi}}{2K_{\rm nc}^2}\right). \tag{7.7}$$

The number of inflationary e-folds in the slow roll regime is:

$$N = \frac{1}{M_{\rm Pl}}\int_{\phi_i}^{\phi_e}\frac{V}{V_{,\phi}\sqrt{K_{\rm nc}}}d\phi. \tag{7.8}$$

The above relations (Eq. (7.4) to Eq. (7.8)) are true for any inflaton potential $V(\phi)$ and we will speculate the particular form of Goldstone inflation in this non-canonical setting in

Sec. 7.3.1. The inflationary observables in this case are:

$$n_s - 1 = 2\eta_V - 6\epsilon_V \tag{7.9}$$

$$r = 16\epsilon_V \tag{7.10}$$

***C*ase- 2**

In this case, $K_{\rm nc}(\phi) \equiv 1$ and $K_{\rm kin}(X) \equiv K_{n+1}X^n$ (for a comprehensive review reader is suggested to consult [213]). Here, the total background dynamics can be constructed in terms of $p(\phi, X) = K(X) - V(\phi)$. The Hubble equation is given as:

$$H^2 = \rho/3, \tag{7.11}$$

where

$$\rho = 2Xp_{,X} - p. \tag{7.12}$$

The speed of sound is

$$c_s^2 = \frac{p_{,X}}{\rho_{,X}} = \frac{K_{,X}}{2XK_{,XX} + K_{,X}}, \tag{7.13}$$

using Eq. (7.12). For the given form of $K(X)$, the sound speed is a constant $c_s^2 = 1/(2n{-}1)$ and the equation of motion (EoM) for the inflaton in this case is modified to:

$$\ddot{\phi} + \frac{3H}{2n-1}\dot{\phi} + \frac{V_{,\phi}}{(2n^2 - n)K_{n+1}X^{n-1}} = 0 \tag{7.14}$$

Now, the slow roll parameters are needed to be calculated to get the expressions for the observables. The two potential slow roll parameters are given as:

$$\epsilon_V = \frac{1}{2}\left(\frac{6^{n-1}}{n}\right)^{\frac{1}{2n-1}}\left(\frac{V'^{2n}}{V^{(3n-1)}}\right)^{\frac{1}{2n-1}} \tag{7.15}$$

$$\eta_V = \left(\frac{6^{n-1}}{n}\right)^{\frac{1}{2n-1}}\left(\frac{V''^{(2n-1)}}{V^n V'^{(2n-2)}}\right)^{\frac{1}{2n-1}} \tag{7.16}$$

The scalar and tensor power spectra are given as:

$$\mathcal{P}_s = \frac{1}{8\pi^2 M_{\rm Pl}^2}\frac{H^2}{\epsilon_V c_s}|_{c_s k=aH}, \tag{7.17}$$

$$\mathcal{P}_t = \frac{2}{\pi^2 M_{\rm Pl}^2}H^2|_{k=aH}. \tag{7.18}$$

Then the inflationary observables can be calculated to be:

$$n_s - 1 = \frac{1}{2n-1}[2n\eta_V - 2(5n-2)\epsilon_V] \tag{7.19}$$

$$r = 16 c_s \epsilon_V \tag{7.20}$$

Finally, the number of e-folds can be expressed in this case as:

$$N = \int_{\phi_e}^{\phi_i}\left(\frac{n}{6^{n-1}}\right)^{\frac{1}{2n-1}}\sqrt{V}\left(\frac{\sqrt{V}}{V'}\right)^{\frac{1}{2n-1}} d\phi \tag{7.21}$$

Here, ϕ_i and ϕ_e represents the field values of the inflaton field at the horizon exit and end of inflation respectively.

7.3 Analysis for Goldstone inflation

Here, we analyse the effect of non-canonial scenarios *Case- 1* and *Case- 2* on the dynamics of Goldstone inflation. We consider the potential for the Goldstone inflation in the form of Eq. (7.1) with $C_\Lambda = \alpha = 1$, $\beta \equiv \frac{\beta}{\alpha}$.

7.3.1 *C*ase-1

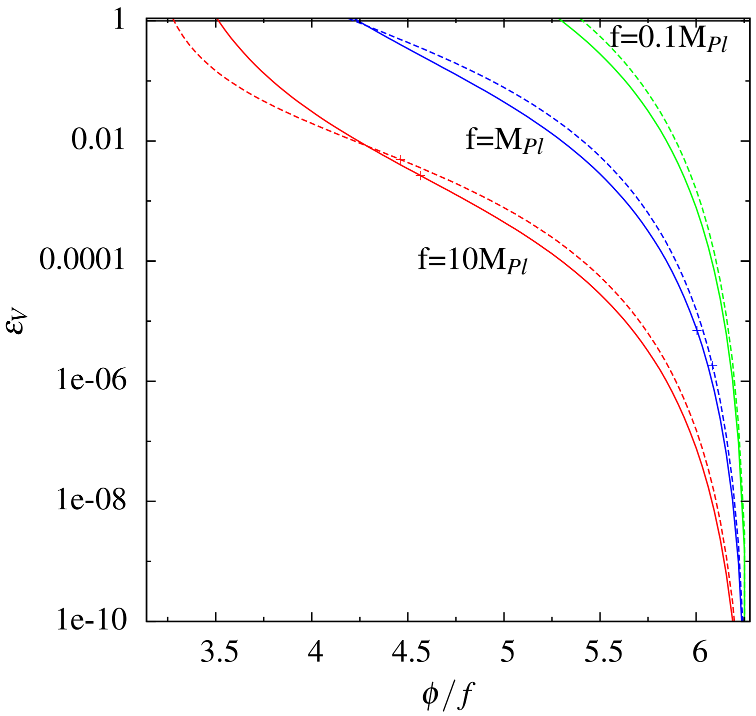

Figure 7.1: The variation of ϵ_V as a function of the field. The dashed lines represent canonical Goldstone inflation whereas the solid lines represent non-canonical Goldstone inflation with $K_{\rm nc}$ switched on and $K_{\rm kin} = X$ (*Case-1*). The pivot field values for 55 e-folds of inflation for the cases $f = M_{\rm Pl}$ and $f = 10M_{\rm Pl}$ are marked with crosses in the curves.

Using the following non-canonical form:

$$K_{\rm kin}(X) = X, \tag{7.22}$$

$$K_{\rm nc}(\phi) = 1 + \alpha\cos(\phi/f) + \beta\sin^2(\phi/f) = \frac{V(\phi)}{\Lambda^4}, \tag{7.23}$$

we arrive at the EoM:

$$\ddot{\phi} + 3H\dot{\phi} + \left(\frac{\dot{\phi}^2}{2} + \Lambda^4\right)\left[\frac{-\alpha\sin(\phi/f) + \beta\sin(2\phi/f)}{f(1+\alpha\cos(\phi/f) + \beta\sin^2(\phi/f))}\right] = 0. \tag{7.24}$$

The slow roll parameters are:

$$\epsilon_V = \frac{\Lambda^4 M_{Pl}^2}{2}\left(\frac{(-\alpha\sin(\phi/f) + \beta\sin(2\phi/f))^2}{f^2(1+\alpha\cos(\phi/f) + \beta\sin^2(\phi/f))^3}\right), \tag{7.25}$$

$$\eta_V = M_{Pl}^2\Lambda^2\frac{-\alpha\cos(\phi/f) + 2\beta\cos(2\phi/f) - \alpha^2 - \beta^2(1-\cos(2\phi/f) + \alpha\beta\cos(\phi/f)(1+\cos^2(\phi/f))}{f^2(1+\alpha\cos(\phi/f) + \beta\sin^2(\phi/f))^3} \tag{7.26}$$

In Fig. 7.1, the variation of ϵ_V is shown as a function of the normalised field value ϕ/f. For the breaking scale $f = 10M_{\rm Pl}$ (red line), the ϵ_V at pivot (marked with cross) is lower in case of non-canonical Goldstone inflation than the canonical case, therefore pointing towards a lower energy scale of inflation. But for $f \leq M_{\rm Pl}$, the pivot energy scale for non-canonical case is higher than the canonical case. This has been depicted by the blue and green lines in the Fig. 7.1. It should be noted that varying α also as a parameter may improve the predictions for observables.

7.3.2 *C*ase- 2

The Natural inflation is a limiting case of the generalised goldstone inflation with $\alpha = 1$ and $\beta = 0$. We start with the analysis of Natural inflation to clarify the dependence of the inflationary observables on the parameters of the model, which is also applicable by extension to generic Goldstone inflation. For Natural inflation, the potential and the kinetic

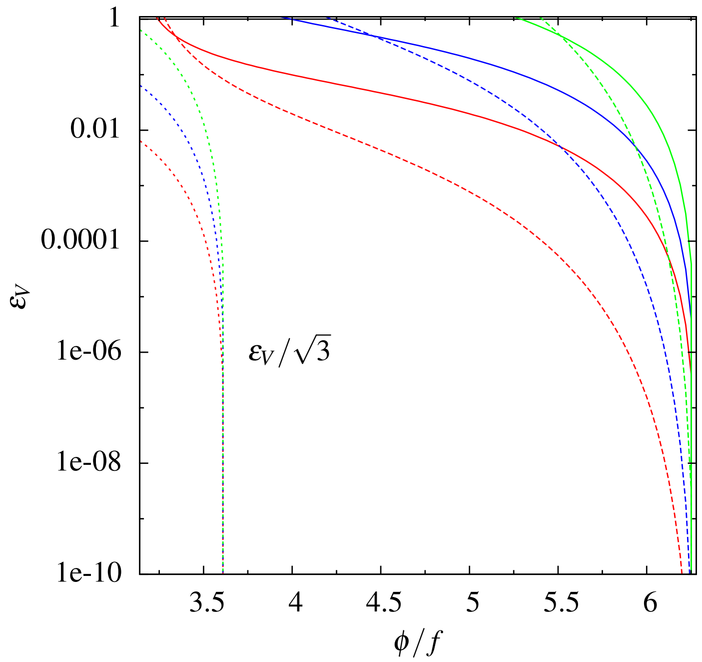

Figure 7.2: The variation of ϵ_V as a function of the field. The dashed lines represent canonical Goldstone inflation whereas the solid lines represent non-canonical Goldstone inflation with $K_{\rm kin}$ switched on and $K_{\rm nc} = 1$. The plots are for $f = 10M_{\rm Pl}$ (in red), $f = M_{\rm Pl}$ (in blue) and $f = 0.1M_{\rm Pl}$ (in green).

functions are given as:

$$V = \Lambda^4(1 + \cos(\phi/f)) \tag{7.27}$$

$$K = K_{n+1}X^n \tag{7.28}$$

Then, the slow roll parameters are:

$$\begin{aligned} \epsilon_V &= \frac{1}{2}\frac{V'}{V}\gamma(n)\left(\frac{V'}{V^n}\right)^{\frac{1}{2n-1}} \\ &= \frac{1}{2}\frac{1}{(K_3\Lambda^4)^{1/3}}\left[\frac{\sin^4(\phi/f)}{(1+\cos(\phi/f))^5}\right]^{1/3} \end{aligned} \tag{7.29}$$

$$
\begin{aligned}
\eta_V &= \gamma(n)\left(\frac{V''^{(2n-1)}}{V^n V'^{(2n-1)}}\right)^{\frac{1}{2n-1}} \\
&= \frac{1}{(K_3\Lambda^4)^{1/3}}\left[\frac{\cos(\phi/f)}{\sin(\phi/f)(1+\cos(\phi/f))^{2/3}}\right],
\end{aligned}
\tag{7.30}
$$

where $\gamma(n) = \left(\frac{6^{n-1}}{nK_{n+1}}\right)^{\frac{1}{2n-1}}$ and in each of the above two equations, the second line is the expression for $n = 2$. The ratio of the scalar power spectra in case of kinetic natural inflation ($n = 2$) to the canonical natural inflation ($n = 1$) can be written as:

$$
\begin{aligned}
\frac{P_s^{n=2}}{P_s^{n=1}} &= \frac{1}{\gamma(2)c_s} \times \frac{V^{8/3}}{V'^{4/3}} \times \frac{V'^2}{V^3} = \frac{1}{\gamma(2)c_s} \times \frac{V^{2/3}}{V'^{1/3}} = \left(\frac{K_3}{3}\right)^{1/3} \times 3^{1/3} \times \frac{V^{2/3}}{V'^{1/3}} \\
&= 3^{1/6} \times K_3^{1/3}\left[\frac{(\Lambda^4/f)^2\sin^2(\phi/f)}{\Lambda^4(1+\cos(\phi/f))}\right]^{1/3} \\
&= 3^{1/6} \times \left(\frac{1}{f^{2/3}}\right) \times (K_3\Lambda^4)^{1/3} \times \left[\frac{\sin^2(\phi/f)}{1+\cos(\phi/f)}\right]^{1/3}
\end{aligned}
\tag{7.31}
$$

Thus, from the equation (7.31) it is clear that:

$$
\frac{P_s^{n=2}}{P_s^{n=1}} \propto \frac{(K_3\Lambda^4)^{1/3}}{f^{2/3}}
\tag{7.32}
$$

From the dependences of ϵ_V and η_V for Natural inflation here, on the factor $(K_3\Lambda^4)^{1/3}$ and on f, it is evident that the slow roll parameters have values (> 1) not compatible with the slow roll condition for most of the inflaton's journey on the slope of the potential. To summarise the point, let us take $f = 10M_{\rm Pl}$. For the sake of a simplistic analysis, let us assume the term in the square bracket in the equation (7.31) is $\mathcal{O}(1)$. Then, the first slow roll parameter is: $\epsilon_V \simeq \frac{3^{1/3}}{2} \times 10^{-4} \times \frac{1}{(K_3\Lambda^4)^{1/3}}$. Thus, for $K_3 = 1$, for any realistic scale of inflation (value of Λ^4) the pivot value of ϵ_V is quite large to have $50 - 60$ e-folds of inflation, which is required from observations. Therefore, it is difficult to achieve enough number of inflationary e-folds for *Case-2* of kinetic natural inflation.

By analogy, for the case of Goldstone inflation in the non-canonical regime of *Case-2*, the combination of parameters $(K_3\alpha\Lambda^4)^{1/3}$ influences the dynamics of inflation in a similar way. The factor $\alpha^{1/3}$ appears since we have considered it as an overall factor in the potential and varied the normalised value of $\beta \equiv \beta/\alpha$ in this case. The variations of the first slow roll parameter ϵ_V as a function of ϕ/f is shown in Fig. 7.2, where, unlike *Case-1*, ϵ_V for a non-canonical *case-2* is higher than that for a canonical case for a particular value of ϕ/f. But, as shown in Eq. (7.20) in Sec. 7.2.2, the energy scale of inflation depends on the speed of sound $c_s = \frac{1}{2n-1} = 1/\sqrt{3}$. This factor appears in the EoM Eq. (7.14) and also in the expression of the pivot quantities. A variation of $\epsilon_V/\sqrt{3}$ in Fig. 7.2 shows that for a particular field value, the non-canonical Goldstone inflation (*Case-2*) points to a lower effective energy scale of inflation (plotted as $\epsilon_V/\sqrt{3}$ in Fig. 7.2) compared to its canonical picture, although at the cost of very steep rolling during inflation.

Therefore, to achieve enough number of e-folds (taken to be $N = 55$ in the analysis) in this case,the combination of $(K_3\alpha\Lambda^4)^{1/3}$ needs to be modified (increased).

7.4 Result

The main observables for inflation in CMB for the ΛCDM model are the scalar spectral index n_s and the tensor-to-scalar ratio r which are measured by PLANCK 2018 [4] with immense precision. The exact values of these parameters with 1σ errors as constrained by PLANCK 2018 are $n_s = 0.9665 \pm 0.0038$ (TT, TE, EE+ lowE+ lensing data), $r < 0.064$ (TT, TE, EE+ lowE +lensing data+ BK14). In this section, we discuss the predictions of the Goldstone inflation in the canonical regime for n_s and r with respect to their values in 1σ and 2σ confidence levels given by PLANCK 2018. We consider two different datasets

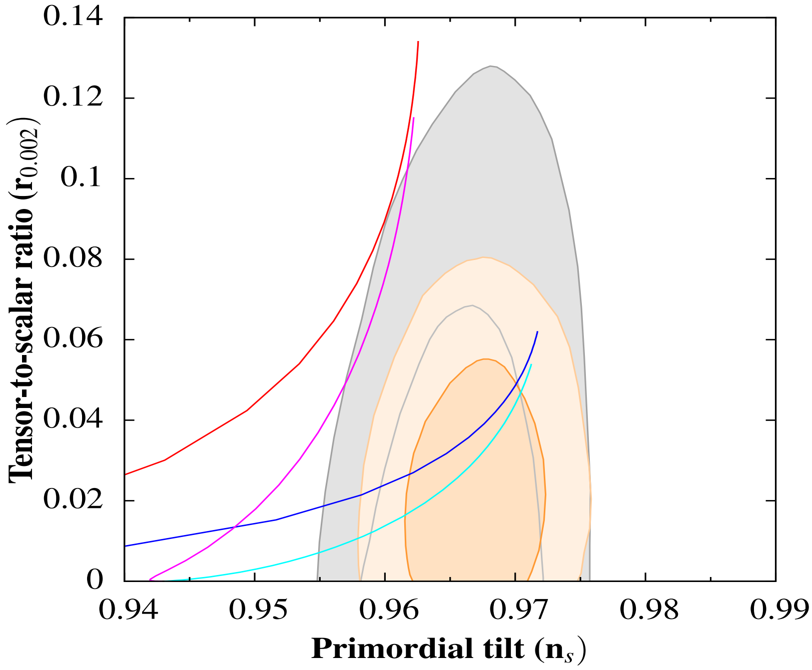

Figure 7.3: Comparison in the n_s-r plane between canonical natural inflation (red), non-canonical natural inflation (blue), canonical Goldstone inflation (magenta) and non-canonical Goldstone inflation (cyan). The Goldstone inflation curves plotted here are for $\beta = 0.5$. The dark and light grey regions signify 68% and 96% confidence limits respectively for PLANCK TT,TE,EE+lowE+lensing data (2018) [4], whereas dark and light yellow regions signify 68% and 96% confidence limits respectively for PLANCK TT,TE,EE+lowE (2018)+lensing+BK14 [31]+BAO data [32–34].

in our analysis: (i) the most constrained PLANCK TT,TE,EE+lowE + lensing + BK14 + BAO and (ii) PLANCK TT,TE,EE+lowE+lensing.

In Fig. 7.3, we compared the predictions for natural inflation and Goldstone inflation in the canonical regime and in the non-canonical regime (*Case-1*). The non-canonical plot here is just for comparison and plotted for $\beta = 0.5$ ($C_\Lambda = 1$, $\alpha = 1$). It is evident from this plot that non-canonical picture $K_{\rm nc}(\phi) = V(\phi)/\Lambda^4$ does improve the predictions for inflation by a significant suppression of r.

In Fig. 7.4, we explored the observables in the n_s-r plane for *Case-1* of non-canonical Goldstone inflation while varying the model parameter β. For each value of β, the solid line

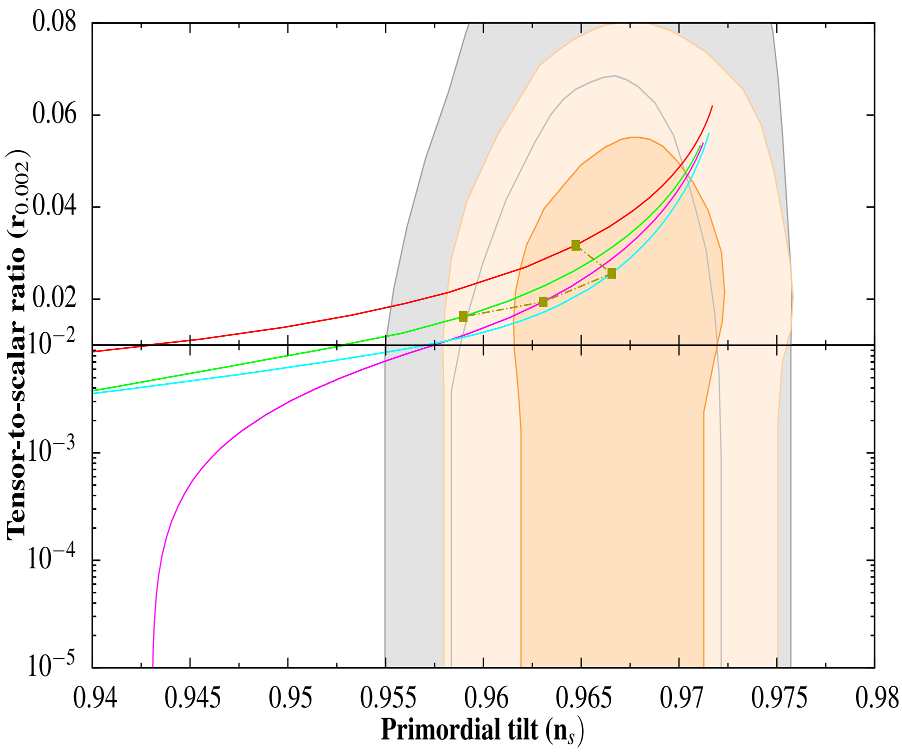

Figure 7.4: Comparison in the n_s-r plane for non-canonical Goldstone inflation with different values of β keeping $\alpha = 1$. $\beta = 0$ (non-canonical natural inflation) is in red, $\beta = 0.25$ in cyan, $\beta = 0.5$ in magenta and $\beta = 0.75$ in green. The green dot-dashed line connects the points with $f = 5M_{\rm Pl}$ in all the curves. The yellow dark and light regions signify 68% and 96% confidence limits respectively for PLANCK TT,TE,EE+lowE+lensing data (2018) [4], whereas grey ark and light regions signify 68% and 96% confidence limits respectively for PLANCK TT,TE,EE+lowE (2018)+lensing+BK14 [31]+BAO data [32–34].

runs for variation of the breaking scale f up to $16M_{\rm Pl}$. The plot shows that for most of the super-Planckian breaking scales $f > M_{\rm Pl}$, the non-canonical scenario (*Case-1*) lowers the tensor-to-scalar ratio r for all values of $\beta < \alpha$. But, similar to the default canonical Natural inflation case, this does not improve the predictions for n_s and r in the sub-Planckian scales $f < M_{\rm Pl}$. This was hinted from Fig. 7.1, where the pivot field value for the non-canonical *Case-1* predicted higher value of ϵ_V for $f \leq M_{\rm Pl}$. Particularly, for $\beta = 0.5$, even though r decreases rapidly with the decrease in f below $M_{\rm Pl}$, the spectral index n_s is outside the current precision bounds by PLANCK.

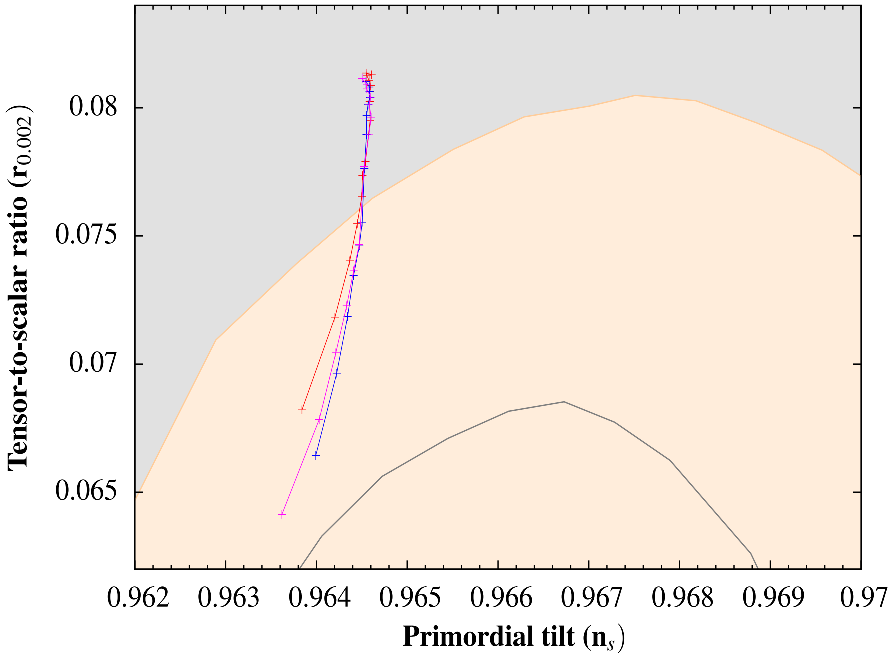

Figure 7.5: The n_s-r plot for kinetic inflation. Kinetic natural inflation curve is plotted in red, whereas kinetic Goldstone inflation curves for $\beta = 0.2$ is in magenta, for $\beta = 0.5$ is in blue. The light grey region pervading all through the plot signifies 96% confidence limit for PLANCK TT,TE,EE+lowE+lensing data (2018) [4], whereas the dark grey contour signifies 68% confidence limit for the same data combination. The yellow shaded region signifies 96% confidence level for PLANCK TT,TE,EE+lowE (2018)+lensing+BK14 [31]+BAO data [32–34]. For each curve, the lowest value of r is for $f = 0.5M_{\rm Pl}$.

Fig. 7.5 shows the predictions for the inflationary observables for *Case-2* of non-canonical Goldstone inflation. Here, we see that the n_s and r values for the sub-Planckian breaking scales $f < M_{\rm Pl}$ are inside the 2σ bounds give by PLANCK dataset (i) for all values of β. But the prediction of r is larger compared to *Case-1*, which makes the Goldstone inflation in kinetc non-canonical regime *Case-2* vulnerable to future precision detections of primordial tensor modes.

In Fig. 7.6, the three solid lines all refer to the same f, but differ in inputs of β. In each of the solid lines, we have compared the three cases: canonical (leftmost point), non-

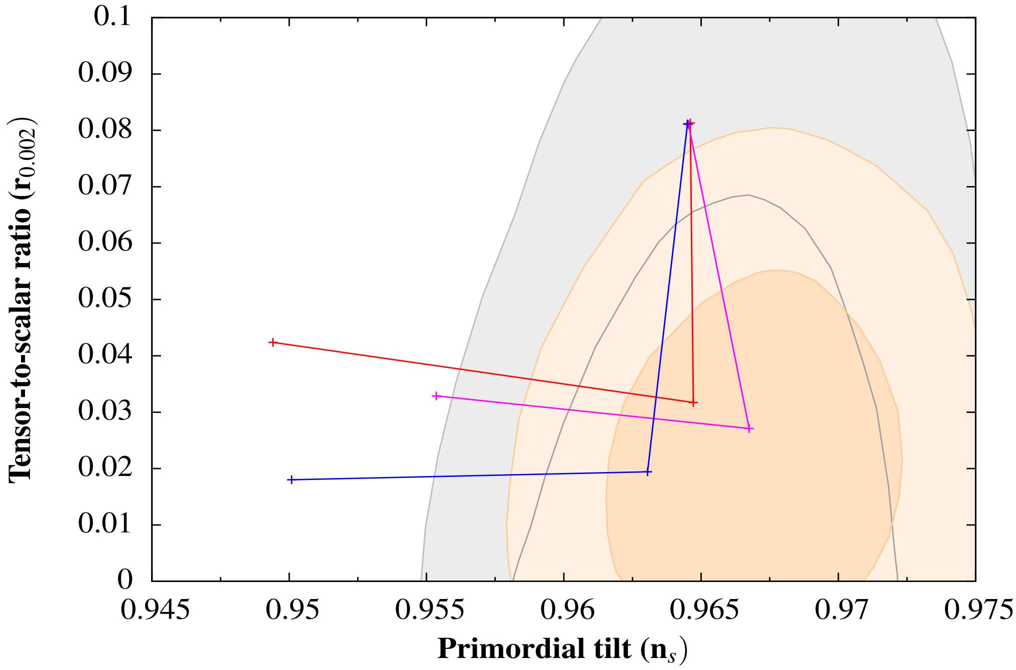

Figure 7.6: Comparison in the n_s-r plane between natural inflation and Goldstone inflation for $f = 5M_{\rm Pl}$ (fixed). The natural inflation curve is plotted in red whereas Goldstone inflation curve for the combination $\alpha = 1$,$\beta = 0.5$ is in blue and for the combination $\alpha = 1$,$\beta = 0.2$ is in magenta. The three points from left to right in each of the curves are for the canonical, non-canonical and kinetic cases respectively. The dark and light grey regions signify 68% and 96% confidence limits respectively for PLANCK TT,TE,EE+lowE+lensing data (2018) [4], whereas dark and light yellow regions signify 68% and 96% confidence limits respectively for PLANCK TT,TE,EE+lowE (2018)+lensing+BK14 [31]+BAO data [32–34].

canonical *Case-1* (middle point) and non-canonical *Case-2* (rightmost point). As hinted in the previous figures, we can see that of the all three cases, the non-canonical *Case-1* provides best predictions for the super-Planckian case $f = 5M_{\rm Pl}$ with reference to current bounds from PLANCK.

7.5 Conclusions and Discussions

With future observations like CMB-S4 [29] and CORE [30] with promising prospects to measure the spectral tilt very precisely ($\Delta n_s \sim 0.002$), and with future possibilities to constrain the primordial tensor modes, a systematic study of the unconventional scenarios of inflation for theoretically motivated models has become essential. Models that are well motivated from theory but facing trouble to predict observable parameters within experimental bounds need to be reevaluated in scenarios such as non-minimal coupling to gravity [214] or non-canonical inflation. Inflaton being a pNGB has a very promising theoretical justification and therefore, a Goldstone potential to drive the inflationary expansion is studied here in the non-canonical scenario constrained from latest CMB data.

We emphasize that using a non-canonical framework in [201] helped to avoid fine-tuning of model parameters, which is unavoidable in the canonical case of Goldstone inflation. For *Case-1*, the prototype $K_{\rm nc}(\phi) = V(\phi)/\Lambda^4$ is just to give an effective flatness to the potential. More forms of $K_{\rm nc}(\phi)$ arising from non-minimal gravitational coupling will be interesting to analyse, as they come naturally from non-trivial Lagrangians in the Jordan frame [13, 85, 215]. We have done the analysis for *Case-2* with only $n = 2$ due to mainly two reasons. Firstly, renormalization of the theory is an issue in any case of kinetic inflation and therefore, it is safe to start with the minimal deviation from the canonical case. Secondly, the observational bound on the cosmological sound speed c_s restricts the power n of the kinetic term.

For non-canonical *Case- 1* we get smaller tensor-to-scalar ratio (r), however we do not achieve enough e-folds of inflation for sub-Planckian f. On the other hand, for *Case- 2* we achieve ~ 55 e-folds of inflation even for sub-Planckian f, but at the cost of r values lying outside the current 68% bound. A generalised kinetic term with both the cases switched on will be interesting in terms of the prediction for observables, if their effects combine in a constructive manner. The next natural step should be to test these models with thorough numerical analysis using Bayesian techniques. Another exciting case would be to check the effects of non-canonical inflation in the brane-world scenarios. As expected in the brane-world scenario, there is a natural tendency of increasing r [216], it would be interesting to check NCI in that paradigm. We hope to return to these problems in near future. Another issue which might need a serious theoretical explanation is the observed anomaly at the low multipole in the CMB power spectrum as observed by PLANCK as well as WMAP. Many explanations [217–221] are being put forward and on that note it would be exciting to check if a non-canonical initial condition could orchestrate such an imprint on such scales.

Finally, we comment regarding the recently proposed Swampland Criteria (fiasco!) [222] which created some sensation in the cosmology community. On that regard, we would like to emphasize that non-canonical inflation, specifically *Case- 2*, with a theoretically well-motivated potential could actually evade the problem and might be a natural answer to it since the Lagrangian for NCI is expected and motivated from String theory. The bounds on c_s from CMB could also play a key role in that as indicated in [223]. This is another interesting problem that we would like to address soon.

CHAPTER 8

CONCLUSIONS

In this chapter, we summarize the results obtained in the works included in the thesis to conclude and discuss future prospects of studies along this line of research. This thesis is focussed on analysing some models of inflation in non-trivial settings that are motivated by high energy theories. These analyses involved establishing deep connections between theoretical studies of the inflationary models to the observables for the primordial power spectrum in CMB, sometimes with a rigorous numerical methodology.

In chapter 1, the idea of cosmology has been introduced. In chapter 2, the standard hot big bang model, its pitfalls and their solutions by the introduction of the inflation epoch have been discussed in detail. In the same chapter, the background and perturbation dynamics of inflation have been produced with an emphasis on the observable quantities in the CMB experiments. In chapter 3, we have discussed how the observed temperature fluctuations in CMB experiments can be related to the power spectrum, which is a function of the basic ΛCDM and inflationary parameters. In the same chapter, the numerical methodology for comparing theoretical predictions for the primordial power spectrum for a particular model of inflation with the observed spectrum at recombination has been discussed. In the chapters 4, 5, 6 and 7, we move on to present the new works done during the time of doctoral research.

It is crucial to understand the true dynamics during inflation since the physics of the universe at such high energies ($\sim$ GUT scale) and such early times is a potential probe of the UV energy scales, which is beyond the access of the standard model of particle physics. In this context, the nature of the scalar field driving inflation and the possible couplings of the inflaton with other degrees of freedom that may be present during inflation is an important input to study the underlying energy budget and evolution during the pre-BBN epoch. For these reasons, model-building to provide the correct action for the epoch of inflation is a major topic in contemporary research of early universe cosmology.

Deviation from the minimal gravitational coupling of the inflaton can accommodate theories that consider modification of gravity at early universe. The generic implications of scalar-tensor theories of gravity, e.g. $f(R)$ theory, Brans-Dicke gravity etc., are studied in [13], specifically with respect to the dependence of the inflationary observables upon the degrees of freedom present in the Lagrangian. Inflation theories arising from such scalar-tensor models has been studied in [13] in the context of attractor models.

In a scenario where the inflaton is energetically coupled to other fields present in a thermal bath during inflation (warm inflation picture) is interesting with respect to various plausible particle physics models including Beyond Standard Model physics. Such warm inflationary scenarios may accommodate inflationary models that are motivated from particle physics, but ruled out by data in their cold inflation descriptions. A thorough numerical analysis of such a model $V = \lambda\phi^4$ has been carried out in [17], where the parameters of 'warm little inflation' have been constrained. The predictions of the previously refuted quartic chaotic model are found to be consistent in the warm inflation picture with recent observations.

The models of inflation that emerge from effective field theory descriptions of string theory are particularly interesting to study due to their prediction of an additional post-inflationary epoch where the energy density is dominated by cold moduli particles. Such a prototype model, namely the Kähler moduli inflation, has been studied from the reheating perspective in [21] and with precision numerical analysis in [22]. Here, the model parameters determine both inflationary observables as well as post-inflationary moduli dominated epoch. Confronting this model with the latest CMB data in [22] by full numerical analysis resulted in the prediction of inflationary observables. We concluded that these models require either exotic reheating scenarios, where the energy density decreases even faster than radiation, or possible introduction of dark radiation in the theory to comply with the recent bounds from CMB observations.

A non-canonical kinetic term is also very frequently encountered in high energy theories; e.g. many inflation models in string theory have a kinetic term of a higher order than the canonical case (kinetic inflation). On the particle physics front, Goldstone bosons are natural candidates for obtaining a quasi-flat inflation potential via shift symmetry. The study of Goldstone inflation in the non-canonical kinetic regime in [201] has concluded that a kinetic treatment of Goldstone inflation can achieve sub-Planckian symmetry breaking scales, while being consistent with the current observations (within 2σ limit) at the same time.

To summarise, the study of this thesis emphasises the importance of precision numerical analysis for the inflationary models which can emerge from viable high energy theories, and to understand the significance of the model parameters and their predictions for inflationary observables. Other than the outlooks discussed at the end of each chapter for each of the scenarios analysed in this thesis, there are many more arenas of inflation that are very interesting to explore, especially with the prospect of future cosmological observations. Detection of primordial B modes by future CMB surveys and direct/indirect detection of primordial gravitational waves will be elemental in resolving among the plethora of inflationary models and also to indicate the energy scale of inflation. The excursion of inflaton is also sensitive to the primordial tensor fluctuations and therefore is a key feature for the viability of inflation models. The possibility of setting a quasi-de Sitter manifold of inflation in swampland is also exciting to explore, especially with non-trivial inflationary scenarios that can evade the slow roll condition for the inflaton potential. Moreover, our lack of knowledge about the post-inflationary epochs up to BBN may be attempted to be improved by better parametrization of the reheating epoch and future detection of primordial gravitational waves from preheating. A better understanding about cosmological inflation and (p)reheating epochs are necessary to obtain a complete picture of the history of the evolution of our universe and this can be achieved by judicially combining relevant theories with latest data via precision numerical and statistical analysis.

BIBLIOGRAPHY

[1] A. H. Guth, *The Inflationary Universe: A Possible Solution to the Horizon and Flatness Problems*, *Phys. Rev.* **D23** (1981) 347–356.

[2] G. F. Smoot, *COBE observations and results*, *AIP Conf. Proc.* **476** (1999) 1–10, [astro-ph/9902027].

[3] WMAP collaboration, G. Hinshaw et al., *Nine-Year Wilkinson Microwave Anisotropy Probe (WMAP) Observations: Cosmological Parameter Results*, *Astrophys. J. Suppl.* **208** (2013) 19, [1212.5226].

[4] PLANCK collaboration, Y. Akrami et al., *Planck 2018 results. X. Constraints on inflation*, 1807.06211.

[5] D. Baumann, *Inflation*, in *Physics of the large and the small, TASI 09, proceedings of the Theoretical Advanced Study Institute in Elementary Particle Physics, Boulder, Colorado, USA, 1-26 June 2009*, pp. 523–686, 2011. 0907.5424. DOI.

[6] R. H. Brandenberger, *Lectures on the theory of cosmological perturbations*, *Lect. Notes Phys.* **646** (2004) 127–167, [hep-th/0306071].

[7] J. Martin, C. Ringeval and V. Vennin, *EncyclopÃędia Inflationaris*, *Phys. Dark Univ.* **5-6** (2014) 75–235, [1303.3787].

[8] J. Martin, C. Ringeval, R. Trotta and V. Vennin, *The Best Inflationary Models After Planck*, *JCAP* **1403** (2014) 039, [1312.3529].

[9] A. D. Linde, *Chaotic Inflation*, *Phys. Lett.* **129B** (1983) 177–181.

[10] A. A. Starobinsky, *A New Type of Isotropic Cosmological Models Without Singularity*, *Phys. Lett.* **B91** (1980) 99–102.

[11] M. Galante, R. Kallosh, A. Linde and D. Roest, *Unity of Cosmological Inflation Attractors*, *Phys. Rev. Lett.* **114** (2015) 141302, [1412.3797].

[12] S. Ferrara, R. Kallosh, A. Linde, A. Marrani and A. Van Proeyen, *Jordan Frame Supergravity and Inflation in NMSSM*, *Phys. Rev.* **D82** (2010) 045003, [1004.0712].

[13] S. Bhattacharya, K. Das and K. Dutta, *Attractor models in scalarâĂŞtensor theories of inflation*, *Int. J. Mod. Phys.* **D27** (2018) 1850079, [1706.07934].

[14] A. Lewis and S. Bridle, *Cosmological parameters from CMB and other data: A Monte Carlo approach*, *Phys. Rev.* **D66** (2002) 103511, [astro-ph/0205436].

[15] A. Berera, *Warm inflation*, *Phys. Rev. Lett.* **75** (1995) 3218–3221, [astro-ph/9509049].

[16] M. Bastero-Gil, A. Berera, R. O. Ramos and J. G. Rosa, *Warm Little Inflaton*, *Phys. Rev. Lett.* **117** (2016) 151301, [1604.08838].

[17] M. Bastero-Gil, S. Bhattacharya, K. Dutta and M. R. Gangopadhyay, *Constraining Warm Inflation with CMB data*, *JCAP* **1802** (2018) 054, [1710.10008].

[18] BICEP2, PLANCK collaboration, P. A. R. Ade et al., *Joint Analysis of BICEP2/$KeckArray$ and $Planck$ Data*, *Phys. Rev. Lett.* **114** (2015) 101301, [1502.00612].

[19] J. P. Conlon, F. Quevedo and K. Suruliz, *Large-volume flux compactifications: Moduli spectrum and D3/D7 soft supersymmetry breaking*, *JHEP* **08** (2005) 007, [hep-th/0505076].

[20] J. P. Conlon and F. Quevedo, *Kähler moduli inflation*, *JHEP* **01** (2006) 146, [hep-th/0509012].

[21] S. Bhattacharya, K. Dutta and A. Maharana, *Constraints on Kähler moduli inflation from reheating*, *Phys. Rev.* **D96** (2017) 083522, [1707.07924].

[22] S. Bhattacharya, K. Dutta, M. R. Gangopadhyay and A. Maharana, *Confronting Kähler moduli inflation with CMB data*, *Phys. Rev.* **D97** (2018) 123533, [1711.04807].

[23] M. J. Mortonson, H. V. Peiris and R. Easther, *Bayesian Analysis of Inflation: Parameter Estimation for Single Field Models*, *Phys. Rev.* **D83** (2011) 043505, [1007.4205].

[24] J. A. Frieman, *Lectures on dark energy and cosmic acceleration*, *AIP Conf. Proc.* **1057** (2008) 87–124, [0904.1832].

[25] A. Albrecht, *Cosmic inflation and the arrow of time*, astro-ph/0210527.

[26] P. Adshead, R. Easther, J. Pritchard and A. Loeb, *Inflation and the Scale Dependent Spectral Index: Prospects and Strategies*, *JCAP* **1102** (2011) 021, [1007.3748].

[27] PLANCK collaboration, N. Aghanim et al., *Planck 2018 results. VI. Cosmological parameters*, 1807.06209.

[28] PLANCK collaboration, P. A. R. Ade et al., *Planck 2015 results. XX. Constraints on inflation*, *Astron. Astrophys.* **594** (2016) A20, [1502.02114].

[29] CMB-S4 collaboration, K. N. Abazajian et al., *CMB-S4 Science Book, First Edition*, 1610.02743.

[30] CORE collaboration, F. Finelli et al., *Exploring cosmic origins with CORE: Inflation*, *JCAP* **1804** (2018) 016, [1612.08270].

[31] BICEP2, KECK ARRAY collaboration, P. A. R. Ade et al., *Improved Constraints on Cosmology and Foregrounds from BICEP2 and Keck Array Cosmic Microwave Background Data with Inclusion of 95 GHz Band*, *Phys. Rev. Lett.* **116** (2016) 031302, [1510.09217].

[32] F. Beutler, C. Blake, M. Colless, D. H. Jones, L. Staveley-Smith, L. Campbell et al., *The 6dF Galaxy Survey: Baryon Acoustic Oscillations and the Local Hubble Constant*, *Mon. Not. Roy. Astron. Soc.* **416** (2011) 3017–3032, [1106.3366].

[33] N. Padmanabhan, X. Xu, D. J. Eisenstein, R. Scalzo, A. J. Cuesta, K. T. Mehta et al., *A 2 per cent distance to z=0.35 by reconstructing baryon acoustic oscillations - I. Methods and application to the Sloan Digital Sky Survey*, *Mon. Not. Roy. Astron. Soc.* **427** (2012) 2132–2145, [1202.0090].

[34] L. Anderson et al., *The clustering of galaxies in the SDSS-III Baryon Oscillation Spectroscopic Survey: Baryon Acoustic Oscillations in the Data Release 9 Spectroscopic Galaxy Sample*, Mon. Not. Roy. Astron. Soc. **427** (2013) 3435–3467, [1203.6594].

[35] Planck Collaboration, R. Adam, P. A. R. Ade, N. Aghanim, M. I. R. Alves, M. Arnaud et al., *Planck 2015 results. X. Diffuse component separation: Foreground maps*, Astron.Astrophys. **594** (Sept., 2016) A10, [1502.01588].

[36] M. Colless et al., *The 2dF Galaxy Redshift Survey: Final data release*, astro-ph/0306581.

[37] SDSS collaboration, K. N. Abazajian et al., *The Seventh Data Release of the Sloan Digital Sky Survey*, Astrophys. J. Suppl. **182** (2009) 543–558, [0812.0649].

[38] E. W. Kolb and M. S. Turner, *The Early Universe*, *Front. Phys.* **69** (1990) 1–547.

[39] PLANCK collaboration, Y. Akrami et al., *Planck 2018 results. I. Overview and the cosmological legacy of Planck*, 1807.06205.

[40] A. H. Guth, *Inflationary universe: A possible solution to the horizon and flatness problems*, Phys. Rev. D **23** (Jan, 1981) 347–356.

[41] J. R. Bond, L. Kofman, S. Prokushkin and P. M. Vaudrevange, *Roulette inflation with Kahler moduli and their axions*, Phys. Rev. **D75** (2007) 123511, [hep-th/0612197].

[42] Z. Lalak, G. G. Ross and S. Sarkar, *Racetrack inflation and assisted moduli stabilisation*, Nucl. Phys. **B766** (2007) 1–20, [hep-th/0503178].

[43] B. de Carlos, J. A. Casas, A. Guarino, J. M. Moreno and O. Seto, *Inflation in uplifted Supergravities*, *JCAP* **0705** (2007) 002, [hep-th/0702103].

[44] V. Mukhanov, *Physical Foundations of Cosmology*. Cambridge University Press, Oxford, 2005.

[45] A. D. Linde, *A New Inflationary Universe Scenario: A Possible Solution of the Horizon, Flatness, Homogeneity, Isotropy and Primordial Monopole Problems*, *Phys. Lett.* **108B** (1982) 389–393.

[46] S. Dodelson, *Modern Cosmology*. Academic Press, Amsterdam, 2003.

[47] W. H. Kinney, *TASI Lectures on Inflation*, astro-ph.CO/0902.1529.

[48] A. Lewis and A. Challinor, *Weak gravitational lensing of the CMB*, *Phys. Rept.* **429** (2006) 1–65, [astro-ph/0601594].

[49] R. K. Sachs and A. M. Wolfe, *Perturbations of a cosmological model and angular variations of the microwave background*, *Astrophys. J.* **147** (1967) 73–90.

[50] R. A. Sunyaev and Ya. B. Zeldovich, *The Observations of relic radiation as a test of the nature of X-Ray radiation from the clusters of galaxies*, *Comments Astrophys. Space Phys.* **4** (1972) 173–178.

[51] LIGO Scientific, Virgo collaboration, B. P. Abbott et al., *GW150914: Implications for the stochastic gravitational wave background from binary black holes*, *Phys. Rev. Lett.* **116** (2016) 131102, [1602.03847].

[52] N. Bartolo et al., *Science with the space-based interferometer LISA. IV: Probing inflation with gravitational waves*, *JCAP* **1612** (2016) 026, [1610.06481].

[53] A. Lewis, *Efficient sampling of fast and slow cosmological parameters*, *Phys.Rev.D* **87** (2013) 103529, [1304.4473].

[54] F. L. Bezrukov and M. Shaposhnikov, *The Standard Model Higgs boson as the inflaton*, *Phys. Lett.* **B659** (2008) 703–706, [0710.3755].

[55] D. S. Salopek, J. R. Bond and J. M. Bardeen, *Designing Density Fluctuation Spectra in Inflation*, *Phys. Rev.* **D40** (1989) 1753.

[56] N. Okada, M. U. Rehman and Q. Shafi, *Tensor to Scalar Ratio in Non-Minimal ϕ^4 Inflation*, *Phys. Rev.* **D82** (2010) 043502, [1005.5161].

[57] F. Bezrukov and D. Gorbunov, *Light inflaton after LHC8 and WMAP9 results*, *JHEP* **07** (2013) 140, [1303.4395].

[58] K. Dutta and A. Maharana, *Inflationary constraints on modulus dominated cosmology*, *Phys. Rev.* **D91** (2015) 043503, [1409.7037].

[59] K. Das, K. Dutta and A. Maharana, *Inflationary Predictions and Moduli Masses*, *Phys. Lett.* **B751** (2015) 195–200, [1506.05745].

[60] M. Cicoli, K. Dutta, A. Maharana and F. Quevedo, *Moduli Vacuum Misalignment and Precise Predictions in String Inflation*, *JCAP* **1608** (2016) 006, [1604.08512].

[61] A. Ijjas, P. J. Steinhardt and A. Loeb, *Inflationary paradigm in trouble after Planck2013*, *Phys. Lett.* **B723** (2013) 261–266, [1304.2785].

[62] D. H. Lyth, *What would we learn by detecting a gravitational wave signal in the cosmic microwave background anisotropy?*, *Phys. Rev. Lett.* **78** (1997) 1861–1863, [hep-ph/9606387].

[63] X. Dong, B. Horn, E. Silverstein and A. Westphal, *Simple exercises to flatten your potential*, *Phys. Rev.* **D84** (2011) 026011, [1011.4521].

[64] S. Ferrara, R. Kallosh, A. Linde, A. Marrani and A. Van Proeyen, *Superconformal Symmetry, NMSSM, and Inflation*, *Phys. Rev.* **D83** (2011) 025008, [1008.2942].

[65] R. Kallosh and A. Linde, *Planck, LHC, and α-attractors*, *Phys. Rev.* **D91** (2015) 083528, [1502.07733].

[66] A. Linde, *Single-field α-attractors*, *JCAP* **1505** (2015) 003, [1504.00663].

[67] J. J. M. Carrasco, R. Kallosh and A. Linde, *α-Attractors: Planck, LHC and Dark Energy*, *JHEP* **10** (2015) 147, [1506.01708].

[68] T. Pinhero and S. Pal, *Non-canonical Conformal Attractors for Single Field Inflation*, 1703.07165.

[69] S. Ferrara, R. Kallosh, A. Linde and M. Porrati, *Minimal Supergravity Models of Inflation*, *Phys. Rev.* **D88** (2013) 085038, [1307.7696].

[70] R. Kallosh and A. Linde, *Superconformal generalizations of the Starobinsky model*, *JCAP* **1306** (2013) 028, [1306.3214].

[71] J. Ellis, D. V. Nanopoulos and K. A. Olive, *No-Scale Supergravity Realization of the Starobinsky Model of Inflation*, *Phys. Rev. Lett.* **111** (2013) 111301, [1305.1247].

[72] W. Buchmuller, V. Domcke and K. Kamada, *The Starobinsky Model from Superconformal D-Term Inflation*, *Phys. Lett.* **B726** (2013) 467–470, [1306.3471].

[73] K. Das, V. Domcke and K. Dutta, *Supergravity Contributions to Inflation in models with non-minimal coupling to gravity*, *JCAP* **1703** (2017) 036, [1612.07075].

[74] R. Kallosh, A. Linde and D. Roest, *Superconformal Inflationary α-Attractors*, *JHEP* **11** (2013) 198, [1311.0472].

[75] B. J. Broy, F. G. Pedro and A. Westphal, *Disentangling the $f(R)$ - Duality*, *JCAP* **1503** (2015) 029, [1411.6010].

[76] Q.-G. Huang, *A polynomial f(R) inflation model*, *JCAP* **1402** (2014) 035, [1309.3514].

[77] S. D. Odintsov and V. K. Oikonomou, *Inflationary α-attractors from $F(R)$ gravity*, *Phys. Rev.* **D94** (2016) 124026, [1612.01126].

[78] S. Nojiri, S. D. Odintsov and V. K. Oikonomou, *Modified Gravity Theories on a Nutshell: Inflation, Bounce and Late-time Evolution*, *Phys. Rept.* **692** (2017) 1–104, [1705.11098].

[79] G. K. Chakravarty and S. Mohanty, *Power law Starobinsky model of inflation from no-scale SUGRA*, *Phys. Lett.* **B746** (2015) 242–247, [1405.1321].

[80] M. Rinaldi, G. Cognola, L. Vanzo and S. Zerbini, *Reconstructing the inflationary $f(R)$ from observations*, *JCAP* **1408** (2014) 015, [1406.1096].

[81] A. Codello, J. Joergensen, F. Sannino and O. Svendsen, *Marginally Deformed Starobinsky Gravity*, *JHEP* **02** (2015) 050, [1404.3558].

[82] I. Ben-Dayan, S. Jing, M. Torabian, A. Westphal and L. Zarate, *$R^2 \log R$ quantum corrections and the inflationary observables*, *JCAP* **1409** (2014) 005, [1404.7349].

[83] H. Motohashi, *Consistency relation for R^p inflation*, *Phys. Rev.* **D91** (2015) 064016, [1411.2972].

[84] A. Linde, *Inflationary Cosmology after Planck 2013*, in *Proceedings, 100th Les Houches Summer School: Post-Planck Cosmology: Les Houches, France, July 8 - August 2, 2013*, pp. 231–316, 2015. 1402.0526. DOI.

[85] B. J. Broy, M. Galante, D. Roest and A. Westphal, *Pole inflation âĂŤ Shift symmetry and universal corrections*, *JHEP* **12** (2015) 149, [1507.02277].

[86] A. B. Goncharov and A. D. Linde, *Chaotic Inflation in Supergravity*, *Phys. Lett.* **139B** (1984) 27–30.

[87] A. Linde, M. Noorbala and A. Westphal, *Observational consequences of chaotic inflation with nonminimal coupling to gravity*, *JCAP* **1103** (2011) 013, [1101.2652].

[88] R. Kallosh and A. Linde, *Superconformal generalization of the chaotic inflation model $\frac{\lambda}{4}\phi^4 - \frac{\xi}{2}\phi^2 R$*, *JCAP* **1306** (2013) 027, [1306.3211].

[89] R. Kallosh, A. Linde and D. Roest, *Universal Attractor for Inflation at Strong Coupling*, *Phys. Rev. Lett.* **112** (2014) 011303, [1310.3950].

[90] R. Kallosh and A. Linde, *Non-minimal Inflationary Attractors*, *JCAP* **1310** (2013) 033, [1307.7938].

[91] D. I. Kaiser and E. I. Sfakianakis, *Multifield Inflation after Planck: The Case for Nonminimal Couplings*, *Phys. Rev. Lett.* **112** (2014) 011302, [1304.0363].

[92] S. Choudhury, *COSMOS-e'- soft Higgsotic attractors*, *Eur. Phys. J.* **C77** (2017) 469, [1703.01750].

[93] R. Kallosh and A. Linde, *Universality Class in Conformal Inflation*, *JCAP* **1307** (2013) 002, [1306.5220].

[94] M. Artymowski and A. Racioppi, *Scalar-tensor linear inflation*, *JCAP* **1704** (2017) 007, [1610.09120].

[95] J. Fumagalli, *Renormalization Group independence of Cosmological Attractors*, *Phys. Lett.* **B769** (2017) 451–459, [1611.04997].

[96] T. Terada, *Generalized Pole Inflation: Hilltop, Natural, and Chaotic Inflationary Attractors*, *Phys. Lett.* **B760** (2016) 674–680, [1602.07867].

[97] N. D. Birrell and P. C. W. Davies, *Quantum Fields in Curved Space*. Cambridge Monographs on Mathematical Physics. Cambridge Univ. Press, Cambridge, UK, 1984, 10.1017/CBO9780511622632.

[98] S. Gottlober, H. J. Schmidt and A. A. Starobinsky, *Sixth Order Gravity and Conformal Transformations*, *Class. Quant. Grav.* **7** (1990) 893.

[99] A. De Felice and S. Tsujikawa, *f(R) theories*, *Living Rev. Rel.* **13** (2010) 3, [1002.4928].

[100] A. L. Berkin and K.-i. Maeda, *Effects of R**3 and R box R terms on R**2 inflation*, *Phys. Lett.* **B245** (1990) 348–354.

[101] L. Sebastiani, G. Cognola, R. Myrzakulov, S. D. Odintsov and S. Zerbini, *Nearly Starobinsky inflation from modified gravity*, *Phys. Rev.* **D89** (2014) 023518, [1311.0744].

[102] L. Amendola, *Cosmology with nonminimal derivative couplings*, *Phys. Lett.* **B301** (1993) 175–182, [gr-qc/9302010].

[103] S. Deser and R. P. Woodard, *Nonlocal Cosmology*, *Phys. Rev. Lett.* **99** (2007) 111301, [0706.2151].

[104] WMAP collaboration, G. Hinshaw et al., *Nine-Year Wilkinson Microwave Anisotropy Probe (WMAP) Observations: Cosmological Parameter Results*, *Astrophys. J. Suppl.* **208** (2013) 19, [1212.5226].

[105] PLANCK collaboration, P. A. R. Ade et al., *Planck 2013 results. XXII. Constraints on inflation*, *Astron. Astrophys.* **571** (2014) A22, [1303.5082].

[106] PLANCK collaboration, P. A. R. Ade et al., *Planck 2015 results. XIII. Cosmological parameters*, *Astron. Astrophys.* **594** (2016) A13, [1502.01589].

[107] R. Fakir and W. G. Unruh, *Improvement on cosmological chaotic inflation through nonminimal coupling*, *Phys. Rev.* **D41** (1990) 1783–1791.

[108] A. Albrecht and P. J. Steinhardt, *Cosmology for Grand Unified Theories with Radiatively Induced Symmetry Breaking*, *Phys. Rev. Lett.* **48** (1982) 1220–1223.

[109] L. Boubekeur and D. H. Lyth, *Hilltop inflation*, *JCAP* **0507** (2005) 010, [hep-ph/0502047].

[110] L. McAllister, E. Silverstein and A. Westphal, *Gravity Waves and Linear Inflation from Axion Monodromy*, *Phys. Rev.* **D82** (2010) 046003, [0808.0706].

[111] E. Silverstein and A. Westphal, *Monodromy in the CMB: Gravity Waves and String Inflation*, *Phys. Rev.* **D78** (2008) 106003, [0803.3085].

[112] A. Albrecht, P. J. Steinhardt, M. S. Turner and F. Wilczek, *Reheating an Inflationary Universe*, *Phys. Rev. Lett.* **48** (1982) 1437.

[113] L. F. Abbott, E. Farhi and M. B. Wise, *Particle Production in the New Inflationary Cosmology*, *Phys. Lett.* **117B** (1982) 29.

[114] P. B. Greene, L. Kofman, A. D. Linde and A. A. Starobinsky, *Structure of resonance in preheating after inflation*, *Phys. Rev.* **D56** (1997) 6175–6192, [hep-ph/9705347].

[115] L. Kofman, A. D. Linde and A. A. Starobinsky, *Towards the theory of reheating after inflation*, *Phys. Rev.* **D56** (1997) 3258–3295, [hep-ph/9704452].

[116] A. Berera and L.-Z. Fang, *Thermally induced density perturbations in the inflation era*, *Phys. Rev. Lett.* **74** (1995) 1912–1915, [astro-ph/9501024].

[117] R. O. Ramos and L. A. da Silva, *Power spectrum for inflation models with quantum and thermal noises*, *JCAP* **1303** (2013) 032, [1302.3544].

[118] M. Bastero-Gil, A. Berera, I. G. Moss and R. O. Ramos, *Cosmological fluctuations of a random field and radiation fluid*, *JCAP* **1405** (2014) 004, [1401.1149].

[119] I. G. Moss and C. Xiong, *Dissipation coefficients for supersymmetric inflatonary models*, hep-ph/0603266.

[120] M. Bastero-Gil, A. Berera and R. O. Ramos, *Dissipation coefficients from scalar and fermion quantum field interactions*, *JCAP* **1109** (2011) 033, [1008.1929].

[121] M. Bastero-Gil, A. Berera, R. O. Ramos and J. G. Rosa, *General dissipation coefficient in low-temperature warm inflation*, *JCAP* **1301** (2013) 016, [1207.0445].

[122] A. Berera, M. Gleiser and R. O. Ramos, *Strong dissipative behavior in quantum field theory*, *Phys. Rev.* **D58** (1998) 123508, [hep-ph/9803394].

[123] J. Yokoyama and A. D. Linde, *Is warm inflation possible?*, *Phys. Rev.* **D60** (1999) 083509, [hep-ph/9809409].

[124] M. A. Cid, S. del Campo and R. Herrera, *Warm inflation on the brane*, *JCAP* **0710** (2007) 005, [0710.3148].

[125] R. Herrera, *G-Warm inflation*, *JCAP* **1705** (2017) 029, [1701.07934].

[126] S. del Campo and R. Herrera, *Warm inflation in the DGP brane-world model*, *Phys. Lett.* **B653** (2007) 122–128, [0708.1460].

[127] H. Mishra, S. Mohanty and A. Nautiyal, *Warm natural inflation*, *Phys. Lett.* **B710** (2012) 245–250, [1106.3039].

[128] L. Visinelli, *Natural Warm Inflation*, *JCAP* **1109** (2011) 013, [1107.3523].

[129] S. Bartrum, M. Bastero-Gil, A. Berera, R. Cerezo, R. O. Ramos and J. G. Rosa, *The importance of being warm (during inflation)*, *Phys. Lett.* **B732** (2014) 116–121, [1307.5868].

[130] M. Bastero-Gil, A. Berera and N. Kronberg, *Exploring the Parameter Space of Warm-Inflation Models*, *JCAP* **1512** (2015) 046, [1509.07604].

[131] V. N. Senoguz and Q. Shafi, *Chaotic inflation, radiative corrections and precision cosmology*, *Phys. Lett.* **B668** (2008) 6–10, [0806.2798].

[132] K. Enqvist and M. Karciauskas, *Does Planck really rule out monomial inflation?*, *JCAP* **1402** (2014) 034, [1312.5944].

[133] G. Ballesteros and C. Tamarit, *Radiative plateau inflation*, *JHEP* **02** (2016) 153, [1510.05669].

[134] M. Benetti and R. O. Ramos, *Warm inflation dissipative effects: predictions and constraints from the Planck data*, Phys. Rev. **D95** (2017) 023517, [1610.08758].

[135] S. Bartrum, A. Berera and J. G. Rosa, *Warming up for Planck*, JCAP **1306** (2013) 025, [1303.3508].

[136] A. Berera, I. G. Moss and R. O. Ramos, *Warm Inflation and its Microphysical Basis*, Rept. Prog. Phys. **72** (2009) 026901, [0808.1855].

[137] N. P. Landsman and C. G. van Weert, *Real and Imaginary Time Field Theory at Finite Temperature and Density*, Phys. Rept. **145** (1987) 141.

[138] A. R. Liddle and S. M. Leach, *How long before the end of inflation were observable perturbations produced?*, Phys. Rev. **D68** (2003) 103503, [astro-ph/0305263].

[139] J. Martin and C. Ringeval, *Inflation after WMAP3: Confronting the Slow-Roll and Exact Power Spectra to CMB Data*, JCAP **0608** (2006) 009, [astro-ph/0605367].

[140] J. Martin and C. Ringeval, *First CMB Constraints on the Inflationary Reheating Temperature*, Phys. Rev. **D82** (2010) 023511, [1004.5525].

[141] J. B. MuÃśoz, E. D. Kovetz, A. Raccanelli, M. Kamionkowski and J. Silk, *Towards a measurement of the spectral runnings*, JCAP **1705** (2017) 032, [1611.05883].

[142] A. Lewis, A. Challinor and A. Lasenby, *Efficient computation of CMB anisotropies in closed FRW models*, Astrophys. J. **538** (2000) 473–476, [astro-ph/9911177].

[143] N. Christensen, R. Meyer, L. Knox and B. Luey, *II. Bayesian methods for cosmological parameter estimation from cosmic microwave background measurements*, *Class. Quant. Grav.* **18** (2001) 2677, [astro-ph/0103134].

[144] A. E. Gelfand, S. K. Sahu and B. P. Carlin, *Efficient parametrisations for normal linear mixed models*, *Biometrika* **82** (1995) 479–488.

[145] F. Wang and D. P. Landau, *Efficient, Multiple-Range Random Walk Algorithm to Calculate the Density of States*, *Phys. Rev. Lett.* **86** (2001) 2050, [cond-mat/0011174].

[146] F. Wang and D. P. Landau, *Efficient, Multiple-Range Random Walk Algorithm to Calculate the Density of States*, *Phys.Rev.Lett.* **86** (Mar., 2001) 2050, [cond-mat/0011174].

[147] W. K. Hastings, *Monte carlo sampling methods using markov chains and their applications*, *Biometrika* **57** (1970) 97–109, [http://biomet.oxfordjournals.org/cgi/reprint/57/1/97.pdf].

[148] R. Arya, A. Dasgupta, G. Goswami, J. Prasad and R. Rangarajan, *Revisiting CMB constraints on warm inflation*, *JCAP* **1802** (2018) 043, [1710.11109].

[149] M. Bastero-Gil, A. Berera, I. G. Moss and R. O. Ramos, *Theory of non-Gaussianity in warm inflation*, *JCAP* **1412** (2014) 008, [1408.4391].

[150] G. Kane, K. Sinha and S. Watson, *Cosmological Moduli and the Post-Inflationary Universe: A Critical Review*, *Int. J. Mod. Phys.* **D24** (2015) 1530022, [1502.07746].

[151] V. Balasubramanian, P. Berglund, J. P. Conlon and F. Quevedo, *Systematics of moduli stabilisation in Calabi-Yau flux compactifications*, *JHEP* **03** (2005) 007, [hep-th/0502058].

[152] S. B. Giddings, S. Kachru and J. Polchinski, *Hierarchies from fluxes in string compactifications*, *Phys. Rev.* **D66** (2002) 106006, [hep-th/0105097].

[153] M. Cicoli, I. GarcÃña-Etxebarria, C. Mayrhofer, F. Quevedo, P. Shukla and R. Valandro, *Global Orientifolded Quivers with Inflation*, *JHEP* **11** (2017) 134, [1706.06128].

[154] L. Dai, M. Kamionkowski and J. Wang, *Reheating constraints to inflationary models*, *Phys. Rev. Lett.* **113** (2014) 041302, [1404.6704].

[155] S. Dodelson and L. Hui, *A Horizon ratio bound for inflationary fluctuations*, *Phys. Rev. Lett.* **91** (2003) 131301, [astro-ph/0305113].

[156] R. Easther and H. V. Peiris, *Bayesian Analysis of Inflation II: Model Selection and Constraints on Reheating*, *Phys. Rev.* **D85** (2012) 103533, [1112.0326].

[157] J. B. Munoz and M. Kamionkowski, *Equation-of-State Parameter for Reheating*, *Phys. Rev.* **D91** (2015) 043521, [1412.0656].

[158] J. L. Cook, E. Dimastrogiovanni, D. A. Easson and L. M. Krauss, *Reheating predictions in single field inflation*, *JCAP* **1504** (2015) 047, [1502.04673].

[159] T. Rehagen and G. B. Gelmini, *Low reheating temperatures in monomial and binomial inflationary potentials*, *JCAP* **1506** (2015) 039, [1504.03768].

[160] Y. Ueno and K. Yamamoto, *Constraints on α-attractor inflation and reheating*, *Phys. Rev.* **D93** (2016) 083524, [1602.07427].

[161] M. Eshaghi, M. Zarei, N. Riazi and A. Kiasatpour, *CMB and reheating constraints to α-attractor inflationary models*, *Phys. Rev.* **D93** (2016) 123517, [1602.07914].

[162] P. Cabella, A. Di Marco and G. Pradisi, *Fiber inflation and reheating*, *Phys. Rev.* **D95** (2017) 123528, [1704.03209].

[163] F. Feroz, M. P. Hobson and M. Bridges, *MultiNest: an efficient and robust Bayesian inference tool for cosmology and particle physics*, *Mon. Not. Roy. Astron. Soc.* **398** (2009) 1601–1614, [0809.3437].

[164] J. Martin, C. Ringeval and R. Trotta, *Hunting Down the Best Model of Inflation with Bayesian Evidence*, *Phys. Rev.* **D83** (2011) 063524, [1009.4157].

[165] J. Martin, C. Ringeval and V. Vennin, *Observing Inflationary Reheating*, *Phys. Rev. Lett.* **114** (2015) 081303, [1410.7958].

[166] J. Martin, C. Ringeval and V. Vennin, *Information Gain on Reheating: the One Bit Milestone*, *Phys. Rev.* **D93** (2016) 103532, [1603.02606].

[167] S. Kachru, R. Kallosh, A. D. Linde and S. P. Trivedi, *De Sitter vacua in string theory*, *Phys. Rev.* **D68** (2003) 046005, [hep-th/0301240].

[168] M. Cicoli, A. Maharana, F. Quevedo and C. P. Burgess, *De Sitter String Vacua from Dilaton-dependent Non-perturbative Effects*, *JHEP* **06** (2012) 011, [1203.1750].

[169] A. Retolaza and A. Uranga, *De Sitter Uplift with Dynamical Susy Breaking*, *JHEP* **04** (2016) 137, [1512.06363].

[170] C. P. Burgess, R. Kallosh and F. Quevedo, *De Sitter string vacua from supersymmetric D terms*, *JHEP* **10** (2003) 056, [hep-th/0309187].

[171] M. Cicoli, D. Klevers, S. Krippendorf, C. Mayrhofer, F. Quevedo and R. Valandro, *Explicit de Sitter Flux Vacua for Global String Models with Chiral Matter*, *JHEP* **05** (2014) 001, [1312.0014].

[172] M. Cicoli, F. Quevedo and R. Valandro, *De Sitter from T-branes*, *JHEP* **03** (2016) 141, [1512.04558].

[173] J. D. Qualls, *Universal Bounds in Even-Spin CFTs*, *JHEP* **12** (2015) 001, [1412.0383].

[174] M. Cicoli, K. Dutta and A. Maharana, *N-flation with Hierarchically Light Axions in String Compactifications*, *JCAP* **1408** (2014) 012, [1401.2579].

[175] R. Allahverdi, R. Brandenberger, F.-Y. Cyr-Racine and A. Mazumdar, *Reheating in Inflationary Cosmology: Theory and Applications*, *Ann. Rev. Nucl. Part. Sci.* **60** (2010) 27–51, [1001.2600].

[176] D. I. Podolsky, G. N. Felder, L. Kofman and M. Peloso, *Equation of state and beginning of thermalization after preheating*, *Phys. Rev.* **D73** (2006) 023501, [hep-ph/0507096].

[177] M. Cicoli, J. P. Conlon and F. Quevedo, *Dark radiation in LARGE volume models*, *Phys. Rev.* **D87** (2013) 043520, [1208.3562].

[178] PLANCK collaboration, R. Adam et al., *Planck 2015 results. X. Diffuse component separation: Foreground maps*, *Astron. Astrophys.* **594** (2016) A10, [1502.01588].

[179] P. F. de Salas, M. Lattanzi, G. Mangano, G. Miele, S. Pastor and O. Pisanti, *Bounds on very low reheating scenarios after Planck*, *Phys. Rev.* **D92** (2015) 123534, [1511.00672].

[180] T. Higaki and F. Takahashi, *Dark Radiation and Dark Matter in Large Volume Compactifications*, *JHEP* **11** (2012) 125, [1208.3563].

[181] J. Ellis, M. A. G. Garcia, N. Nagata, D. V. Nanopoulos and K. A. Olive, *Starobinsky-like Inflation, Supercosmology and Neutrino Masses in No-Scale Flipped SU(5)*, *JCAP* **1707** (2017) 006, [1704.07331].

[182] D. Baumann and L. McAllister, *Inflation and String Theory*. Cambridge Monographs on Mathematical Physics. Cambridge University Press, 2015, 10.1017/CBO9781316105733.

[183] K. Nakayama, S. Saito, Y. Suwa and J. Yokoyama, *Probing reheating temperature of the universe with gravitational wave background*, *JCAP* **0806** (2008) 020, [0804.1827].

[184] S. Kuroyanagi, C. Gordon, J. Silk and N. Sugiyama, *Forecast Constraints on Inflation from Combined CMB and Gravitational Wave Direct Detection Experiments*, *Phys. Rev.* **D81** (2010) 083524, [0912.3683].

[185] L. Aparicio, M. Cicoli, B. Dutta, S. Krippendorf, A. Maharana, F. Muia et al., *Non-thermal CMSSM with a 125 GeV Higgs*, *JHEP* **05** (2015) 098, [1502.05672].

[186] L. Aparicio, M. Cicoli, B. Dutta, F. Muia and F. Quevedo, *Light Higgsino Dark Matter from Non-thermal Cosmology*, *JHEP* **11** (2016) 038, [1607.00004].

[187] R. H. Cyburt, B. D. Fields, K. A. Olive and T.-H. Yeh, *Big Bang Nucleosynthesis: 2015*, *Rev. Mod. Phys.* **88** (2016) 015004, [1505.01076].

[188] N. Sasankan, M. R. Gangopadhyay, G. J. Mathews and M. Kusakabe, *New observational limits on dark radiation in braneworld cosmology*, *Phys. Rev.* **D95** (2017) 083516, [1607.06858].

[189] N. Sasankan, M. R. Gangopadhyay, G. J. Mathews and M. Kusakabe, *Limits on Brane-World and Particle Dark Radiation from Big Bang Nucleosynthesis and the CMB*, *Int. J. Mod. Phys.* **E26** (2017) 1741007, [1706.03630].

[190] J. J. Blanco-Pillado, D. Buck, E. J. Copeland, M. Gomez-Reino and N. J. Nunes, *Kahler Moduli Inflation Revisited*, *JHEP* **01** (2010) 081, [0906.3711].

[191] R. Easther, J. Frazer, H. V. Peiris and L. C. Price, *Simple predictions from multifield inflationary models*, *Phys. Rev. Lett.* **112** (2014) 161302, [1312.4035].

[192] K. D. Lozanov and M. A. Amin, *Equation of State and Duration to Radiation Domination after Inflation*, *Phys. Rev. Lett.* **119** (2017) 061301, [1608.01213].

[193] K. D. Lozanov and M. A. Amin, *Self-resonance after inflation: oscillons, transients and radiation domination*, *Phys. Rev.* **D97** (2018) 023533, [1710.06851].

[194] K. Freese, J. A. Frieman and A. V. Olinto, *Natural inflation with pseudo - Nambu-Goldstone bosons*, *Phys. Rev. Lett.* **65** (1990) 3233–3236.

[195] G. Schwarz, *Estimating the Dimension of a Model*, *Annals of Statistics* **6** (July, 1978) 461–464.

[196] R. Trotta, *Bayes in the sky: Bayesian inference and model selection in cosmology*, *Contemporary Physics* **49** (Mar., 2008) 71–104, [0803.4089].

[197] V. F. Mukhanov and G. V. Chibisov, *Quantum Fluctuations and a Nonsingular Universe*, *JETP Lett.* **33** (1981) 532–535.

[198] A. Sen, *Stable nonBPS states in string theory*, *JHEP* **06** (1998) 007, [hep-th/9803194].

[199] A. Sen, *Stable nonBPS bound states of BPS D-branes*, *JHEP* **08** (1998) 010, [hep-th/9805019].

[200] A. Sen, *Tachyon condensation on the brane anti-brane system*, *JHEP* **08** (1998) 012, [hep-th/9805170].

[201] S. Bhattacharya and M. R. Gangopadhyay, *A study in non-canonical domain of Goldstone inflaton*, 1812.08141.

[202] N. Arkani-Hamed, H.-C. Cheng, P. Creminelli and L. Randall, *Extra natural inflation*, *Phys. Rev. Lett.* **90** (2003) 221302, [hep-th/0301218].

[203] A. D. Linde, *Hybrid inflation*, *Phys. Rev.* **D49** (1994) 748–754, [astro-ph/9307002].

[204] J. E. Kim, H. P. Nilles and M. Peloso, *Completing natural inflation*, *JCAP* **0501** (2005) 005, [hep-ph/0409138].

[205] S. Dimopoulos, S. Kachru, J. McGreevy and J. G. Wacker, *N-flation*, *JCAP* **0808** (2008) 003, [hep-th/0507205].

[206] A. R. Liddle, A. Mazumdar and F. E. Schunck, *Assisted inflation*, *Phys. Rev.* **D58** (1998) 061301, [astro-ph/9804177].

[207] E. J. Copeland, A. Mazumdar and N. J. Nunes, *Generalized assisted inflation*, *Phys. Rev.* **D60** (1999) 083506, [astro-ph/9904309].

[208] N. Arkani-Hamed, H.-C. Cheng, P. Creminelli and L. Randall, *Pseudonatural inflation*, *JCAP* **0307** (2003) 003, [hep-th/0302034].

[209] D. Croon, V. Sanz and J. Setford, *Goldstone Inflation*, *JHEP* **10** (2015) 020, [1503.08097].

[210] C. Csaki, N. Kaloper, J. Serra and J. Terning, *Inflation from Broken Scale Invariance*, *Phys. Rev. Lett.* **113** (2014) 161302, [1406.5192].

[211] R. Contino, Y. Nomura and A. Pomarol, *Higgs as a holographic pseudoGoldstone boson*, *Nucl. Phys.* **B671** (2003) 148–174, [hep-ph/0306259].

[212] C. Armendariz-Picon, T. Damour and V. F. Mukhanov, *k - inflation*, *Phys. Lett.* **B458** (1999) 209–218, [hep-th/9904075].

[213] S. Li and A. R. Liddle, *Observational constraints on K-inflation models*, *JCAP* **1210** (2012) 011, [1204.6214].

[214] K. Nozari and S. D. Sadatian, *Non-Minimal Inflation after WMAP3*, *Mod. Phys. Lett.* **A23** (2008) 2933–2945, [0710.0058].

[215] C. Pallis, *Non-Minimally Gravity-Coupled Inflationary Models*, *Phys. Lett.* **B692** (2010) 287–296, [1002.4765].

[216] M. R. Gangopadhyay and G. J. Mathews, *Constraints on Brane-World Inflation from the CMB Power Spectrum: Revisited*, *JCAP* **1803** (2018) 028, [1611.05123].

[217] D. K. Hazra, A. Shafieloo, G. F. Smoot and A. A. Starobinsky, *Wiggly Whipped Inflation*, *JCAP* **1408** (2014) 048, [1405.2012].

[218] J. McDonald, *Hemispherical Power Asymmetry from a Space-Dependent Component of the Adiabatic Power Spectrum*, *Phys. Rev.* **D89** (2014) 127303, [1403.2076].

[219] G. J. Mathews, M. R. Gangopadhyay, K. Ichiki and T. Kajino, *Possible Evidence for Planck-Scale Resonant Particle Production during Inflation from the CMB Power Spectrum*, *Phys. Rev.* **D92** (2015) 123519, [1504.06913].

[220] M. R. Gangopadhyay, G. J. Mathews, K. Ichiki and T. Kajino, *Explaining low ℓ anomalies in the CMB power spectrum with resonant superstring excitations during inflation*, *Eur. Phys. J.* **C78** (2018) 733, [1701.00577].

[221] N. Kitazawa and A. Sagnotti, *A string-inspired model for the low-ℓ CMB*, *Mod. Phys. Lett.* **A30** (2015) 1550137, [1503.04483].

[222] G. Obied, H. Ooguri, L. Spodyneiko and C. Vafa, *De Sitter Space and the Swampland*, 1806.08362.

[223] W. H. Kinney, S. Vagnozzi and L. Visinelli, *The Zoo Plot Meets the Swampland: Mutual (In)Consistency of Single-Field Inflation, String Conjectures, and Cosmological Data*, 1808.06424.